AD NUMBER

AD488151

NEW LIMITATION CHANGE

TO

Approved for public release, distribution unlimited

FROM

Distribution authorized to U.S. Gov't. agencies and their contractors; Operational and Administrative Use; May 1966. Other requests shall be referred to the Flight Dynamics Laboratory [FDCL], Wright-Paatterson AFB, OH, 45433.

AUTHORITY

AFFDL ltr, 31 May 1973

AFFDL-TR-65-204

STUDY OF APPLICATION OF RELIABILITY PREDICTION TECHNIQUES ON FLIGHT CONTROL COMPONENTS

J. B. WERTZ, et al

BATTELLE MEMORIAL INSTITUTE
COLUMBUS, OHIO

TECHNICAL REPORT AFFDL-TR-65-204

MAY 1966

AIR FORCE FLIGHT DYNAMICS LABORATORY
RESEARCH AND TECHNOLOGY DIVISION
AIR FORCE SYSTEMS COMMAND
WRIGHT-PATTERSON AIR FORCE BASE, OHIO 45433

(6)

STUDY OF APPLICATION OF RELIABILITY PREDICTION TECHNIQUES ON FLIGHT CONTROL COMPONENTS.

(9) Technical rept. 15 Mar 64 – 30 Jun 65,

J. B. WERTZ, *et al*

BATTELLE MEMORIAL INSTITUTE
COLUMBUS, OHIO

(10) J. B. Wertz, J. R Goldgraben, M. E. Hassfurther, J. V. Baum J. L. Easterday

(11) May 66

(12) 129 p.

(15) AF33(615)-1527

(16) AF-8025

(18) AFFDL (19) TR-65-204

(05-2 HOC)

FOREWORD

This report was prepared by Battelle Memorial Institute under United States Air Force Contract No. AF33(615)-1527, "Study of Application of Reliability Prediction Techniques". The work was administered under the direction of the AF Flight Dynamics Laboratory, Research and Technology Division, with Mr. V. R. Schmitt as Technical Monitor.

The research was administered and conducted by the Advanced Electronics Division and the Systems Engineering Division of the Engineering Physics Department of Battelle, and by the Kinematics and Mechanisms Division of the Mechanical Engineering Department of Battelle. Individual contributions from the Engineering Physics Department included: over-all project administration, L. H. Stember, Jr., Division Chief; project coordination and reliability, J. L. Easterday; administration and technical consultation for the momentum-exchange system studies, M. E. Hassfurther; modeling, analog studies, and technique application, J. B. Wertz, R. E. Thompson, and R. J. Conlon. Work by the Mechanical Engineering Department on the NaK system and the servo valve were administrated by J. V. Baum who was supported by J. R. Goldgraben and R. K. Mitchell on the analog studies and reliability analyses, and J. M. Harris on data evaluation and laboratory testing.

This report covers the period from March 15, 1964, to June 30, 1965.

This technical report has been reviewed and is approved.

H. W. BASHAM
Chief, Control Elements Branch
Flight Control Division
AF Flight Dynamics Laboratory

ABSTRACT

A previous reliability research effort by Battelle generated an analytical technique called the Moment method for predicting drift-type failures in components and systems. This technique is based on the Propagation of Variance formula, which combines data derived from the system or system model, and parameter tolerance data, to formulate an estimate of the probability that the system will perform within specifications at the initial or some future time of operation.

This report discusses the application of the reliability-prediction technique to a momentum-exchange-type attitude control and stabilization subsystem for a satellite, a liquid-metal servo actuating subsystem, and an electrohydraulic servo valve.

A mathematical model was completed for the momentum-exchange-type attitude control (fluid flywheel), significant system parameters identified, the analysis of the expected system degradation over time was made, and a prediction of efficiency and reliability is presented in the report.

Performance characteristics used to define system performance for the fluid-flywheel system were:

(1) Settling time for an input step

(2) Open-loop peak efficiency.

Since parameter variability data as a function of time were essentially nonexistent, it was estimated that system gain and fluid-friction factor would be the system parameters most likely to drift over time. (A test plan designed to obtain the desired parameter variability data is appendixed to the report.) Settling time was observed to be a discontinuous function of both system gain and friction factor due to the definition of settling time rather than a physical phenomenon. Open-loop peak efficiency for the flywheel is defined in the same way as the efficiency for an a-c or d-c servo motor. The results of the investigation give the parameters to which their performance criteria are most sensitive and the percentage contribution of each parameter to the performance criteria variances.

The pump and actuator portion of the liquid-metal servo actuating subsystem were similarly modeled, sensitive system parameters identified, and critical points of degradation estimated from analysis of the Propagation of Variance study. Study of the analog model for the pump and actuator yielded the partial derivatives of system and component performance characteristics with respect to those parameters that were identified as being susceptible to degradation. The results indicated that wear in the actuator piston rings is probably the most critical area in the system with respect to drift reliability. This is based on the assumption that the rod seal and bearing in the actuator perform satisfactorily. The servo control valve was not analyzed because the design for this component is incomplete.

The servovalve was modeled on the analog computer, and the sensitivity of performance characteristics with respect to variations in the physical parameters was investigated. Design optimization was achieved through reduction of those partials of the Propagation of Variance Formula that had large values and/or were related to

parameters whose time rate of change was expected to be significant. The second step in this study was the development of a quantitative prediction of the relative reliability improvement expected from a new valve design with respect to the characteristic of peak quiescent flow. The third activity on this task was the performance of life tests on two modified and two unmodified servo valves. The modified valves were those constructed in accordance with the findings of the analysis of the analog model. The predicted improvements in quiescent leakage and frequency response were verified by the laboratory tests. In addition, a significant improvement in feedback-wire-tip wear occurred in the redesigned valves.

TABLE OF CONTENTS

TABLE OF CONTENTS
(Continued)

ILLUSTRATIONS

ILLUSTRATIONS
(Continued)

ILLUSTRATIONS
(Continued)

ILLUSTRATIONS
(Continued)

TABLES

SYMBOLS

Symbols for Task I

A	Diffuser ratio
A_i	Performance characteristic
$\bar{A}_i$	Mean value of the performance characteristic
a	Friction-factor constant at equilibrium
$a-b$	Initial value of the friction-factor constant
α	Friction-factor time constant
$\underline{B}$, B	Magnetic-flux density
C	Diffuser constant
D_S	Sensor dead band
D_1	Loop diameter
D_2	Tube diameter
E	Peak efficiency
E_0	Peak efficiency at system lifetime of zero hours (initial peak efficiency)
E_S	Thevenin voltage source
E_b	Back emf
$E_{500\ hours}$	Peak efficiency at system lifetime of 500 hours
$E_{5\ years}$	Peak efficiency at system lifetime of 5 years
e	Base of natural logarithms
η_D	Diffuser efficiency
f_c	Friction-factor constant
$\underline{F}$, F	Force
f	Fanning friction factor
g	Acceleration due to earth's gravity
γ_F	Fluid weight density (mercury)
H	Angular momentum
h	Pump channel height
I	Amplifier output current (pump input current)
I_S	Norton current source
$\underline{i}_p$, I_p	Current in the pumping channel
J_V	Moment of inertia of the vehicle
J_f	Moment of inertia of the fluid flywheel
K_L	Loop-loss constant
K_V	Voltage-amplifier gain
K_{V_0}	Initial value of voltage-amplifier gain
K_a	Current-amplifier gain
K_b	Back-emf loss constant
K_d	Diffuser loss constant
K_g	Pump-gain constant
K_1	First rate constant for voltage-amplifier gain change
K_2	Second rate constant for voltage-amplifier gain change
L	Electrode length
$\underline{L}$	Length of the current path in magnetic field
λ	Constant associated with calculating diffuser efficiency
μ	Fluid viscosity (mercury)
n_L	Number corresponding to the portion of a distribution below the lower specification limit
n_U	Number corresponding to the portion of a normal distribution above the upper specification limit
ω_f	Fluid angular velocity in the loop
P_i	Input power to system
P_{FL}	Fixed power loss in system electronics
P_L	Pressure drop in loop
P_O	System power output
P_d	Pressure drop in diffuser
P_j	Parameter
P_n	Net system pressure
P_{n_L}	Portion of the distribution corresponding to n_L
P_{n_U}	Portion of the distribution corresponding to n_U
P_p	Pressure drop in pump

Symbols for Task I
(Continued)

P_t	Pressure developed by the pump
$\overline{P}_j$	Mean value of the parameter
R_C	Mercury-electrode contact resistance
R_S	Amplifier-output resistance
R_a	Sum of amplifier-output resistance and mercury-electrode contact resistance
R_e	Reynolds number
R_f	Pump fringing resistance
R_p	Pump channel resistance
ρ_{rs}	Correlation coefficient
SL_L	Lower specification limit
SL_U	Upper specification limit
σ_E	Standard deviation of the open-loop peak efficiency
σ_{A_i}	Standard deviation of the performance characteristic
σ_{P_j}	Standard deviation of the parameter
σ_{K_V}	Standard deviation of voltage-amplifier gain
$\sigma_{K_{V_0}}$	Initial standard deviation of voltage-amplifier gain
σ_{K_1}	First rate constant for voltage-amplifier standard-deviation change
σ_{K_2}	Second rate constant for voltage-amplifier standard-deviation change
σ_{t_s}	Standard deviation of the settling time
T_L	Torque loss in loop
T_b	Torque loss due to back emf
T_d	Torque loss in diffuser
T_g	Torque without system losses
T_n	Net torque available to accelerate the fluid
T_p	Torque loss in pump
t	Time
t_S	Settling time
t_{S_0}	Settling time at system lifetime of zero hours (initial settling time)
$t_{S_{500\ hours}}$	Settling time at system lifetime of 500 hours
$t_{S_{5\ years}}$	Settling time at system lifetime of 5 years
θ_c	Angular-position input command signal
θ_e	Angular-position error signal
$\theta_{e_{DB}}$	Angular-position error-signal output from sensor dead band
θ_P	Angular position of pitch axis
θ_R	Angular position of roll axis
θ_Y	Angular position of yaw axis
θ_r	Vehicle angular-position response
$\underline{V}$, V	Fluid velocity
V_S	Voltage saturation level
w	Pump channel width

Symbols for Task II

Main Characters

A	Area (in.^{2})
a	Diametral clearance (in.)
C	Coefficient
C_{RA}	Actuator piston radial clearance (in.)
D^*	Hydraulic radius (in.)
d	Diameter (in.)
g	Gravitational constant (ft/sec.^{2})
H	Head (ft)
K_1	See Equation (46) (in.^{2})
K_2	See Equation (46) (in.^{2})
K_5	See Equation (51) (in.^{2})
L	Flow length [See Equation (48) (in.)]
ℓ	Leakage length (in.)
M	Mass
m	Slip factor
P	Pressure (psi)
Q	Flow (cis)

Symbols for Task II (Continued)

Main Characters (Continued)

q	Leakage (cis)
R	Radius (in.)
R_e	Reynolds number
t	Impeller-blade circumferential thickness (in.)
u	Tangential velocity of impeller tip (in./sec)
V	Velocity (in./sec)
w	Impeller-blade width (in.)
X	Impulse factor or distance
Z	Number of blades on impeller
α	Direction of absolute velocity, diffuser vane angle (deg) (see Figure 31)
β	Impeller-blade angle (deg) or bulk modulus (psi)
γ	Density of NaK ($lb/in.^3$)
δ	Axial clearance (in.)
ϵ	R_2/R_1
E	Ratio of radii that bound a radial leakage path
λ	See Equation (48)
μ	Absolute viscosity of NaK ($lb\ sec/in.^2$)
ν	μ/ρ, kinematic viscosity ($in.^2/sec$)
ξ	Damping factor
ω	Rotational speed at frequency (radians/second)
ϕ_M	See Equation (57)
$\phi_2(m)$	See Equation (53)
ϕ_3	See Equation (54)
ρ	Mass density of NaK ($lb^2\ sec^2/in.^4$)
ψ	Cot α_1 prerotation factor

Subscripts

0 - 5	Position identification in pump (See Figure 32)
A	Actuator
a - j	Stage identification (See Figure 31)
DI	Diffuser inlet
DO	Diffuser outlet
EQ	Equivalent
F	Front bearing, front seal, or friction
ID	Impulse at diffuser
IO	Impulse at inlet
L	Loss, load, or leakage
M	Mixing, middle bearing
N	Natural
R	Rear bearing
S	Pump supply
SA	Supply area
th	Theoretical
b	Impeller blade
P	Piston
p	Pump outlet (pressure)
r	Radial
s	Spool
tb	Thrust bearing
u	Tangential

Symbols for Task III

A_N	Nozzle area ($in.^2$)
A_O	Orifice area ($in.^2$)
$C_{BLLI-DP}$	Bushing leakage coefficient, load Port No. 1 to drain (cis/psi)
C_D	Drain-orifice flow coefficient
C_N	Nozzle flow coefficient
C_O	Orifice flow coefficient
C_{OI}	Orifice flow coefficient (one side only)
C_{PSL}	Spool leakage coefficient (cis %/psi)
C_q	Spool-bushing port discharge coefficient
C_{RB}	Bushing radial clearance (in.)

Symbols for Task III (Continued)

C_{RS}	Seal radial clearance (in.)
$C_{SLL1-DP}$	Spool leakage coefficient, load Port No. 1 to drain (cis/psi)
D	Nozzle diameter (in.)
d	Orifice diameter (in.)
d_B	Bushing diameter (in.)
d_s	Spool diameter (in.)
FR	Frequency response (db)
h_1	Nozzle flapper distance on one side with no armature deflection (in.)
i	Torque-motor differential current (ma)
I_{Null}	Null current (ma)
K	Erosive wear constant [$in.^3$ of solid eroded per $in.^3$ of fluid per unit of fluid velocity (in./sec)]
K_{fbs}	Feedback-wire spring rate (lb/in.)
K_p	Spool-bushing port pressure drop characteristic (psi $\%^2/cis^2$)
ℓ	Leakage-path length (in.)
M	Abrasive wear constant (in. mg/cycle %)
N	Number of operational cycles
n	Number of spool-bushing flow ports on each end
P_A	Pressure in Load Line A
P_B	Pressure in Load Line B
P_{DP}	Drain-port pressure (psi)
P_{LI}	Load pressure in control line (psi)
P_{N1}, P_{N2}	Pressure in Nozzles 1, 2 (psi)
P_S	Supply pressure (psi)
ΔP_N	Nozzle differential pressure or control pressure (psi)
ΔQ	Spool leakage
Q_1, Q_2	Nozzle flows (cis)
Q_{END}	Laminar spool end leakage (cis)
Q_ℓ	Quiescent leakage flow (cis)

Symbols for Task III (Continued)

$Q_{\ell a}$	Abrasion-sensitive quiescent leakage (cis)
$Q_{\ell e}$	Erosion-sensitive quiescent leakage (cis)
Q_v	Valve flow (cis)
w	Slot width (in.)
X_{SMAX}	Spool maximum stroke from center (in.)
Y_S	Spool position (percent of maximum stroke from center)
Y_{S2}	Spool position corresponding to minimum spool leakage-path length (%)
Y_{SLAP}	Underlap (% of maximum stroke from center)
y	Spool displacement gain (% of maximum stroke per milliamp)
δ	Armature deflection (% of maximum rotation from center)
ϕ	Dynamic phase lag (deg)
μ	Fluid viscosity (lb sec/$in.^2$)
ρ	Mass density (lb $sec^2/in.^4$)

INTRODUCTION

Most present reliability analysis and estimating techniques are based on statistical techniques and catastrophic failures. This approach is not appropriate for electromechanical devices and small-quantity production items, such as advanced vehicles, which are designed to be subjected to extreme environments. In addition to small-quantity production, the development and evaluation of new concepts and designs for advanced missions and environments are constrained by increasing reliability requirements, decreasing calendar time for the evolution of a design, more complex functions, and smaller packaging. New methods must be developed to predict the reliability of new and critical flight-control components having unique design and application, small-production quantities, and relatively short design lead time.

Battelle has been conducting research on the development of the Moment method of analysis of drift failures in electromechanical devices and, under the present contract, has undertaken the task of extending and modifying the techniques developed and applying these techniques to three specified systems: a momentum-exchange-type attitude-control and stabilization subsystem, a liquid-metal servo-actuating subsystem, and an electrohydraulic servo valve. These systems and components have been simulated mathematically on the analog computer. The results show the relationships between system performance characteristics and individual parameters, thus providing information for design optimization and reliability predictions.

Although the technique may be considered as still in its basic stage of development with some simplifying assumptions required to implement it, the applications demonstrated in this project indicate its feasibility, as well as providing guidelines for similar applications to other systems. The technique described is of proven value for design analysis and optimization, and reliability prediction of drift parameter degradation. Battelle has been conducting research and development of the technique for 3 years under Air Force contract. The initial study, conducted under Contract No. AF 33(657)-7978, to develop the analytical techniques was reported in Technical Documentary Report No. ASD-TDR-63-287 dated January, 1963. The research was continued through the application and further development of the techniques, using as an example an electrohydraulic servo valve and an associated flight-type linear hydraulic actuator. This work, conducted under the same contract, is reported in Technical Documentary Report No. FDL-TDR-64-50 dated August, 1964.

This report is divided into three distinct sections, each representing a complete and independent report for its respective task. Lists of symbols are applicable only to the particular section of the report with which they are associated. Brief abstracts, summaries, and conclusions are contained within each of the three report sections. Supplemental material containing information which may be considered proprietary by other contractors has been delivered to the program Technical Monitor. Included in this supplemental material are:

(1) Equations for Mathematical Model of Centrifugal Pumps

(2) Derivation of a Method for Determining the Nonsteady-State Power Requirements for a Centrifugal Pump

(3) Approximate Method for Determining the Pressure Differential Across the Faces of a Centrifugal Impeller Blade

(4) Analog Computer Wiring Diagram and Potentiometer Settings for Pump Simulation Program

(5) Relationship Between Volume of Eroded Material and Increase in Lap Space.

SUMMARY

General

This research has been concerned primarily with the application of the Moment method of variability analysis as a means of reliability prediction applied to three specific flight-control systems. Emphasis was on the application of this previously developed technique to provide a basis for others to utilize it with their own systems. The analysis is concerned with the gradual shift in one or more performance characteristics as a result of internal parameter variations produced by environmental and time-dependent effects, thus causing the performance to shift outside of specification limits. The goal then is to predict the probability that a device will exhibit performance characteristics within the required limits for a specified period of time in the specified environment. The Moment method is based on the Propagation of Variance formula, equating total variability for each performance characteristic to the sum of the contributions of variability from all the related internal and input parameters. The results of the analyses identify the relationships between the input parameters and the output characteristics, and provide a weighting of these relationships, thus enabling identification of those parameters most likely to cause severe degradation of the system and permitting a prediction of system reliability over time if the input parameter data are known.

The three systems studied on this project were: (1) momentum-exchange-type attitude control and stabilization subsystem, (2) liquid metal (NaK) servo-actuating system, and (3) an electrohydraulic servovalve. The research was conducted in three separate tasks, and this report has been organized accordingly.

Task I. Momentum-Exchange-Type Attitude Control and Stabilization Subsystem

The investigation into the drift reliability of the fluid-flywheel system considered the system performance specified by the performance characteristics: (1) settling time for an input step and (2) open-loop peak efficiency. Settling time was given an upper specification limit of 14.5 seconds, and peak efficiency was given a lower specification limit of 3 percent.

Parameter-variability data as a function of time were essentially nonexistent. Battelle generated a test plan designed to obtain the parameter-variability data. The test plan is submitted as an appendix to this report.

From manufacturers' information and past Battelle experience, it was decided that system gain and the fluid-friction factor would be the system parameters most likely to drift over time. The system gain was assumed to decrease linearly over time, and the friction factor was considered to have an exponential increase over time. The results of the investigation give the parameters to which the performance criteria are most sensitive and the percentage contribution of each parameter to the performance criteria variances.

Settling time was observed to be a discontinuous function of both system gain and friction factor. A sharp decrease in settling time occurred after 1/2 year of operation. The discontinuous relationship is a result of the standard definition for settling time and not the result of physical phenomena, which indicates the need to consider carefully what performance characteristics are to be used to specify system performance. Initially, the nominal settling time was 13.25 seconds, with a tolerance of ±1.08 seconds and a reliability estimate of 0.9999. After 5 years of operation, the nominal settling time was 11.75 seconds, with a tolerance of ±2.56 seconds and a reliability estimate of 0.9999. The high reliability estimate at the end of 5 years is due to the decrease in nominal value that resulted from the discontinuous relationship.

Open-loop peak efficiency for the flywheel has the same definition as that for an a-c or d-c servo motor and is a continuous function of the parameters. The nominal value of peak efficiency decreased steadily over time, and its tolerance value increased steadily over time. Initially, the nominal peak efficiency was 4.27 percent, with a tolerance of ±0.576 percent and a reliability estimate of 1.000. After 5 years of operation, the nominal peak efficiency was 3.25 percent, with a tolerance of ±1.31 percent and a reliability estimate of 0.7164.

The Moment method for predicting drift-type failures requires quantitative data on the degradation of parameters as a function of time. Since these data were lacking for this system, it was necessary to rely on qualitative information, which proved to be sufficient to make reasonable assumptions for the analysis. It was concluded that the system has a high reliability with respect to the characteristics chosen and the arbitrarily assigned specification limits. It has been demonstrated that the Moment method has the ability to provide insight to a designer on the behavior of the system characteristics being considered as a means of performance evaluation.

Task II. Liquid-Metal (NaK-77) Servo-Actuating Subsystem

A satisfactory model of a centrifugal pump and linear actuator was developed, and manipulation of the analog model yielded the necessary partial derivatives of system and component performance characteristics with respect to those parameters identified as being susceptible to degradation.

The analysis of the liquid-metal servo-actuating subsystem has shown that the variance of the system performance characteristics, in this example the actuator frequency response, is due primarily to tolerances in the effective clearance around the actuator piston rings. Tolerances in pump parameters contribute only 15 to 25 percent of the total variance in system performance. System performance is, however, sensitive to degradations in the tip radius of the pump impeller and in the angle of the blade tip, and these parameters produce up to twice the change in system performance as an equal percentage increase in the piston-ring clearance. Leakage between stages of the centrifugal pump has only a slight influence on the pump and system performance.

Study of the pump and actuator configurations leads to the conclusion that changes in blade-tip radius and angle due to liquid-metal erosion would be very slight. Also, since interstage leakage does not significantly affect frequency response, it could be

expected that wear in the piston rings of the linear actuator would be the most critical wear area in the system (assuming satisfactory performance of the actuator rod seal and bearing over the required life of the system). If this is not the case, the bearing and seal may be the most critical because degradation can lead to a "catastrophic" type of failure.

The results of this study indicate the ability of the Moment method, of variability analysis, in conjunction with mathematical and analog models, to predict the variation that can be expected in the performance of a servo control system and in the individual system components. The reliability observations provide useful design guidance during development stages of new equipment by establishing a basis upon which to reduce or increase manufacturing tolerances on parts affecting various system parameters. Further, study of the normalized partial derivatives indicating the sensitivity of performance to changes in system parameters assists in pinpointing critical wear areas, thus identifying subjects for reliability improvement.

Task III. Redesign of an Electrohydraulic Servo Valve

The first part of the analytical study for the electrohydraulic servo valve employed an analog computer simulation of a two-stage servo valve to obtain partial derivatives of various performance characteristics with respect to valve parameters that are susceptible to degradation. The partial derivatives were calculated and plotted for different values by key design parameters. These plots were evaluated and their interrelationships noted in order to identify design changes that would reduce the over-all sensitivity of the valve to parameter degradation and to the effects of parameter variations introduced in the manufacturing process.

The study showed that the existing design was already close to optimum as far as the critical areas of degradation were concerned, and it was not expected that design changes would bring about significant improvement in the gross reliability of the valve. The critical areas were identified in previous programs as those parts of the spool and bushing that influence the quiescent leakage at null. In the reliability-improvement derivation for quiescent leakage, it was shown that in the statistical sense, i.e., for the averaged histories of a large number of valves, a definite improvement would occur in time to failure with regard to allowable leakage.

The experimental life-testing program carried out on a sample of two modified and two unmodified valves essentially confirmed the above conclusions. Because the spread in initial characteristics of the valves was relatively great, in both the intersample and the intrasample sense, and because of the small sample size, the observed improvement cannot be confirmed on a statistical basis.

The design changes that were ultimately derived did reduce slightly the sensitivity of quiescent leakage to degradation effects, and also reduced the initial value of quiescent leakage and improved the frequency response of the valve. In addition, these modifications reduced significantly the sensitivity of several performance characteristics to degradations in the first-stage orifice and nozzle-flow characteristics.

An interesting unexpected difference between the designs was a noticeable improvement in the wear of the ball on the end of the feedback wire in the new design. It is felt that this improvement would lead to significantly better performance of the "aged" valve in the critical areas very close to null.

Since the existing valve was already at a near optimum design, the reliability improvement anticipated from the design modifications was relatively minor. However, the results of the study are significant because the successful application of the Moment method of variability analysis to the redesign and improvement of an existing control-system component was successful, and both the feasibility of application and the predicted results were confirmed by practice.

REVIEW OF THE MOMENT METHOD ANALYSIS

There are two ways in which a system can fail. The first is caused by drifts in system parameter values occurring over a period of time, which results in overall system performance outside of specification limits. Examples of this type of failure would be changes in transistor characteristics, chemical reaction between a fluid and its container that would be sufficient to change the characteristics of the fluid but not weaken the container, and wear between moving surfaces. The second cause of failure is some radical or catastrophic occurrence, such as a break between a power supply and its load, a rupture in a hydraulic line, or a break in a mechanical linkage. This reliability-prediction technique applies only to the drift type of failure.

A detailed discussion of the technique has been reported in previous reports and papers[1,2,3]*; therefore, only a general description will be given here. The Propagation of Variance formula (Figure 1) states that the variability of a performance characteristic, A_i, represented by its standard deviation σ_{A_i}, depends on the sensitivity of the performance characteristic to parameter changes represented by the partials $(\partial A_i/\partial P_j)_{\bar{P}_j}$, the variability of the parameters P_j represented by σ_{P_j}, and any cross coupling between parameters represented by ρ_{rs}.

Information Necessary to Perform Analysis

In order to perform the necessary computation to obtain the variability of a performance characteristic, a mathematical model of the system must be established so that the partials may be obtained. Data must also be available that give the variability of the parameters. To obtain a reliability estimate, a set of specification limits that defines failure for critical performance characteristics must be known and the shape of the distribution curve for the performance characteristic must be determined. In order to make any prediction on future performance, the variability of each parameter with time must be known.

The partials can be determined analytically from the system model or empirically by programming the model on a digital or analog computer and varying the parameters one at a time to show the resulting changes in the performance characteristic. If the system has any nonlinearities, the use of a computer is practically a necessity. Knowledge of parameter variability might be obtained from component manufacturers, independent tests, or knowledge of the present state of the art of component variability. For computational purposes, the tolerance values on the parameters are considered equivalent to 3 σ_{P_j} for each parameter. The task or mission for a system often provides the specifications for that system.

The shape of the distribution curve is not obtained from the Propagation of Variance formula. However, it is known that, as the number of parameters affecting a performance characteristic increases, the distribution curve for that characteristic approaches a Gaussian or normal distribution. In applying the reliability technique, the distribution curves of the performance characteristics are considered normal.

*References are on page 128.

$$\sigma_{A_i}^2 = \sum_{j=1}^{N} \left(\frac{\partial A_i}{\partial P_j}\right)_{\bar{P}_j}^2 \sigma_{P_j}^2 + 2 \sum_{r=1}^{N-1} \sum_{s=r+1}^{N} \rho_{rs} \sigma_{P_r} \sigma_{P_s} \left(\frac{\partial A_i}{\partial P_r}\right)_{\bar{P}_r} \left(\frac{\partial A_i}{\partial P_s}\right)_{\bar{P}_s}$$

$\sigma_{A_i}^2$ is the variance* of component performance characteristic A_i

N is the number of contributing parameters

$\sigma_{P_j}^2$ is the variance of contributing parameter P_j

$\bar{P}_j$ is the mean value** of parameter P_j

$\left(\frac{\partial A_i}{\partial P_j}\right)_{\bar{P}_j}$ is the first partial derivative of component performance characteristic A_i with respect to parameter P_j evaluated at $\bar{P}_j$

ρ_{rs} is the correlation coefficient that relates parameters P_r and P_s

* σ^2 = Variance is defined as the second moment of a distribution about its mean value.
σ = Standard deviation is defined as the square root of the variance.

** Mean value is defined as the first moment of a distribution about the origin.

FIGURE 1. PROPAGATION OF VARIANCE FORMULA

The variability of each parameter with time and environment is very difficult to obtain in present practice. To determine these values, strong reliance must be placed on previous life tests for components and component parts. On occasion, the time-dependent variability values (or functions) would be generated from knowledge or insight gained from experience in working with a component or a part. When the partial derivatives are known, worst-case operation can be obtained and compared with the performance specifications. (Worst-case operation is system operation at the extreme values of each parameter that maximizes and/or minimizes a performance characteristic, depending on whether the specification limits considered are upper and/or lower bounds.)

Procedure to Obtain Reliability Estimate

When the mean value of the performance characteristic $\bar{A}_i$ has been determined from the mean values of the parameters $\bar{P}_j$ and the variability of the performance characteristic σ_{A_i} has been determined by the Propagation of Variance formula, the following steps will give the reliability estimate:

(1) Assume that the distribution of the performance characteristic is normal. This has the effect of defining the shape of the distribution in terms of known values, i.e., the mean (nominal) value and the variance.

(2) Determine two values n_L and n_U so that n_L = mean value of the performance ($\bar{A}_i$) minus the lower specification limit (SL_L), the difference divided by the standard deviation, σ_{A_i}, which is defined as the square root of the variance $\left(\sigma^2_{A_i}\right)$. Therefore, $n_L = \dfrac{\bar{A}_i - SL_L}{\sigma_{A_i}}$ and

$n_U = \dfrac{SL_U - \bar{A}_i}{\sigma_{A_i}}$ by a similar reasoning for the upper specification limit. If there is either no upper specification limit (SL_U) or no lower specification limit (SL_L), then let n_U or n_L respectively equal infinity.

(3) From a statistical table for the normal distribution, determine the portion of the distribution corresponding to n_L and n_U. The sum of the two is the probability that the performance characteristic values will fall within the tolerance limits. This probability is the reliability estimate.

When the partial derivatives and the variances are normalized, the critical system parameters and the proportion each parameter contributes to the variance of the performance characteristic are easily distinguished. Critical parameters are those to which the system is most sensitive.

Limitation of the Technique

The use of the Propagation of Variance formula to determine reliability presents three possible areas for error that would affect the results obtained by this technique:

(1) The first two moments of a parameter distribution, mean value and variance, used in the Propagation of Variance formula are not sufficient to completely describe a distribution that is not normal. The Propagation of Variance equation can consider higher moments; however, from model and data accuracy consideration, only the first two moments were used. The characteristics of non-normal distribution are not reflected in the Propagation of Variance formula.

(2) The partial derivatives used in the Propagation of Variance formula are considered constant over the tolerance value of the parameter ($\pm 3\sigma_{p_j}$).

In actuality, the partial for any parameter may be a function of the parameter value over the tolerance interval. A plot of the partial over the tolerance interval may give a curved line rather than the straight line signified by the constant partial value. The degree of curvature will affect the results of the technique, since some straight-line approximation must be made to calculate the performance characteristic variance, $\sigma^2_{A_i}$.

(3) Any prediction of future reliability will only be as good as the variation estimates of the parameter values and variances with time and environment.

Complete details of the technique development and procedures are contained in Technical Documentary Report No. ASD-TDR-63-287 (AD 412496), dated January, 1963, and Technical Documentary Report No. FDl-TDR-64-50, dated August, 1964.

TASK I. MOMENTUM-EXCHANGE-TYPE ATTITUDE-CONTROL AND STABILIZATION SUBSYSTEM

Introduction

A previous reliability research effort by Battelle generated an analytical technique called the Moment method for predicting drift-type failures in components and systems.[1, 2, 3] This technique is based on the Propagation of Variance formula, which combines data derived from the system or system model and parameter variability data to formulate an estimate of the probability that the system will perform within specifications at initial or future times of operation. The probability value is interpreted as the reliability estimate.

This report discusses the application of the reliability-prediction technique to a momentum-exchange-type attitude-control and stabilization subsystem for a satellite. Several types of controllers would fit into the momentum-exchange category. This report considers the type called a fluid flywheel. The principle of the fluid flywheel is to accelerate a fluid within a closed loop in the satellite. This action generates a torque about the axis of the loop to which the satellite responds and consequently is repositioned.

Engineering Activity

Description of Fluid-Flywheel System

The fluid flywheel considered in this report is one designed and built by the General Electric Company. General Electric's goal was to prove the feasibility of a fluid flywheel as an attitude-control device. All numerical values for the system parameters, most of the parameter tolerance values, and most of the system equations are presented in the General Electric report on the fluid flywheel.[4] There is effectively one flywheel for each of the three axes of a satellite, all powered from a single electrical-energy source.

Functional Block Diagram and General Discussion. The functional block diagram for one of the three axes of the fluid-flywheel system is shown in Figure 2. The operation of each of the three axes of the flywheel is identical, with the exception of the loading imposed by the inertia of the satellite about each axis.

General Electric tested for cross-coupling between the axes and found that no appreciable amount exists.* Therefore, Battelle's investigation considered the operation about a single axis with no cross-coupling.

The torque to maintain a given attitude under disturbances and to obtain a desired attitude, given a position error indication, is generated by accelerating a fluid in a

*Wells, R., General Electric Company, Johnson City, New York, telephone conversation, December 4, 1964.

closed loop (loops) about the appropriate axis (axes). The action is similar to a servo-motor-driven inertia wheel for attitude control. The torque available for control is proportional to the product of the fluid inertia value and its acceleration.

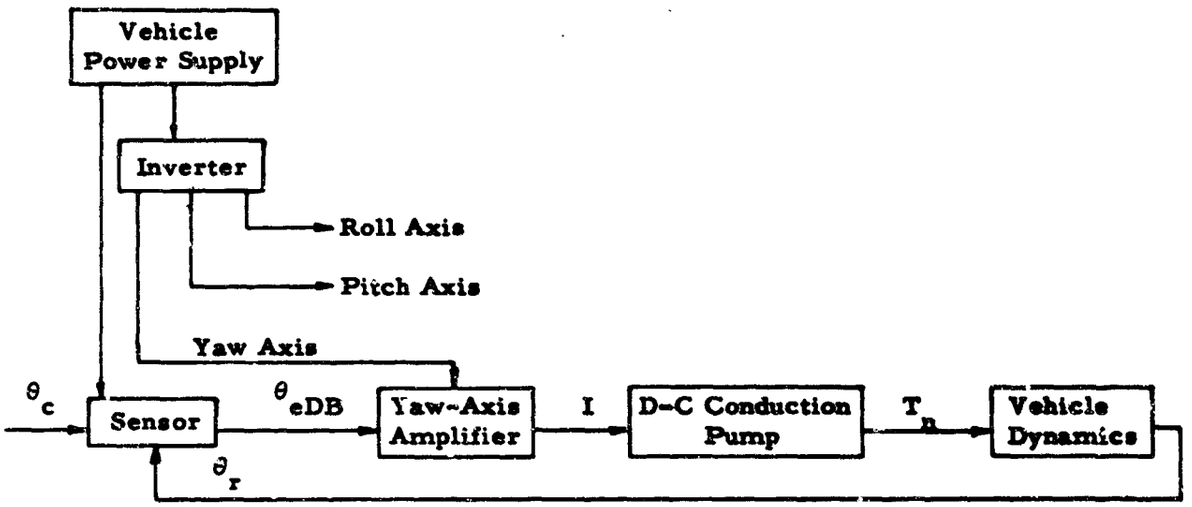

FIGURE 2. FUNCTIONAL BLOCK DIAGRAM OF FLUID-FLYWHEEL ATTITUDE-CONTROL SYSTEM

The heart of the fluid flywheel is the pump, which accelerates the fluid. (In this flywheel the fluid was mercury.) The pump is an electromagnetic d-c conduction pump (E.M. pump), which operates on the same basic principles as an electric d-c motor. For the operation of this type of pump, the fluid must be a liquid metal.

Brief Discussion of Electromagnetic Pump. The electromagnetic pump is not a new device. It has been used since the early 1950's for pumping liquid metals, particularly sodium and NaK (mixture), as coolants of nuclear reactors. Other liquid metals considered as coolants have been bismuth, lithium, and magnesium. The basic construction of the pump is also applicable to metering liquid-metal flow rates. A liquid metal that flows within a constant magnetic field will generate a current proportional to the flow rate. Electromagnetic pumps vary in size from those pumping less than 1 gpm and requiring several amperes to those pumping 30 gpm and requiring several thousand amperes. The development of electromagnetic pumps has received good coverage in the literature.[5, 6, 7, 8, 9, 10, 11, 12, 13]

The pumping of the mercury is achieved by passing an electric current through the mercury under the influence of a magnetic field. The mercury flow path, the current path, and the magnetic field are mutually orthogonal. The interaction of the current and magnetic field applies a force to the mercury, causing the mercury to move. The back electromotive force of the pump and the fluid losses in the loop provide sufficient damping so that no rate feedback or other compensation is required.

System Electronics. The force that accelerates the mercury is proportional to the current flow generated by the error signal from the attitude error sensor. The

error signal is amplified by a voltage-to-current amplifier. The load presented to the amplifier by the mercury is in the milliohm range. Therefore, a prime design goal is to keep the output impedance of the amplifier as small as possible.

The amplifier used was designed by General Electric, and is based on the use of parallel transistors to reduce the output impedance seen by the pump. The amplifier schematic diagram is shown in Figure 3. Detailed discussions of the voltage-to-current amplifier and its development have been recorded previously by General Electric authors. (4, 14, 15)

Efficiency of the fluid-flywheel system is quite low due to the fluid losses in the loop and electrical losses at the amplifier-pump interface. The amplifier gave approximately a 4 to 1 ratio between amplifier output impedance and mercury load resistance. Improved high-current, low-voltage characteristics of new transistors give promise of amplifier output impedance to mercury resistance ratios of 0.4 to 1. *

System Model

A model of the fluid flywheel was reported by Nichol. (4) This model considers the sensor-amplifier combination as an ideal current amplifier with a gain, a small dead band, and a saturation level that limits the current to 60 amperes. In most respects, Nichol's model parallels the models described in previous reports. (5, 9, 13)

A sketch of the electromagnetic d-c conduction pump is shown in Figure 4. The basic equation for system operation is the vector force equation

$$\underline{F} = \underline{i}_p \, w \times \underline{B}$$

for the force exerted on the fluid to accelerate it,
where

i_p is the current in the pumping channel

w is the width of channel

B is the magnetic flux.

With the current path at a right angle to the flux field and using the pound-feet system of units:

$$\underline{F} = \underline{i}_p \, w \times \underline{B} = 6.87 \times 10^{-6} \, Bi_p w \text{ lb}, \qquad (1)$$

with B in gauss.

The pressure developed in the pump is

$$P_t = \frac{F}{wh} = 6.87 \times 10^{-6} \, \frac{Bi_p}{h} \text{ lb/ft}^2 \quad , \qquad (2)$$

and can be written in terms of the voltage generated by the amplifier by considering the circuit shown in Figure 5.

*McComb, R., General Electric Company, Schenectady, New York, Battelle-G.E. conference, October 6, 1964.

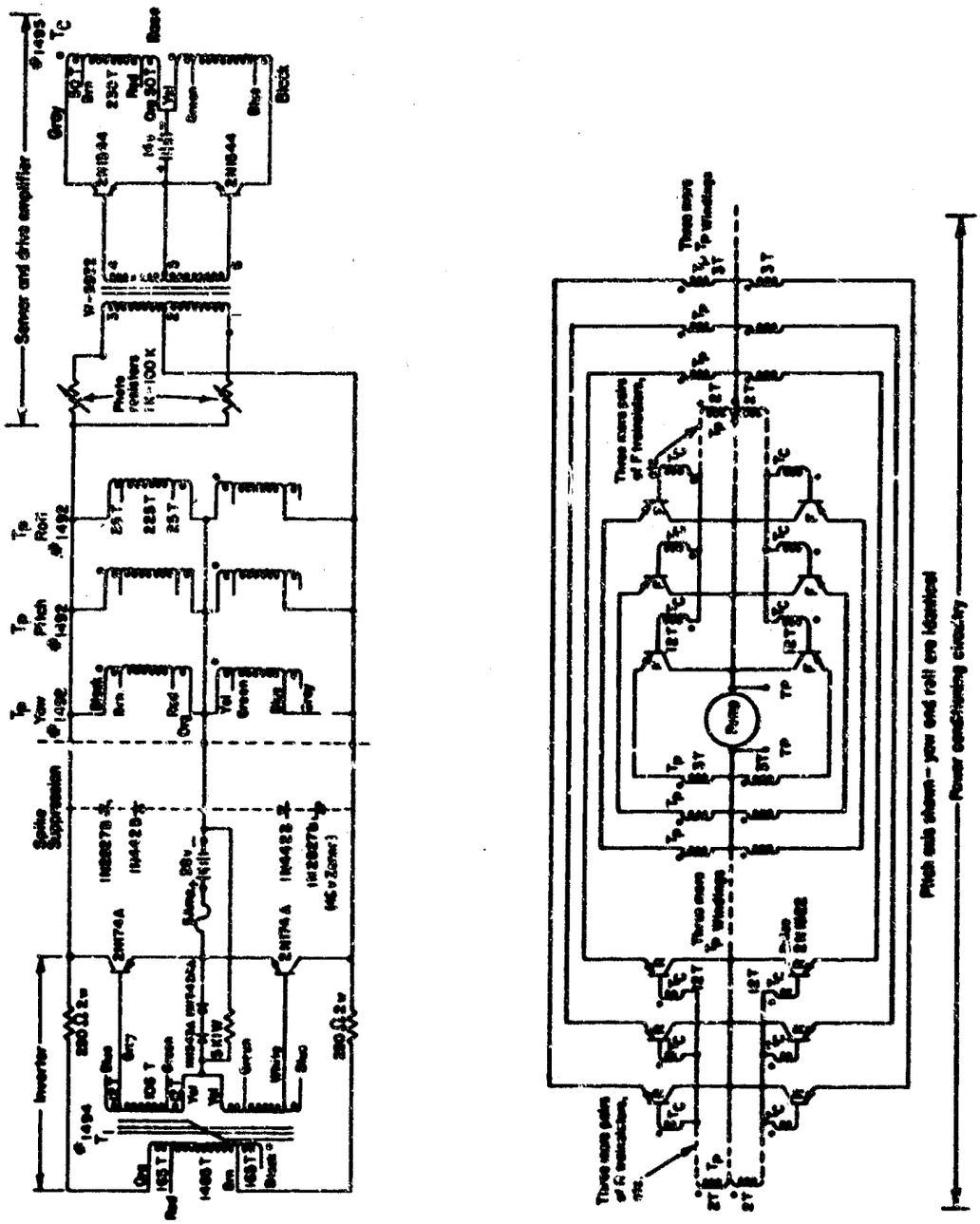

FIGURE 3. SCHEMATIC OF FLUID-FLYWHEEL CONTROL

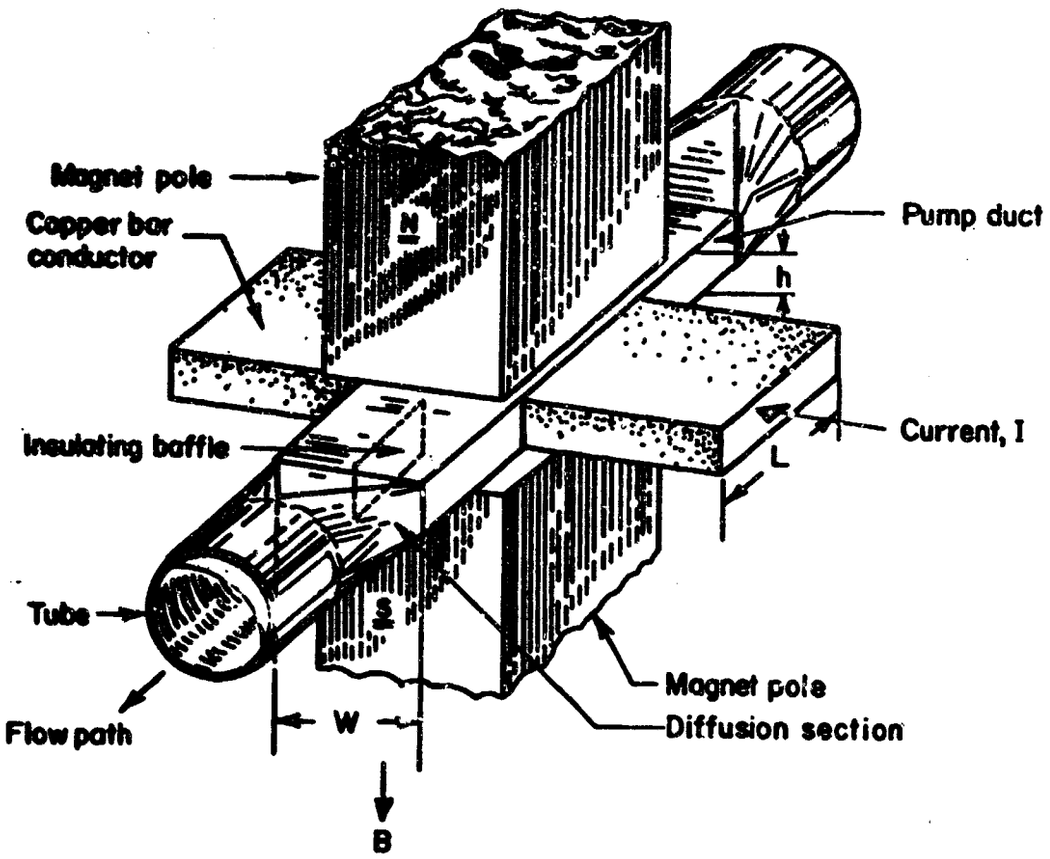

FIGURE 4. D-C CONDUCTION PUMP

FIGURE 5. EQUIVALENT CIRCUIT OF AMPLIFIER-PUMP INTERFACE (BATTELLE)

Figure 5 represents the interface between the amplifier and the pump. From Figure 5 and standard circuit-analysis procedures, it can be shown that

$$i_p = \frac{K_V \theta e_{DB} R_f - E_b (R_a + R_f)}{R_a R_f + R_a R_p + R_p R_f} \tag{3}$$

and

$$P_t = \frac{6.87 \times 10^{-6} B i_p}{h} = \frac{6.87 \times 10^{-6} B}{h} \quad \frac{K_V \theta e_{DB} R_f - E_b (R_a + R_f)}{R_a R_f + R_a R_p + R_p R_f} \quad . \tag{4}$$

An expression for E_b is needed in terms of the system parameters and the fluid angular velocity, ω_f, and is obtained from the vector equation

$$E_b = \text{back emf} = \oint (\underline{V} \times \underline{B}) \cdot d\underline{L} \quad . \tag{5}$$

The fluid velocity, $\underline{V}$, the flux density, $\underline{B}$, and the length, $\underline{L}$, of the current-carrying medium (which in this case is the pump channel width) are mutually orthogonal, and therefore

$$E_b = 9.3 \times 10^{-6} BwV. \tag{6}$$

The fluid velocity through the pump channel can be expressed in terms of the fluid angular velocity in the loop, ω_f, by

$$V = \frac{\pi D_2^2 D_1 \omega_f}{8hw} \quad , \tag{7}$$

giving

$$E_b = \frac{9.3 \times 10^{-6} \pi B D_2^2 D_1 \omega_f}{8h} \tag{8}$$

Nichol defines an overall diffuser ratio, A, as

$$A = \frac{\pi D_2^2}{4hw} \quad .$$

The diffuser ratio should be greater than one to keep the magnetic gap small and to obtain a large magnetic flux with small-sized magnets. Substituting A into Equation (8) gives

$$E_b = \frac{9.3 \times 10^{-6}\ BAw\ D_1 \omega_f}{2} \quad . \tag{9}$$

The expression for i_p is now

$$i_p = \frac{K_V \theta_{e_{DB}} R_f - 4.65 \times 10^{-6}\ BAw D_1 \omega_f (R_a + R_f)}{R_a R_f + R_a R_p + R_p R_f} \quad . \tag{10}$$

Nichol does not consider the amplifier-pump interface to be represented by the circuit in Figure 5 but rather that shown in Figure 6.

FIGURE 6. EQUIVALENT CIRCUIT OF AMPLIFIER-PUMP INTERFACE (NICHOL)

From Figure 5 and standard circuit-analysis procedures, it can be shown that

$$i_p = \frac{K_a \theta_{e_{DB}} R_f - E_b}{R_p + R_f} \quad ,$$

and substituting for E_b,

$$i_p = \frac{K_a \theta_{e_{DB}} R_f - 4.65 \times 10^{-6}\ BAwD_1 \omega_f}{R_p + R_f} \quad . \tag{11}$$

The expressions for i_p give it as a function of the angular error after passing through the sensor dead band, $\theta_{e_{DB}}$, and of the angular velocity, ω_f. However, from Figure 5, $K_V \theta_{e_{DB}}$ represents a voltage source, E_S, and from Figure 6, $K_a \theta_{e_{DB}}$ represents a current source, I_S. The question arises, "Can the interface representation in Figure 5 be substituted for that in Figure 6 without any change in the pressure developed (P_t)?" Nichol gives

$$P_t = \frac{6.87 \times 10^{-6}\ R_f B}{h(R_f + R_p)}\ I - \frac{6.43 \times 10^{-11}\ \pi B^2 D_2^2 D_1}{8h^2(R_f + R_p)}\ \omega_f$$

$$P_t = K_g I - K_b \omega_f \quad , \tag{12}$$

and Battelle gives

$$P_t = \frac{6.87 \times 10^{-6} R_f B}{h(R_a R_f + R_a R_p + R_p R_f)} E_S - \frac{6.43 \times 10^{-11} \pi B^2 D_2^2 D_1 (R_a + R_f)}{8h^2(R_a R_f + R_a R_p + R_p R_f)} \omega_f$$

$$= K_g^* E_S - K_b^* \omega_f . \tag{13}$$

The question arises, "Does $K_g^* E_S - K_b^* \omega_f = K_g I - K_b \omega_f$?"

From Figure 5,

$$E_S = \left[R_a + \frac{R_p R_f}{R_p + R_f} \right] I + \left[\frac{9.3 \times 10^{-6} \pi B D_1 D_2^2 R_f}{8h(R_f + R_p)} \right] \omega_f \tag{14}$$

Substituting the expression for E_S into Equation (13) does give, with some manipulation, Nichol's expression for P_t and the equality holds:

$$K_g^* E_S - K_b^* \omega_f = K_g I - K_b \omega_f . \tag{15}$$

It is necessary to determine the value for K_V shown in Figure 5. Nichol states that the sensor-amplifier combination effectively saturates at an input error of two degrees, since the current I is limited to 60 amperes. For a maximum current of 60 amperes, the fluid velocity at steady state is 1.18 radians/second. From Nichol's characteristic less curves in Figure 7, it can be determined that

$$\omega_f = \frac{H}{J_f} = \frac{1.1 \text{ ft lb sec}}{0.935 \text{ ft lb sec}^2} = 1.18 \text{ radians/second.}$$

Realizing that during transient operation there is a wide range of possible combinations for the input error, source current, and fluid angular velocity, Battelle decided to determine the values of K_V for steady-state operation when the input error, θ_e, was two degrees, I was 60 amperes, and ω_f was 1.18 radians/second. This can be accomplished by using Equation (14), where E_S is equal to $K_V \theta_{e_{DB}}$, and substituting in the known values for $\theta_{e_{DB}}$ and all the terms on the right-hand side of the equation. This gives

$$K_V = 0.355 \text{ volts/degree.}$$

The pressure developed by the pump, P_t, is opposed by the fluid drag in the fluid-flywheel loop. The fluid drag is the sum of three pressure drops, which are expressed as follows:

(1) Pressure drop in the pump $\quad P_p = \dfrac{f \gamma_F L A^2 D_1^2 \omega_f^2}{4g \left(\dfrac{hw}{h + w} \right)}$

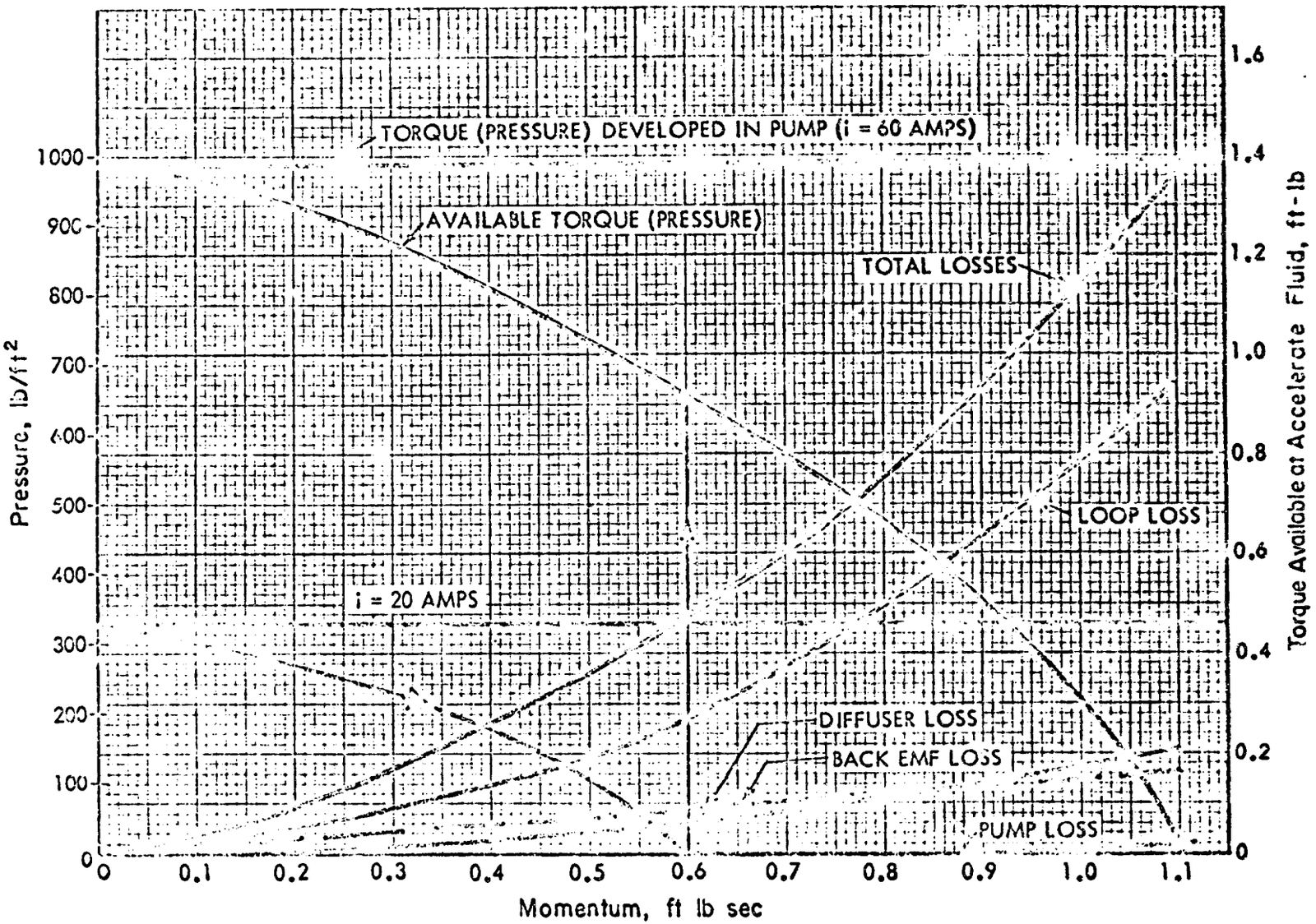

FIGURE 7. FLUID-FLYWHEEL-MODEL PERFORMANCE CURVES

(2) Pressure drop in the diffuser $P_d = \dfrac{(1 - \eta_D)\gamma_F A^2 D_1^2 \omega_f^2}{8g}$

(3) Pressure drop in the loop $P_L = \dfrac{\pi f \gamma_F D_1^3 \omega_f^2}{2gD_2}$.

The expressions for the pressure drops are correct for turbulent flow only. Battelle has checked Nichol's claim that laminar flow considerations are not necessary and found this claim to be valid. In Battelle's analog simulation of the system, provision was made for reading out the Reynolds number as a function of time during a dynamic response test of the flywheel. A plot of the Reynolds number readout is shown in Figure 8 for the system excited by a step function of two degrees. During the response, the Reynolds number was in the range of turbulent flow ($R_e > 2,000$) for the critical portions of the response (large errors), and remained in the laminar flow range for very small values of error toward the end of the response.

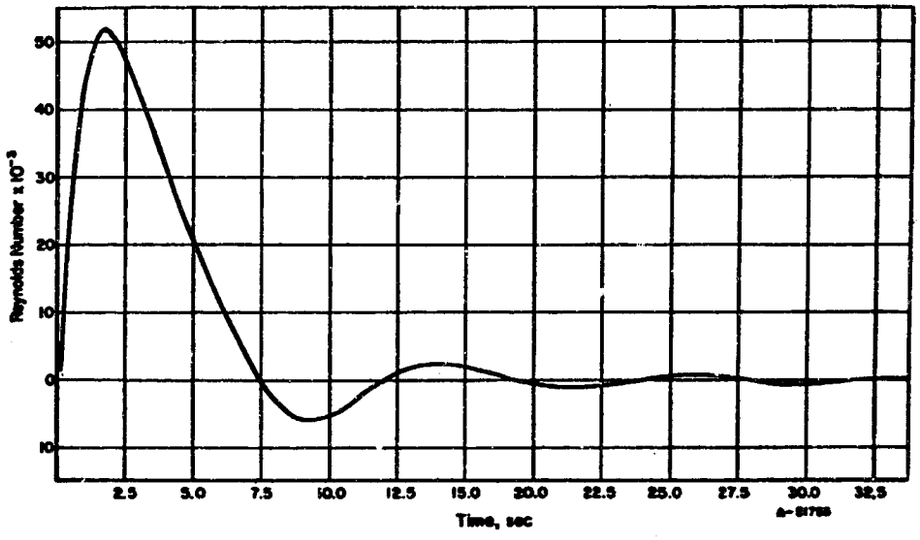

FIGURE 8. REYNOLDS NUMBER VERSUS TIME FOR A SYSTEM INPUT STEP OF TWO DEGREES

The Fanning friction factor, f, is given as

$$f = \frac{f_c}{(R_e)0.16} ,$$

with the friction-factor constant f_c initially equal to 0.031. The f appears in the pump and loop drops. The Reynolds numbers for the pump and loop are given[4] as

$$R_e \text{ (pump)} = \frac{\gamma_F A D_1 hw}{\mu(h + w)} \omega_f \qquad (16)$$

and

$$R_e \text{ (loop)} = \frac{\gamma_F D_1 D_2}{2\mu} \omega_f \quad . \tag{17}$$

Substituting the above values for the Reynolds numbers in the appropriate equations gives the following relationships:

$$P_p = \frac{f_c \gamma_F^{0.84} L(A D_1)^{1.84} (h + w)^{1.16} \mu^{0.16}}{4g(hw)^{1.16}} \omega_f^{1.84} \quad .$$

Defining K_p as

$$K_p \equiv \frac{f_c \gamma_F^{0.84} L(A D_1)^{1.84} (h + w)^{1.16} \mu^{0.16}}{4g(hw)^{1.16}} \quad , \tag{18}$$

$$P_p = K_p \omega^{1.84} \quad . \tag{19}$$

$$P_L = \frac{\pi f_c \gamma_F^{0.84} D_1^{2.84} \mu^{0.16}}{(2)^{1.16} g D_2^{1.16}} \omega_f^{1.84}$$

Defining K_L as

$$K_L \equiv \frac{\pi f_c \gamma_F^{0.84} D_1^{2.84} \mu^{0.16}}{(2)^{1.16} g D_2^{1.16}} \tag{20}$$

$$P_L = K_L \omega_f^{1.84} \tag{21}$$

The maximum theoretical diffuser efficiency, η_D, is given by Nichol to be

$$\eta_D = \frac{(1 - \lambda)}{A^2} + \lambda \quad , \tag{22}$$

where

$$\lambda = \frac{0.88[G(R_e)] (A^2 - C^2) + 2(C - 1)}{A^2 - 1} \quad ,$$

and $G(R_e) = 1$ for $R_e > 10^5$

$G(R_e) = 0.325 \log R_e - 0.625$ for $2 \times 10^3 \leq R_e \leq 10^5$,

and

$C = 1$ for $R_e > 10^5$

$$C = \frac{1}{0.088[\,G(R_e)]} \quad \text{for } 2 \times 10^3 \leq R_e \leq 10^5 .$$

The diffuser efficiency depends upon the transition from the rectangular pump section to the cylindrical tubing. General Electric performed numerous tests to determine the best geometric configuration to maximize η_D.[14]

The expression given by Nichol for η_D shows that η_D should be a function of the Reynolds number and would consequently vary over any dynamic response. From the analog mechanization shown in Figure 13, the variable value of η_D was computed over a dynamic response and inserted in the expression for diffuser pressure drop. The response of the fluid-flywheel system to a step in input position signal when η_D was variable was similar to the response of the system when the constant value for η_D of 65 percent suggested by Nichol was used. Further investigation showed that, for a major portion of the dynamic response, the diffuser efficiency was effectively a constant value, but equivalent to 79.5 percent, not 65 percent. Figure 9 shows a plot of system error in the yaw axis for a step input to the flywheel system, with η_D equal to 65 percent, η_D equal to 79.5 percent, and η_D calculated over the dynamic response. The plot for η_D of 65 percent is distinguishable from the calculated η_D and the η_D of 79.5 percent. The plots for the calculated η_D during a response and the constant η_D of 79.5 percent overlap throughout the response range. As a result, a constant Reynolds number of 39,000, corresponding to a nominal value of η_D of 79.5 percent, was used in this investigation. It was concluded that the system response was relatively insensitive to changes in Reynolds number. For the reliability analysis, the diffuser efficiency value changed for different dynamic responses due to changes in parameter values that appear in the defining equation for diffuser efficiency.

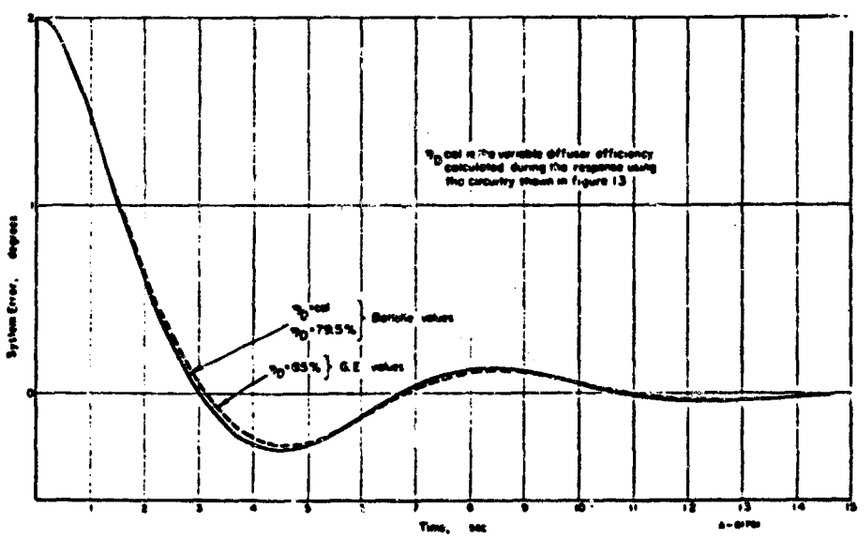

FIGURE 9. COMPARISON OF DIFFUSER EFFICIENCY VALUES, η_D

The change in the nominal η_D value does not change the diffuser pressure-drop expression in its literal form:

$$P_d = \frac{(1 - \eta_D)\gamma_F A^2 D_1^2}{8g} \omega_f^2 = K_d \omega_f^2 . \quad (23)$$

The net pressure to accelerate the mercury at any time is

$$P_n = P_t - P_p - P_d - P_L$$

$$P_n = K_g^* E_S - K_b^* \omega_f - (K_p + K_L) \omega_f^{1.84} - K_d \omega_f^2 , \quad (24)$$

where K_p and K_L are as defined in Equations (18) and (20).

The pressure, P_n, develops a torque with the relationship

$$T_n = P_n \text{ (cross-sectional area) (moment arm)}$$

$$= P_n \left[\pi \left(\frac{D_2}{2}\right)^2\right] \left(\frac{D_1}{2}\right)$$

$$= \frac{\pi D_2^2 D_1}{8} P_n$$

$$T_n = \frac{\pi D_2^2 D_1}{8} (K_g^* E_S - K_b^* \omega_f - (K_p + K_L) \omega_f^{1.84} - K_d \omega_f^2) \quad (25)$$

$$T_n = K_g' E_S - K_b' \omega_f - (K_p' + K_L') \omega_f^{1.84} - K_d' \omega_f^2 \quad (26)$$

The last two terms in the expression for T_n may cause some confusion since, in a dynamic run, the mercury flow can change direction indicating a positive and negative value for ω_f. To account for this possibility, the expression for the torque should be rewritten as

$$T_n = K_g' E_S - K_b' \omega_f - (K_p' + K_L') |\omega_f|^{1.84} \text{ sgn } \omega_f - K_d' |\omega_f|^2 \text{ sgn } \omega_f . \quad (27)$$

$$T_n = T_g - T_b - (T_p + T_L) - T_d .$$

The torque accelerates the mercury and the satellite about the axis of the mercury loop. The loading effects of the mercury and the satellite on the system are their respective inertias. Figure 10 shows the closed-loop block diagram of the system model used.

Nichol considers a torque-momentum expression (as shown in Figure 6), rather than the torque-angular velocity expression used here. The expressions are equivalent in that momentum, H, is

$$H = J_f \omega_f , \quad (28)$$

the product of the mercury inertia and its angular velocity, and H/J_f is substituted for ω_f in the torque expression.

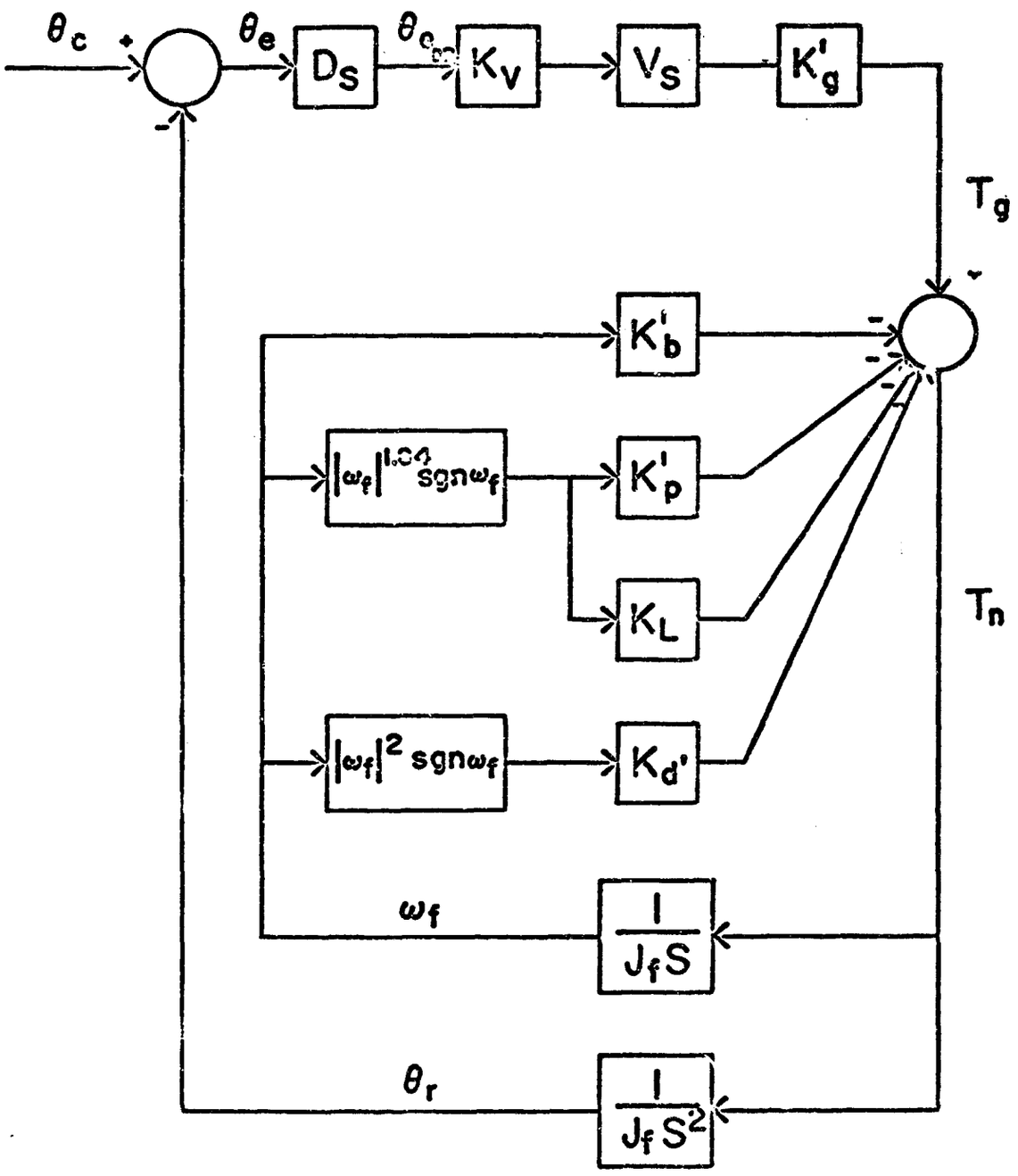

FIGURE 10. BLOCK DIAGRAM OF FLUID-FLYWHEEL MODEL

Battelle performed dynamic runs using the model in Figure 10 for comparison with the actual system responses reported by Nichol. Figure 11a shows the closed-loop responses of the three system axes as reported by Nichol, and Figure 11b gives the model responses as obtained by Battelle. In all three cases, the agreement between the curves is excellent.

The numerical parameter values used in the model simulation are:

$\gamma_F = 850$ (lb)/ft^2

$\mu = 1.045 \times 10^{-3}$ lb/ft sec

$B = 18,800$ gauss

$D_1 = 4$ feet

$D_2 = 3 \times 10^{-2}$ ft

$h = 6 \times 10^{-3}$ ft

$w = 4 \times 10^{-2}$ ft

$L = 2.08 \times 10^{-2}$ ft

$R_S = 10^{-2}$ ohms

$R_C = 2 \times 10^{-5}$ ohms

$R_p/R_f = 3 \times 10^{-1}$

$(R_p+R_f) = 6.33 \times 10^{-3}$ ohms

$\eta_D = 79.5$ percent

$g = 32.2$ ft/sec^2

$J_\cdot = 9.35 \times 10^{-1}$ ft/lb/sec^2

$J_V = 53.0$ ft/lb/sec^2

$D_S = 10^{-2}$ degrees

$V_S = 7.04 \times 10^{-1}$ volts

$K_V = 3.55 \times 10^{-1}$ volts/degree.

The flywheel-system model was mechanized on the analog computer as shown in Figure 12. The computer circuitry for calculating diffuser efficiency is shown in Figure 13. Figure 14 shows the computer mechanization for generation and readout of power efficiency, which is discussed in the following sections on performance criteria and results.

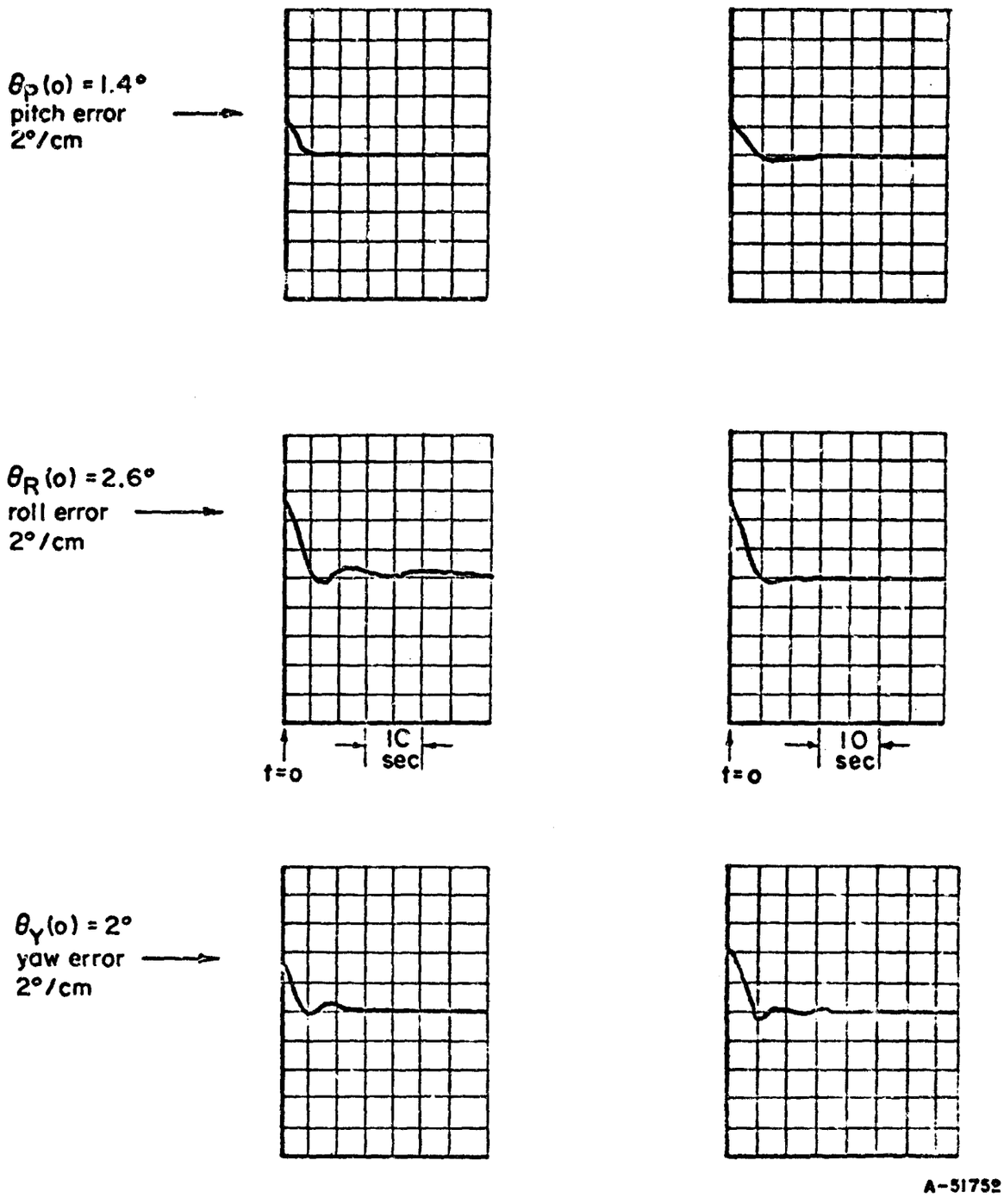

a. Nichol's Response Curves

b. Battelle's Response Curves

FIGURE 11. SYSTEM RESPONSE CURVES FOR STEP INPUTS

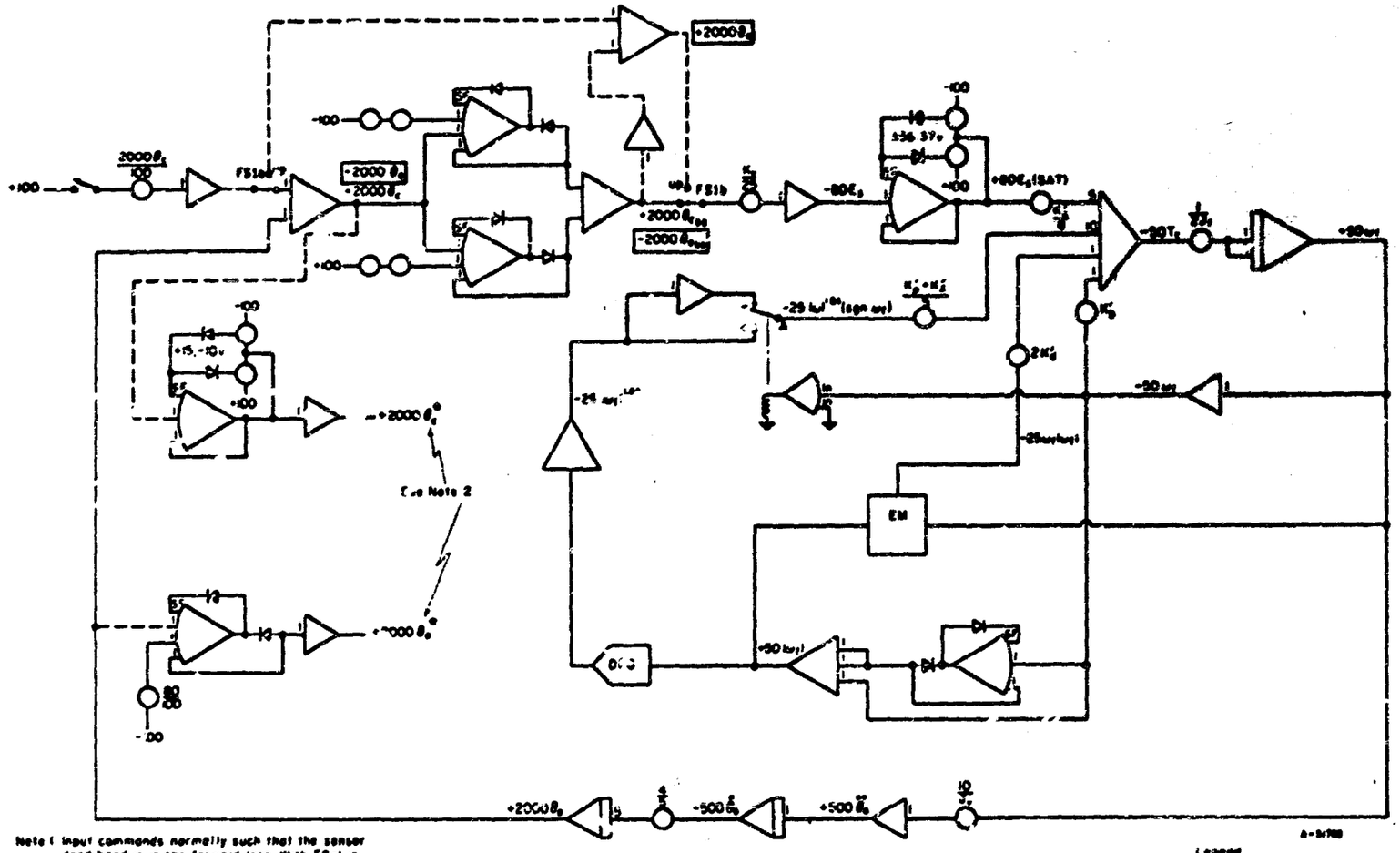

Note 1 Input commands normally such that the sensor dead band is in the forward loop. With FS-1 in the up position, the dead band is in the feedback loop and the enclosed terms ▭ apply.

Note 2 θ_c^* and θ_o^* are used as readouts only and were devised to allow for expanded recordings of portions of θ_c and θ_o.

Note 3 Voltage scaled, real time

Legend
EM-Electronic multiplier
DFG-Diode function generator
SP-input signal to feedback connection

FIGURE 12. MECHANIZATION OF FLUID FLYWHEEL

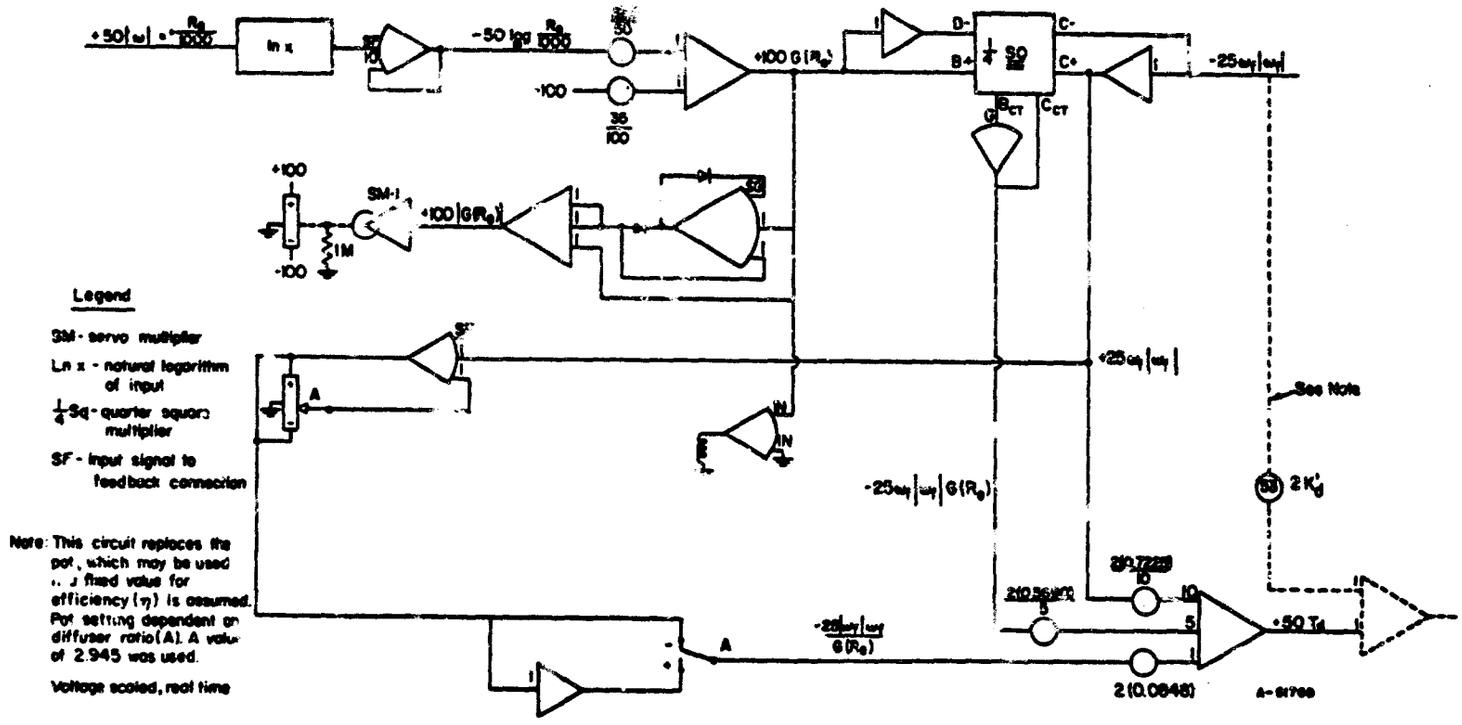

FIGURE 13. MECHANIZATION FOR VARIABLE DIFFUSER EFFICIENCY (η_D)

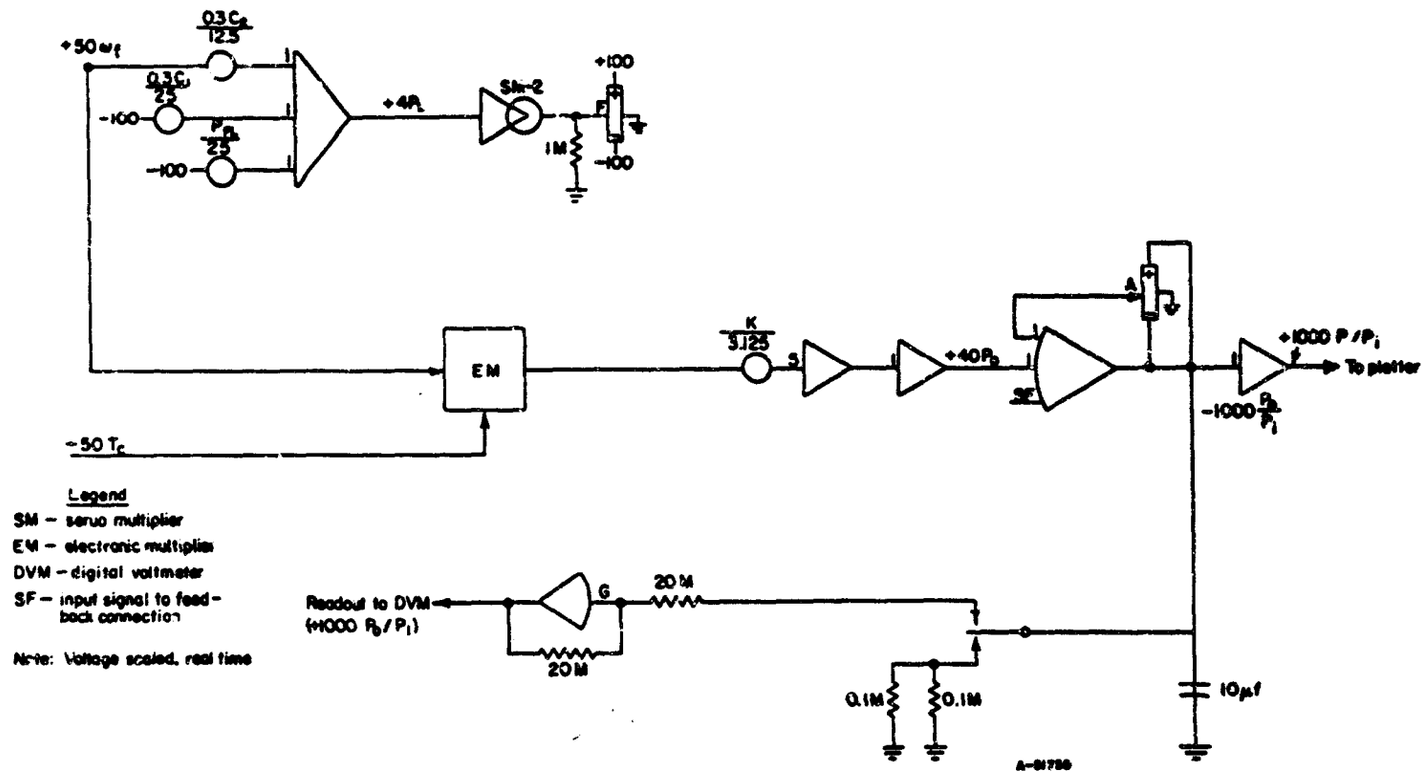

FIGURE 14. MECHANIZATION FOR GENERATION AND READOUT OF POWER EFFICIENCY

Performance Criteria

Other than the ability to operate in a space environment, no specifications were imposed and no mission was given for the fluid flywheel. General Electric did operate the flywheel system in the temperature range of -19 to 90 F and noticed no change in the system-response characteristics. General Electric's temperature range of operation does not signify the meeting of any specification, but it does indicate what temperature variations could be accepted easily.

The lack of specifications makes the choice of performance criteria somewhat arbitrary. However, in light of the previous comments on damping and efficiency, the following two performance criteria were chosen:

(1) Settling time for an input step in position. This criterion is for a closed-loop response and provides a measure of the damping of the system.

(2) Open-loop peak efficiency. This criterion presents an efficiency measure similar to that used to evaluate a servomotor.

Settling Time. Settling time is defined arbitrarily as the amount of time it takes the satellite position to settle to within five times the nominal dead-band value when excited by an input step in an angular position of 2.5 degrees. The 2.5-degree input is large enough to force the system into saturation, and small enough not to bury the intended parameter variations in a saturated response. Battelle considered only one axis of the General Electric flywheel, namely the yaw axis, with moment-of-inertia of 53 foot pound seconds^2. The dead band of the sensor was 0.01 degree; this determined the settling time to be the time required to decrease to and stay within the error bounds of ±0.05 degree.

Open-Loop Peak Efficiency. General Electric considered efficiency as a performance criterion of the system and mentioned that an efficiency of 4 to 5 percent should be expected when efficiency was defined as

$$\text{Efficiency} = \frac{\text{power out (mechanical)}}{\text{power in (electrical)}} .$$

Discussions with General Electric disclosed that no standard exists with which to reference the characteristics of a fluid flywheel. General Electric further pointed out that, while the definition given for efficiency is good, one must be careful in talking about flywheel efficiency. It is important to know exactly how the power terms are obtained, and what the ground rules are, in any discussion of efficiency.

General Electric obtained their efficiency values by a method used for determining the efficiency of servomotor-driven flywheels (disks). The procedure for obtaining efficiency was to excite the flywheel, at rest and under open-loop conditions, with a signal sufficient to obtain maximum momentum. When the momentum reached one-third of its maximum value, the power-in and power-out measurements were made. The ratio of these two values was determined, giving the efficiency value. In performing the

measurements necessary to obtain efficiency, no standard load was used, which permits a possible variation in efficiency for a particular flywheel with different loads.

Efficiency and momentum curves are nonlinear, and the one-third maximum momentum as the reference value for the efficiency measurement is somewhat arbitrary. Battelle decided on an approach for determining efficiency using the General Electric definition, but eliminating a particular momentum value as a measurement reference. Battelle also decided to use open-loop peak efficiency as a performance criterion. Open-loop peak efficiency is obtained in precisely the same manner as that for a servomotor. It is the maximum value of the power-out to power-in ratio from the standard speed-torque characteristic curves, independent of the fraction of maximum momentum at which it occurs.

Battelle obtained its power-out term directly from the analog simulation by taking the product of the mercury angular velocity and the developed torque, and multiplying by the conversion factor 1.356 to obtain the power-out in watts:

$$\text{Power out} = P_O = 1.356\ T_n\ \omega_f \text{ watts.} \qquad (29)$$

The power-in term cannot be obtained directly from the analog simulation. The problem arises from the fact that the electronic amplifier was simulated as a Thevenin equivalent circuit. A Thevenin circuit is sufficient for giving voltage-transfer relationships, but a power value obtained from the product of the Thevenin circuit voltage and its current output does not give, in general, the power of the device being represented by the Thevenin circuit. Briefly stated, calculations involving the load on an equivalent circuit (Thevenin and Norton) are valid, but calculations concerning the source are not.

Battelle's investigation of the flywheel electronics shown in Figure 3 disclosed that the correct operation of the electronic amplifier was not as a variable-voltage source proportional to angular error with a fixed source impedance, but rather as a fixed-voltage source with a source impedance that varied as a function of the angular error. The equivalent circuit describing the operation of the electronic amplifier as simulated on the analog computer is shown in Figure 15.

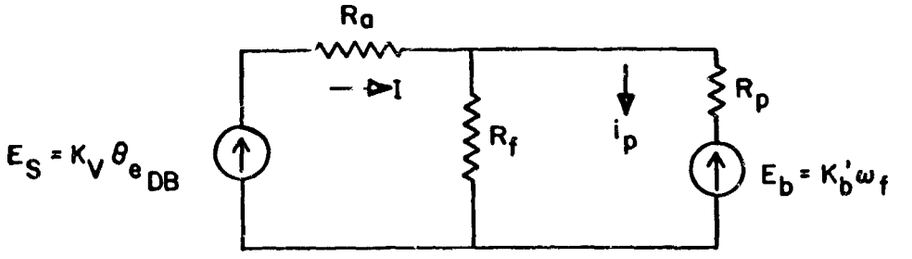

FIGURE 15. EQUIVALENT CIRCUIT OF AMPLIFIER-PUMP INTERFACE SIMULATED ON THE ANALOG COMPUTER

However, Battelle's investigation showed that the equivalent circuit describing the operation of the electronic amplifier is actually as shown in Figure 16.

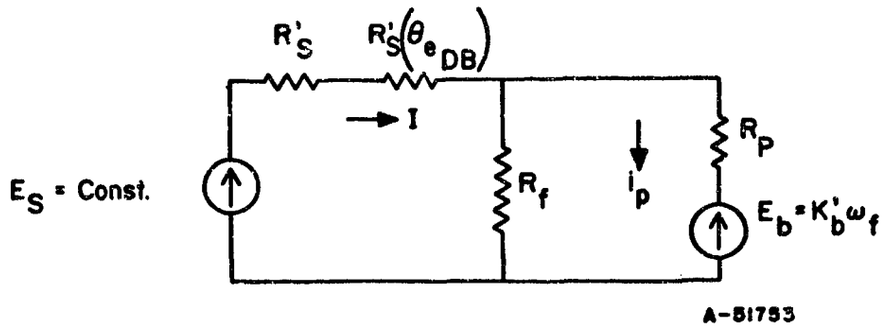

FIGURE 16. RESULTANT EQUIVALENT CIRCUIT OF AMPLIFIER-PUMP INTERFACE FROM BATTELLE'S INVESTIGATION OF THE ELECTRONICS

The analytic expression for $R_S(\theta_{e_{DB}})$ is not obtainable from the electronic circuitry shown in Figure 3, and to Battelle's knowledge, it has not been determined empirically. Battelle performed a brief investigation into possible functions $R_S(\theta_{e_{DB}})$ which would relate Figures 15 and 16 to obtain identical outputs for corresponding inputs. It was concluded that $R_S(\theta_{e_{DB}})$ was a nonlinear function of $\theta_{e_{DB}}$ and would have to be determined empirically.

A reasonable question at this point is "If the simulation of the electronic amplifier is not for the actual operation of the electronic amplifier, can values of power-in truly be obtained"? The answer is yes, and the contribution to power-in from the electronic amplifier is obtained as the product of the fixed-voltage source (E_S = 0.3 volt) and the source current to the pump (I):

$$\text{Power in} = P_L = 0.3\,I$$

This product does represent the amplifier power-in contribution to the system due to the fact that current from the fixed-voltage source is the current to the pump. (No other current flow paths exist for the current from the fixed-voltage source.)

As shown in Figures 15 and 16, the source current will be the sum of the currents through the fringing resistance (R_f) and the pump channel. The pump channel has a resistance (R_p) and an internal voltage generator, which is a function of the fluid angular velocity. By appropriate manipulation of terms for a specific set of parameters and a specific input, the expression for I reduces to

$$I = C_1 - C_2\omega_f \ ,$$

where

$$C_1 = \frac{K_V (R_p + R_f)\theta_e}{R_p R_e + R_p R_f + R_f R_e}$$

and

$$C_2 = \frac{4.56 \times 10^{-6} ABD_1 R_f W}{R_p R_e + R_p R_f + R_f R_e}$$

A constant value, $P_{FL} = 0.6$ watt was added to the product of $E_S I$ to represent the power losses in the electronic inverter and power supplies, shown in Figure 2, to give the total system power input. The inverter and power-supply losses were obtained from a G. E. report.[14]

One change was necessary in the system model for obtaining peak efficiency. This was the elimination of the saturation limiter. The excitation signal was a two-degree position step, which would normally saturate the system and bury the effects of the parameter variations. The two-degree input was considered necessary to obtain a peak efficiency value at near-maximum driving conditions for comparison with G. E.'s estimated value of 4 to 5 percent. A two-degree input also is analogous to obtaining a servomotor characteristic curve at rated operating voltage.

Degradation Factors. General Electric has done a substantial amount of developing and testing on the pump and flywheel. However, their emphasis was not on obtaining degradation factors and degradation rates, but rather on selection of materials, design of the pump, fabrication of parts, reduction of weight, and optimization of certain parameters.[15, 16] In lieu of anticipated data from General Electric, Battelle investigated the system to try to obtain degradation factors for the system parameters. A considerable amount of time was expended in this effort, the result of which was a suggested test plan for determining the degradation factors and their time rates. The necessity for writing a test plan points to the lack of information available regarding degradation factors for this type of system.

Battelle's Experimental Physics Division was contacted to investigate possible drift-type failures in the pump and tubing section, and to make suggestions for possible degradation factors and their time rates. The investigation showed that a strong possibility existed for an increase in the friction-factor constant over time due to chemical reaction between the mercury and pump and tubing and due to mass transfer between dissimilar materials because of temperature differences around the flow loop. Past experience of the Experimental Physics Division has shown that this phenomenon takes place in all systems of this type, with rates of reactions depending on the particular liquid metal and its container material. It was stated that a noticeable, but not large, amount of material would go into solution and the process would probably take several years. The reaction takes place at a more rapid rate initially and drops off as the process of solid dissolving into the liquid tends toward an equilibrium state.

It has been noted that the rate of change of this process is exponential in nature, indicating that the functional expression for the friction factor "constant" is of the form

$$f_c = a - be^{-\alpha t} \quad , \tag{30}$$

where a is the friction factor constant at equilibrium and a-b is the initial value of the friction factor constant. Nichol[4] gives the initial value as

$$a - be^{-\alpha t} = a - b = 0.031, \text{ at } t = 0 \quad .$$

The values of a and α would have to be determined experimentally. For this work, a and α were chosen in the following manner. Nichol states that the friction factor constant is a function of the wetting of the stainless steel tubing by the mercury. If water were in the tubing rather than mercury, the friction factor would be 0.040. General Electric realized that mercury would not wet stainless steel as water would, and experimentally determined the initial friction-factor constant as 0.031. Battelle decided to choose the final value of the friction-factor constant to be equivalent to that of water:

$$a = 0.040.$$

Battelle chose 5 years as the time for attaining equilibrium. A reasonable expression for the friction-factor "constant" as a function of time, and the one used in this report is

$$f_c = 0.040 - 0.009\, e^{(-t/1.25)}, \qquad (31)$$

where t is in years. The Fanning friction factor used in the flow-loss equation now becomes

$$f = \frac{f_c}{(R_e)^{0.16}} = \frac{0.040 - 0.009\, e^{(-t/1.25)}}{(R_e)^{0.16}}$$

The tolerance value on f_c was assumed to be ± 5 percent and was assumed to remain fixed over time.

Delco Radio Division of General Motors Corporation, Kokomo, Indiana, was contacted to supply and discuss information pertaining to possible degradation factors in the transistors that were used in the electronic amplifier. The transistors were Delco Type 7276361 TO-36. From conversations with Delco and from the base-current characteristic curve at a constant collector current of 5 amperes versus time, the transistor gain (h_{f_e}), and consequently the system voltage "constant", K_V, was determined to vary with time. From the above-mentioned curve, it was noted that the gain decreased linearly with time, but at two different rates. Initially, the gain decreased at a constant rate until about 500 hours had elapsed and then decreased at a lower constant rate for the rest of the time. The functional expression for K_V as a function of time is

$$K_V = K_{V_0} - K_1 t \quad \text{first 500 hours}$$

$$K_V = (K_{V_0} - 500\, K_1) - K_2 t \quad \text{after first 500 hours,}$$

where t is in hours and

$$K_{V_0} = 0.355 \frac{\text{volts}}{\text{degree}} \qquad K_1 = \frac{6.39 \times 10^{-5} \text{ volts}}{\text{degree-hour}} \qquad K_2 = \frac{1.13 \times 10^{-6} \text{ volts}}{\text{degree-hour}}$$

It was also noted that the tolerance value of K_V varied over time in a similar fashion as K_V with the following functional expression:

$$\sigma K_V = \sigma_{K_{V_0}} + \sigma_{K_1} t \quad \text{first 500 hours}$$

$$\sigma_{K_V} = (\sigma_{K_{V_0}} + \sigma_{K_1} 500) + \sigma_{K_2} t \quad \text{after first 500 hours,}$$

where t is in hours and

$$\sigma_{K_{V_0}} = 6.67\% \quad \sigma_{K_1} = \frac{1.69 \times 10^{-3}\%}{\text{hour}} \qquad \sigma_{K_2} = \frac{1.67 \times 10^{-4}\%}{\text{hour}} .$$

This report assumes that only the friction-factor constant, the amplifier gain, and the amplifier-gain tolerance values vary over time.

Results

The partial derivatives of the two performance characteristics, settling time and open-loop peak efficiency, were obtained from analog computer data. The analog data were generated by varying each parameter in predetermined increments from its nominal value with all other parameters at their nominal values, and exciting the system with fixed inputs. Each analog run gave one point of a "performance characteristic variation" versus "change of parameter" plot. Several runs gave points through which a curve could be drawn. The slope of this curve was considered the partial derivative of the performance characteristic with respect to the parameter considered.

Settling Time. The time for the system to settle to within 0.05 degree at system lifetime t = 0 for an input step excitation of 2.5 degrees was 13.25 seconds. System output and error curves versus time are shown in Figure 17. The characteristic loss curves for the flywheel are shown in Figure 18. Figure 18 differs from Nichol's plot in Figure 7 in the values of diffuser and back emf losses. This inconsistency is due to Battelle's changing the model of the system by increasing the diffuser efficiency and replacing the current source by a voltage source. The system changes did not cause any noticeable change in system response, which can be noted from Figure 11. Table I lists the parameters, their tolerances, partials, and variances, and gives the evaluation of the variance equation and a breakdown of the variance in percent. The results of the evaluation of the variance equation shows that the tolerance value on the settling-time characteristic is $\pm 3\sigma_{t_s}$, which is equal to ±1.08 seconds. The settling time can be expressed as

$$t_{S_0} = 13.25 \pm 1.08 \text{ seconds}$$

at the time vehicle operation initially starts. As can be seen from the normalized partial derivatives $\frac{\partial t_s}{\partial P_j} \overline{P}_j$ in Table I, the parameters to which the system settling time is most sensitive are tubing diameter, D_2, magnetic-flux density, B, pump channel height, h, amplifier output impedance, R_S, and the amplifier gain, K_V. The parameter

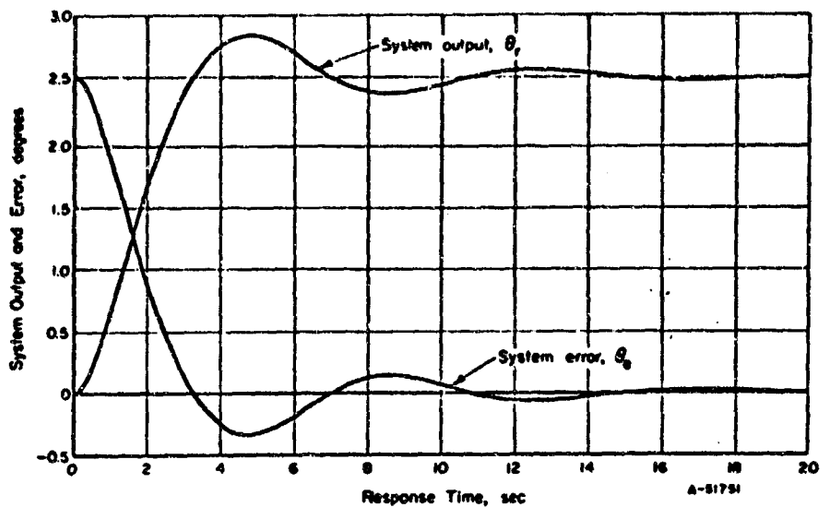

FIGURE 17. SYSTEM OUTPUT AND ERROR VERSUS TIME, SYSTEM LIFETIME 0

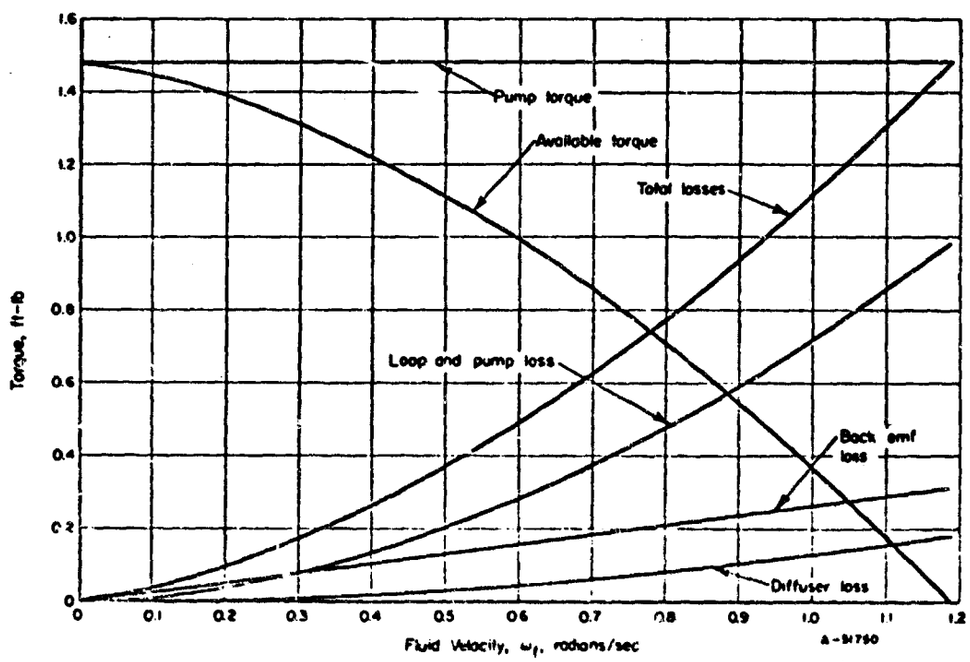

FIGURE 18. CHARACTERISTIC LOSS CURVES, SYSTEM LIFETIME 0

TABLE I. FOR SYSTEM LIFETIME OF 0, THE PARAMETER PARTIAL DERIVATIVES AND VARIANCES FOR THE PERFORMANCE CHARACTERISTIC OF SETTLING TIME

Evaluation of the Settling Time Variance, $\sigma_{t_s}^2$, and a Breakdown of σ_{t_s} in the Percent Contribution From Each Parameter

Parameter P_j	Symbol	Parameter Value and Tolerance	$\frac{\partial t_s}{\partial P_j}$	$\frac{\partial t_s}{\partial P_j} \overline{P}_j$	σ_{P_j}	$\sigma_{P_j}^2$	$\sigma_{P_j}^2 / \overline{P}_j^2$	$\left(\frac{\partial t_s}{\partial P_j}\right)^2 \sigma_{P_j}^2$	Breakdown of σ_{t_s}, %
Sensor dead band	D_s	$1 \times 10^{-2} \pm 3 \times 10^{-4}$	$+6.67 \times 10$	+0.667	1×10^{-4}	1×10^{-8}	1×10^{-4}	4.45×10^{-3}	0.03430
Amplifier gain	K_V	$3.55 \times 10^{-1} \pm 7.1 \times 10^{-2}$	-1.24×10	-4.40	2.365×10^{-2}	5.6×10^{-4}	4.46×10^{-3}	8.61×10^{-2}	66.42
Magnetic-flux density	B	$1.78 \times 10^4 \pm 5.64 \times 10^2$	-5.02×10^{-6}	-9.44	1.88×10^2	3.54×10^4	1×10^{-4}	8.96×10^{-3}	6.923
Loop diameter	D_1	$4 \pm 8 \times 10^{-2}$	-7.29×10^{-1}	-2.92	2.67×10^{-2}	7.13×10^{-4}	4.46×10^{-5}	3.78×10^{-4}	0.2914
Tubing diameter	D_2	$3 \times 10^{-2} \pm 8.33 \times 10^{-5}$	-3.81×10^2	-11.43	2.775×10^{-5}	7.71×10^{-10}	8.58×10^{-7}	1.18×10^{-4}	0.08635
Pump channel height	h	$6 \times 10^{-3} \pm 9 \times 10^{-5}$	$+1.095 \times 10^3$	+6.58	3×10^{-5}	9×10^{-10}	2.5×10^{-5}	1.079×10^{-3}	0.8319
Pump channel width	w	$4 \times 10^{-2} \pm 6 \times 10^{-4}$	$+3.85 \times 10$	+1.538	2×10^{-4}	4×10^{-8}	2.5×10^{-5}	8.99×10^{-5}	0.06567
Electrode length	L	$2.08 \times 10^{-2} \pm 3.12 \times 10^{-4}$	-8.07×10	-1.677	1.04×10^{-4}	1.08×10^{-8}	2.5×10^{-5}	7.03×10^{-5}	0.0542
Amplifier output impedance	R_g	$1 \times 10^{-2} \pm 1 \times 10^{-3}$	$+5.43 \times 10^2$	+5.43	3.33×10^{-4}	1.11×10^{-7}	1.11×10^{-3}	3.28×10^{-2}	25.29
Friction factor constant	f_c	$3.1 \times 10^{-2} \pm 1.55 \times 10^{-3}$	-8.6	-0.267	5.17×10^{-4}	2.67×10^{-7}	2.78×10^{-4}	1.97×10^{-5}	0.01156
Voltage saturation level	V_s	$7.04 \times 10^{-1} \pm 3.52 \times 10^{-2}$	-1.015	-0.715	1.173×10^{-2}	1.38×10^{-4}	2.78×10^{-4}	1.42×10^{-4}	0.01094
								$\sigma_{t_s}^2 = 1297 \times 10^{-4}$	
								$\sigma_{t_s} = 0.360$	

values with the larger tolerance values are amplifier gain, K_V, amplifier output impedance, R_S, friction factor constant, f_c, and voltage saturation level, V_S. The breakdown of the variance of settling time shows that the amplifier gain, K_V, amplifier output impedance, R_S, and magnetic-flux density, B, are the parameters that have the strongest effect on the settling-time tolerance value. These results show that decisions concerning the important parameters must take into account both sensitivity (partial derivatives) and tolerance values.

A worst-case analysis actually showed that the settling time would be shortened to 7.5 seconds if the parameter values were at their extremes; a case that would supposedly lengthen the settling time. This apparent discrepancy is considered later in the report.

For an arbitrary upper-limit settling time of 14.5 seconds (and no lower limit), the reliability estimate is computed by means of the Moment method as follows:

$$n_L = \frac{13.25 - (-\infty)}{0.360} = \infty \qquad n_U = \frac{14.50 - 13.25}{0.360} = \frac{1.25}{0.360} = 3.47$$

$$\text{Percent } P_{n_L = \infty} = 50 \qquad \text{Percent } P_{n_U = 3.47} = 49.99$$

Total = 99.99 percent.

The probability of a flywheel having a settling time of less than 14.5 seconds is 0.9999. The reliability estimate is the probability value, 0.9999.

At system lifetime t = 500 hours, the settling time was 13.85 seconds. System output and error curves versus time are shown in Figure 19. Figure 20 gives the characteristic loss curves for the flywheel system. Table II gives the same information as Table I but considers a system lifetime of 500 hours. The tolerance value on the settling-time characteristic is ±1.02 seconds. The settling time can be expressed as

$$t_{S_{500\ \text{hours}}} = 13.85 \pm 1.02 \text{ seconds.}$$

Tubing diameter, D_2, and magnetic-flux density, B, are the two most important parameters affecting the sensitivity of settling time and are of equal consequence. The other important parameters affecting the sensitivity of settling time to parameter shifts are the pump channel height, h, and the friction factor constant, f_c. The breakdown of the variance of settling time shows that the parameters having the greatest effect on the tolerance value for settling time are amplifier gain, K_V, magnetic flux density, B, amplifier output impedance, R_S, and the friction factor constant, f_c. The rearrangement in the parameters affecting the sensitivity of settling time and the change in the breakdown of settling-time variance point to the fact that the partial derivatives are not constant over the variation of the parameters.

A worst-case analysis showed that the settling time would be 8.7 seconds. The reliability estimate is as shown on page 40.

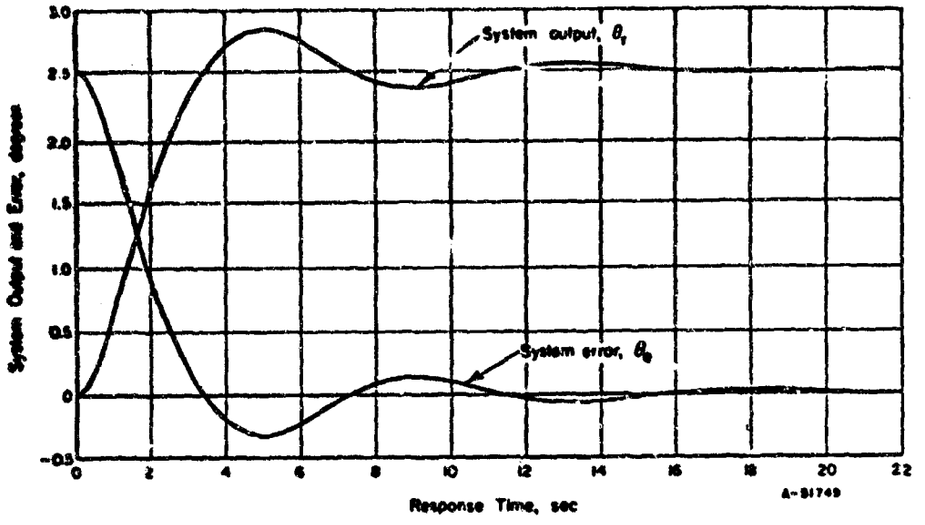

FIGURE 19. SYSTEM OUTPUT AND ERROR VERSUS TIME, SYSTEM LIFETIME 500 HOURS

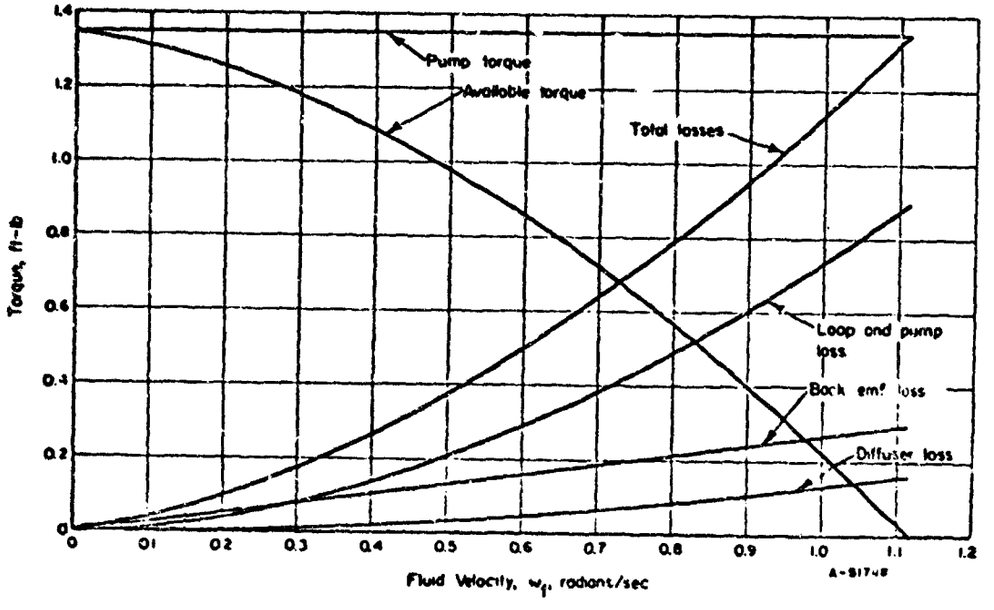

FIGURE 20. CHARACTERISTIC LOSS CURVES, SYSTEM LIFETIME 500 HOURS

TABLE II. FOR SYSTEM LIFETIME OF 500 HOURS, THE PARAMETER PARTIAL DERIVATIVES AND VARIANCES FOR THE PERFORMANCE CHARACTERISTIC OF SETTLING TIME

Evaluation of the Settling-Time Variance, $\sigma_{t_S}^2$, and a Breakdown of σ_{t_S} in the Percent Contribution From Each Parameter

Parameter P_j	Symbol	Parameter Value and Tolerance	$\frac{\partial t_S}{\partial P_j}$	$\frac{\partial t_S}{\partial P_j} \overline{P}_j$	σ_{P_j}	$\sigma_{P_j}^2$	$\sigma_{P_j}^2 / \overline{P}_j^2$	$\left(\frac{\partial t_S}{\partial P_j}\right)^2 \sigma_{P_j}^2$	Breakdown of σ_{t_S}, %
Sensor dead band	D_S	$1 \times 10^{-2} \pm 3 \times 10^{-4}$	$+6.16 \times 10$	+0.616	1×10^{-4}	1×10^{-8}	1×10^{-4}	3.8×10^{-5}	0.03295
Amplifier gain	K_V	$3.23 \times 10^{-1} \pm 7.26 \times 10^{-2}$	-1.19×10	-3.84	2.42×10^{-2}	5.88×10^{-4}	5.62×10^{-3}	8.33×10^{-2}	72.24
Magnetic flux density	B	$1.88 \times 10^{4} \pm 5.64 \times 10^{2}$	-5.97×10^{-4}	-11.22	1.88×10^{2}	3.54×10^{4}	1×10^{-4}	1.26×10^{-2}	10.92
Loop diameter	D_1	$4 \pm 8 \times 10^{-2}$	-1	-4	2.67×10^{-2}	7.13×10^{-4}	4.46×10^{-5}	7.13×10^{-4}	0.6183
Tubing diameter	D_2	$3 \times 10^{-2} \pm 8.33 \times 10^{-5}$	-3.73×10^{2}	-11.2	2.775×10^{-5}	7.71×10^{-10}	8.58×10^{-7}	1.072×10^{-4}	0.09297
Pump channel height	h	$6 \times 10^{-3} \pm 9 \times 10^{-5}$	$+9.53 \times 10^{2}$	+5.72	3×10^{-5}	9×10^{-10}	2.5×10^{-5}	8.17×10^{-4}	0.7085
Pump channel width	w	$4 \times 10^{-2} \pm 6 \times 10^{-4}$	$+5.56 \times 10$	+2.22	2×10^{-4}	4×10^{-8}	2.5×10^{-5}	1.24×10^{-4}	0.1075
Electrode length	L	$2.08 \times 10^{-2} \pm 3.12 \times 10^{-4}$	-1.97×10^{2}	-4.09	1.04×10^{-4}	1.08×10^{-8}	2.5×10^{-5}	4.19×10^{-4}	0.3633
Amplifier output impedance	R_S	$1 \times 10^{-2} \pm 1 \times 10^{-3}$	$+2.30 \times 10^{2}$	+2.60	3.35×10^{-4}	1.11×10^{-7}	1.11×10^{-3}	8.70×10^{-3}	7.545
Friction factor constant	f_c	$3.14 \times 10^{-2} \pm 1.55 \times 10^{-3}$	-1.64×10^{2}	-5.17	5.23×10^{-4}	2.74×10^{-7}	2.78×10^{-4}	7.36×10^{-3}	6.388
Voltage saturation level	V_S	$7.04 \times 10^{-1} \pm 3.52 \times 10^{-2}$	-2.843	-2.00	1.173×10^{-2}	1.38×10^{-4}	2.78×10^{-4}	1.12×10^{-3}	0.9713
								$\sigma_{t_S}^2 = 115 \times 10^{-3}$	
								$\sigma_{t_S} = 0.340$	

$$n_L = \frac{13.85 - (-\infty)}{0.340} = \infty \qquad n_U = \frac{14.5 - 13.85}{0.340} = \frac{0.65}{0.34} = 1.91.$$

Percent $P_{n_{L=\infty}} = 50$ Percent $P_{n_{U=1.91}} = 47.19$

Total = 97.19 percent

The reliability estimate is 0.9719.

At system lifetime t = 5 years, the settling time was 11.75 seconds. System output and error curves versus time are shown in Figure 21. The characteristic loss curves for the flywheel system are shown in Figure 22. Table III gives the same information as Tables I and II but considers system lifetime of 5 years. The tolerance value on the settling-time characteristic is 2.56 seconds. The settling time can be expressed as

$$t_{S_{5\ \text{years}}} = 11.75 \pm 2.56 \text{ seconds.}$$

The parameters to which the settling time is most sensitive are tubing diameter, D_2, loop diameter, D_1, magnetic-flux density, B, amplifier gain, K_V, and pump channel height, h, and amplifier output impedance, R_S, of equal consideration. The variance of settling-time breakdown shows that amplifier gain, K_V, and amplifier output impedance, R_S, have the greatest effect on the variance.

A worst-case analysis showed that the settling time would be 15.9 seconds. The reliability estimate is as follows:

$$n_L = \frac{11.75 - (-\infty)}{0.854} = \infty \qquad n_U = \frac{14.5 - 11.75}{0.854} = \frac{2.75}{0.854} = 3.22$$

Percent $P_{n_{L=\infty}} = 50$ Percent $P_{n_{L=3.22}} = 49.99$

Total = 99.99 percent

The reliability estimate is 0.9999.

An obvious difference between the results of 5-year operation and both the initial starting operation and 500-hour operation is that the nominal settling time at 5 years has decreased. The decrease is quite large, being greater than the settling-time tolerance values for both system lifetimes of t = 0 and t = 500 hours. The three settling-time expressions are repeated here:

$$t_{S_{0\ \text{hours}}} = 13.25 \pm 1\ 08 \text{ seconds} \qquad t_{S_{5\ \text{years}}} = 11.75 \pm 2.56 \text{ seconds.}$$

$$t_{S_{500\ \text{hours}}} = 13.85 \pm 1.02 \text{ seconds}$$

The distribution curves for each of the three settling times are shown in Figure 23.

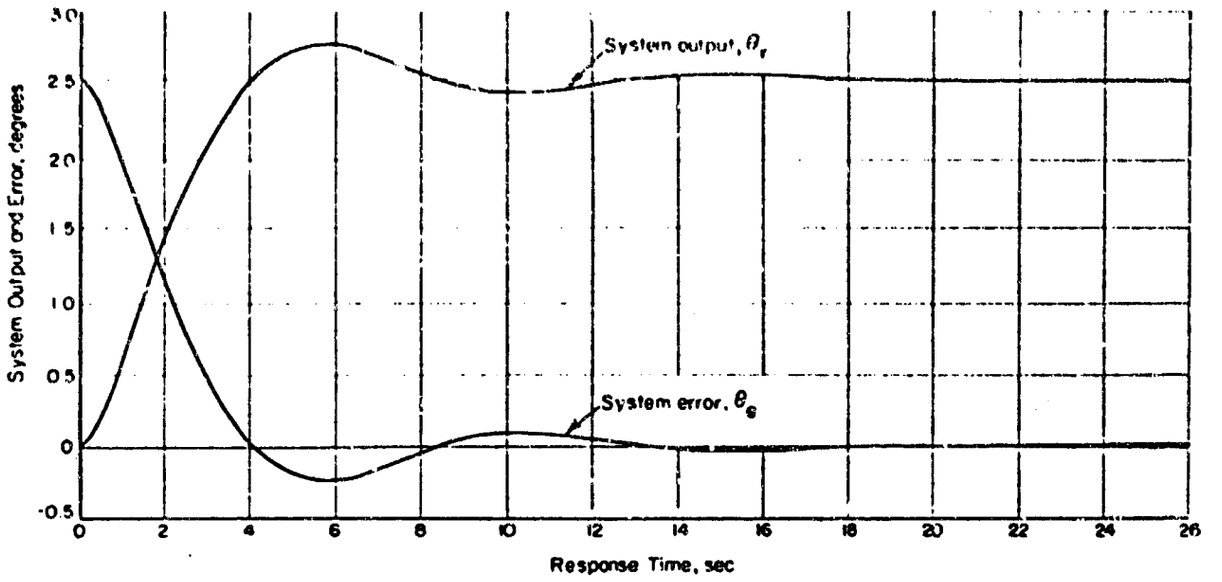

FIGURE 21. SYSTEM OUTPUT AND ERROR VERSUS TIME, SYSTEM LIFETIME 5 YEARS

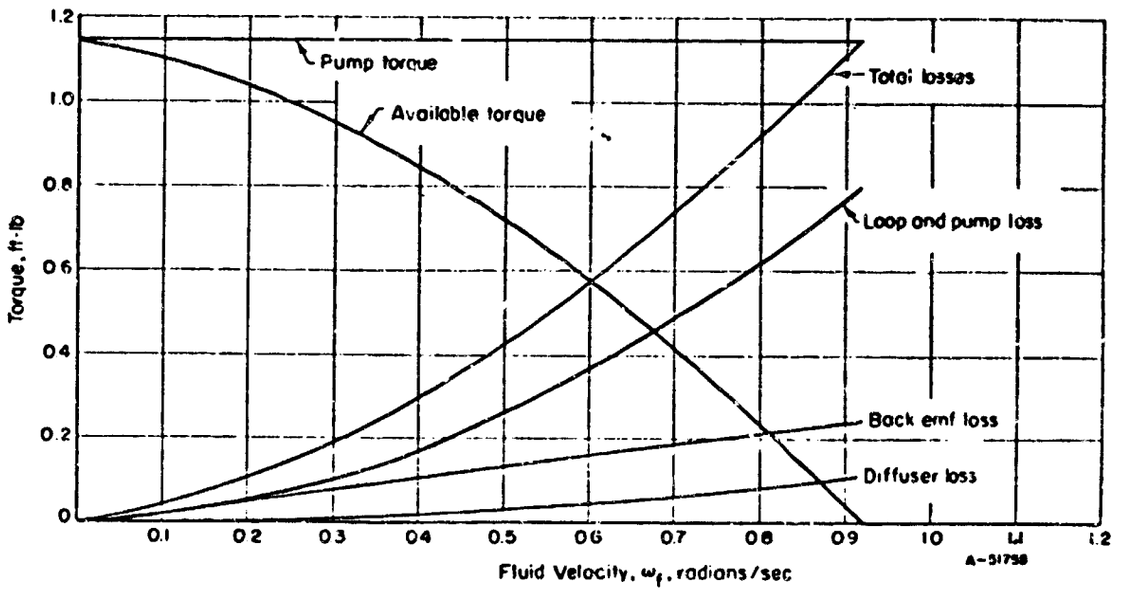

FIGURE 22. CHARACTERISTIC LOSS CURVES, SYSTEM LIFETIME 5 YEARS

TABLE III. FOR SYSTEM LIFETIME OF 5 YEARS, THE PARAMETER PARTIAL DERIVATIVES AND VARIANCES FOR THE PERFORMANCE CHARACTERISTIC OF SETTLING TIME

Evaluation of the Settling-Time Variance, $\sigma_{t_S}^2$, and a Breakdown of σ_{t_S} in the Percent Contribution From Each Parameter

Parameter P_j	Symbol	Parameter Value and Tolerance	$\frac{\partial t_S}{\partial P_j}$	$\frac{\partial t_S}{\partial P_j} \overline{P}_j$	σ_{P_j}	$\sigma_{P_j}^2$	$\sigma_{P_j}^2 \Big/ \overline{P}_j^2$	$\left(\frac{\partial t_S}{\partial P_j}\right)^2 \sigma_{P_j}^2$	Breakdown of σ_{t_S}, %
Sensor dead band	D_S	$1 \times 10^{-2} \pm 3 \times 10^{-4}$	$+7.7 \times 10$	+0.77	1×10^{-4}	1×10^{-8}	1×0^{-4}	5.93×10^{-5}	0.00813
Amplifier gain	K_V	$2.735 \times 10^{-1} \pm 1.173 \times 10^{-1}$	-2.12×10	-5.80	3.92×10^{-2}	1.535×10^{-3}	2.06×10^{-2}	6.91×10^{-1}	94.72
Magnetic-flux density	B	$1.88 \times 10^4 \pm 5.64 \times 10^2$	-3.19×10^{-4}	-6.00	1.88×10^2	3.54×10^4	1×10^{-4}	3.61×10^{-3}	0.4948
Loop diameter	D_1	$4.0 \pm 8 \times 10^{-2}$	-1.8	-7.20	2.67×10^{-2}	7.13×10^{-4}	4.46×10^{-5}	2.305×10^{-3}	0.3159
Tubing diameter	D_2	$3 \times 10^{-2} \pm 8.3 \times 10^{-5}$	-3.2×10^2	-9.61	2.775×10^{-5}	7.71×10^{-10}	8.58×10^{-7}	7.90×10^{-5}	0.01082
Pump channel height	h	$6 \times 10^{-3} \pm 9 \times 10^{-5}$	$+8.88 \times 10^2$	+5.33	3×10^{-5}	9×10^{-10}	2.5×10^{-5}	7.10×10^{-4}	0.09732
Pump channel width	w	$4 \times 10^{-2} \pm 6 \times 10^{-4}$	+6.25	+0.25	2×10^{-4}	4×10^{-8}	2.5×10^{-5}	1.563×10^{-6}	0.0002138
Electrode length	L	$2.08 \times 10^{-2} \pm 3.12 \times 10^{-4}$	-4.37×10	-0.91	1.04×10^{-4}	1.08×10^{-8}	2.5×10^{-5}	2.07×10^{-5}	0.002837
Amplifier output impedance	R_S	$1 \times 10^{-2} \pm 1 \times 10^{-3}$	$+5.33 \times 10^2$	+5.33	3.33×10^{-4}	1.11×10^{-7}	1.11×10^{-3}	3.15×10^{-2}	4.318
Friction factor constant	f_c	$3.984 \times 10^{-2} \pm 1.55 \times 10^{-3}$	$+2.065 \times 10$	+0.823	5.64×10^{-4}	4.41×10^{-7}	2.78×10^{-4}	1.885×10^{-4}	0.02581
Voltage saturation level	V_S	$7.04 \times 10^{-1} \pm 3.52 \times 10^{-2}$	-3.55×10^{-1}	-0.25	1.173×10^{-2}	1.38×10^{-4}	3.78×10^{-4}	1.74×10^{-5}	0.002385
								$\sigma_{t_S}^2 = 729 \times 10^{-3}$	
								$\sigma_{t_S} = 0.854$	

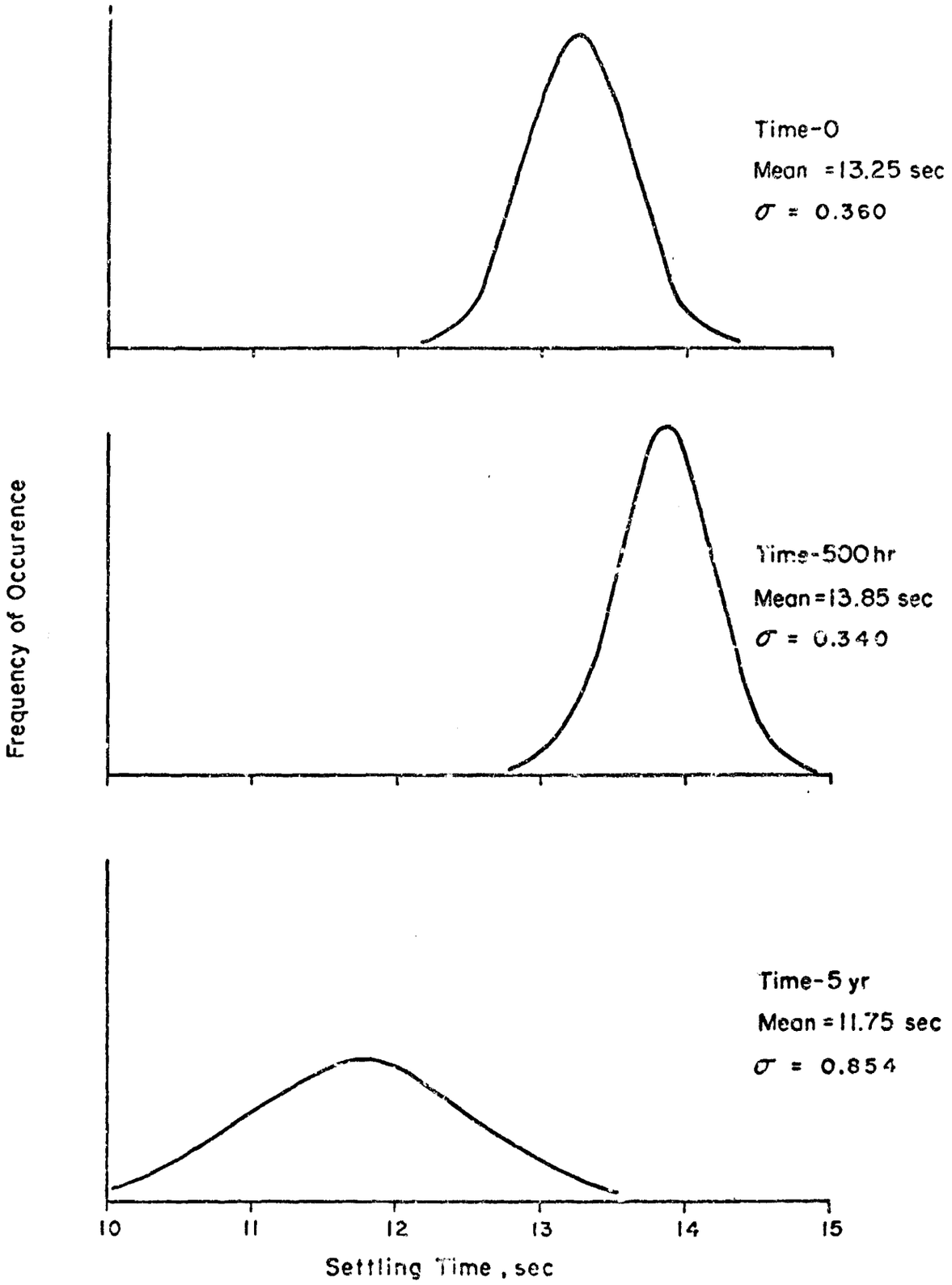

FIGURE 23. SETTLING-TIME FREQUENCY DISTRIBUTIONS

The large decrease in the nominal settling-time value for a system lifetime of 5 years can be explained by the fact that the performance-characteristic settling time is not a continuous function of the system parameters. The physical explanation of this result can be given by considering the effect of decreasing the system gain (K_V) and increasing system damping (f_c) in any underdamped closed-loop system and considering the general definition of settling time.

A general definition of settling time is the time it takes for the error of a system excited by a step input to settle within a given magnitude. The acceptable error magnitude used for defining settling time effectively defines two boundaries about the zero-error axis. The time at which the error enters the region between boundaries and remains in that region thereafter is the settling time. If a system is underdamped, the system error will oscillate about zero error and possibly enter, leave, and re-enter the region between the two boundaries several times before settling between the boundaries.

As the system gain is decreased and the system damping is increased, the magnitude of the oscillation about the zero-error axis is decreased. Each cycle of oscillation about zero-error axis will approach zero error from a positive-error value on one-half the cycle and from a negative-error value on the other half of the cycle. As the gain is decreased and damping is increased, the magnitude of the half-cycle peak is decreased until they are enclosed by the boundaries defining settling time. As the half cycle on which settling time occurs is enclosed by a boundary due to decreasing gain and increasing damping, the settling-time point "jumps" to the preceding half cycle, causing the discontinuity in settling time. The situation described here would occur if only one of the two causes, decreasing gain or increasing damping, took place.

Figure 24 demonstrates the discontinuity in the settling-time characteristic by plotting the distribution curves and the line of nominal settling-time variation versus time. It can be seen from Figure 24 that only one "jump" occurs in the time period being considered, and that it occurs at approximately a system lifetime of 1/2 year. If the time period were extended, more "jumps" would occur, signifying other half-cycle peaks had been enclosed in defining settling-time boundaries.

The results of using settling time as a measure of performance demonstrates what one can expect from a performance characteristic that is a discontinuous function of the system parameters. A discontinuity in the nominal value of a performance characteristic as a function of time may or may not be a serious problem in determining whether to use the performance characteristic as a measure of drift-type failure. For the case of the fluid flywheel, the "jump" in the settling-time value was not an unfavorable occurrence since the jump in settling time was away from the specification limit and was faborable to operation. Had the jump increased settling time, or had there been a lower limit on settling time, then the jump would present a problem. Knowledge of a jump in an important system performance characteristic is useful information for design regardless of whether the jump is favorable.

The worst-case analyses for the first two system lifetimes considered were much better than the actual settling times obtained with the nominal parameter values. The worst-case results are considered much better than their nominal value counterparts since the worst-case settling times are much lower than the nominal settling times. This contradictory result is due to a discontinuous relationship between the settling-time characteristic of the system and the system parameters. This result could have

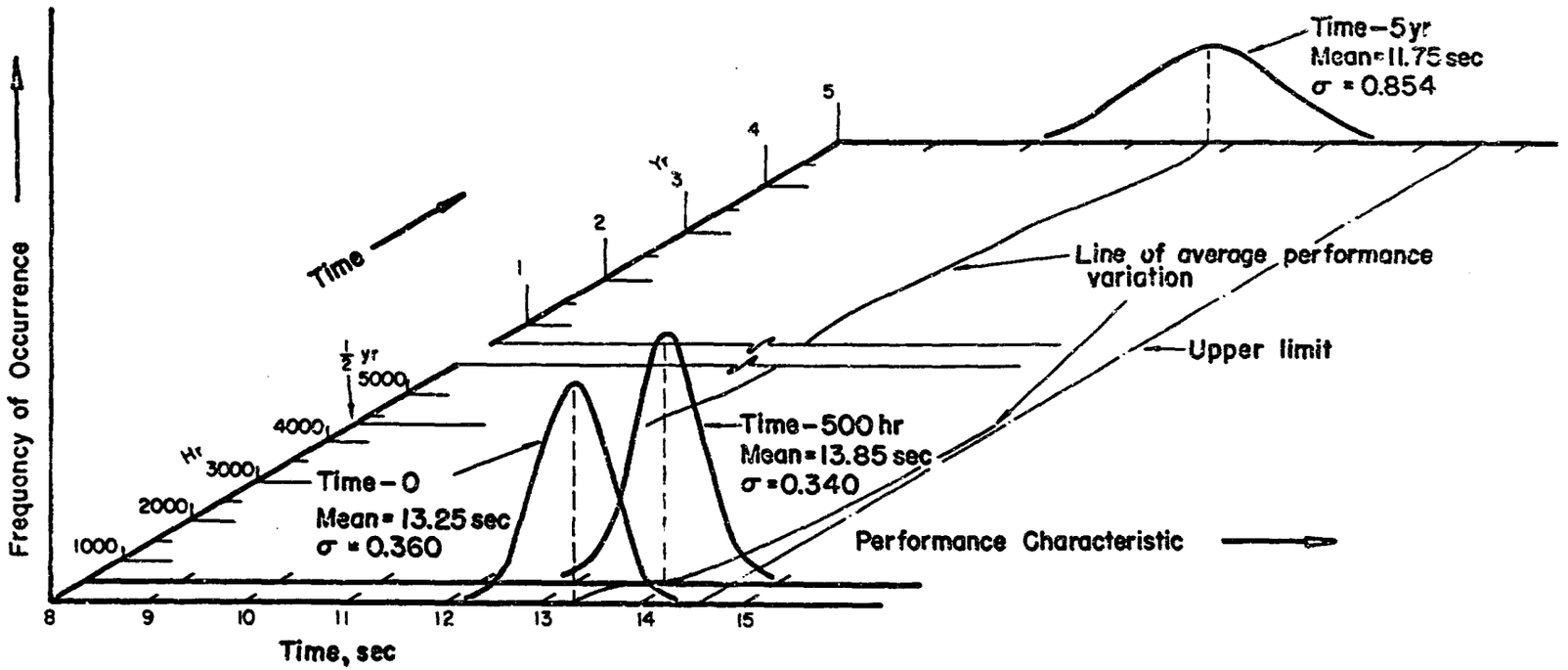

FIGURE 24. SETTLING-TIME FREQUENCY DISTRIBUTIONS, TIME RELATIONSHIPS

been surmised from the data in Tables I through III by noting that the partial derivative of settling time with respect to amplifier gain, K_V, is negative in sign. The negative slope indicates that, for worst-case considerations, the K_V should be decreased. The question can now be asked, "Why did the settling time decrease if the partial has a negative slope and the K_V was decreased?"

The question is answered by the curve shown in Figure 25, which is a plot of settling time versus the parameter, K_V. The plot is general in that no numerical values appear for either settling time or amplifier gain. Figure 25 applies to any underdamped system when the system gain is changed. It can be seen from the plot that, other than when a jump in the curve occurs, the slope is negative. The overriding factor in settling time as a function of system gain is the discontinuity and not the partial derivative. The condition of discontinuities (jumps) in the plot does not continue as the gain is continually reduced. The system eventually becomes overdamped, and further reduction in gain will always increase the settling time.

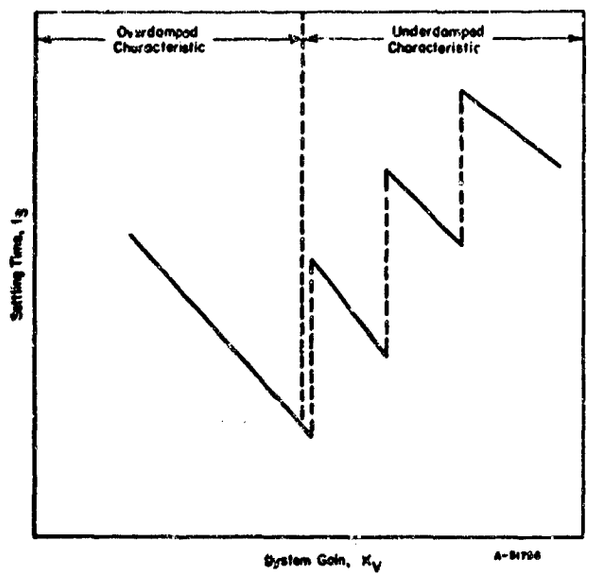

FIGURE 25. PLOT OF SETTLING TIME VERSUS SYSTEM GAIN

Peak Efficiency. At system lifetime t = 0, the open-loop peak-efficiency nominal value was 4.37 percent. The characteristic curves for the flywheel are shown in Figure 26. Table IV gives the same information as Table I but considers open-loop peak efficiency rather than settling time. The tolerance value on the peak-efficiency characteristic is $\pm 3\sigma_E = \pm 0.576$ percent. The peak efficiency can be expressed as

$$E_O = 4.27 \pm 0.576 \text{ percent.}$$

The most important parameters affecting peak-efficiency sensitivity are tubing diameter, D_2, magnetic-flux density, B, and pump channel height, h; of equal consequence are amplifier gain, K_V, and amplifier output impedance. The breakdown in percent of peak efficiency variance shows that amplifier gain, K_V, amplifier output impedance, R_S, and magnetic-flux density, B, have the greatest effect on variance.

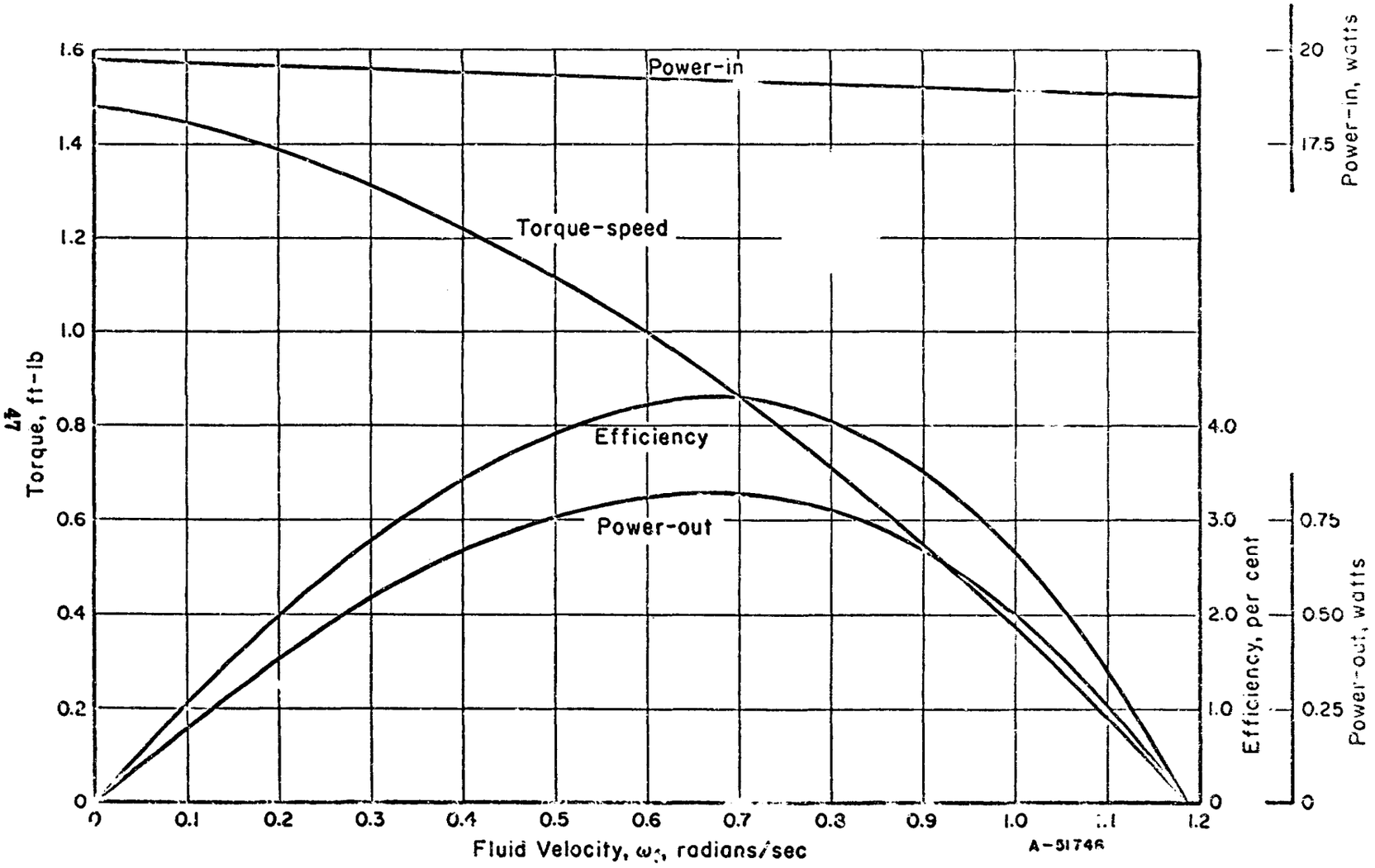

FIGURE 26. SYSTEM CHARACTERISTIC CURVES, SYSTEM LIFETIME 0

TABLE IV. FOR SYSTEM LIFETIME OF 0, THE PARAMETER PARTIAL DERIVATIVES AND VARIANCES FOR THE PERFORMANCE CHARACTERISTIC OF OPEN-LOOP PEAK EFFICIENCY

Evaluation of the Open-Loop Peak Efficiency Variance, σ_E^2, and a Breakdown of σ_E in the Percent Contribution From Each Parameter

Parameter P_j	Symbol	Parameter Value and Tolerance	$\frac{\partial E}{\partial P_j}$	$\frac{\partial E}{\partial P_j}\bar{P}_j$	σ_{P_j}	$\sigma_{P_j}^2$	$\sigma_{P_j}^2/\bar{P}_j^2$	$\left(\frac{\partial E}{\partial P_j}\right)^2 \sigma_{P_j}^2$	Breakdown of σ_E, %
Sensor dead band	D_3	$1 \times 10^{-2} \pm 3 \times 10^{-4}$	0	0	1×10^{-4}	1×10^{-8}	1×10^{-4}	0	0
Amplifier gain	K_V	$3.55 \times 10^{-1} \pm 7.1 \times 10^{-2}$	+6.77	+2.4	2.365×10^{-2}	5.6×10^{-4}	4.46×10^{-3}	2.57×10^{-2}	69.67
Magnetic-flux density	B	$1.88 \times 10^{4} \pm 5.64 \times 10^{2}$	$+5.04 \times 10^{-4}$	+5.72	1.88×10^{2}	3.54×10^{4}	1×10^{-4}	3.27×10^{-3}	8.864
Loop diameter	D_1	$4 \pm 8 \times 10^{-2}$	-4.75×10^{-1}	-1.9	2.67×10^{-2}	7.13×10^{-4}	4.46×10^{-5}	1.607×10^{-4}	0.4356
Tubing diameter	D_2	$3 \times 10^{-2} \pm 8.33 \times 10^{-5}$	$+2.41 \times 10^{2}$	+7.22	2.775×10^{-5}	7.71×10^{-10}	8.58×10^{-7}	4.48×10^{-5}	0.1214
Pump channel height	h	$6 \times 10^{-3} \pm 9 \times 10^{-5}$	-7.5×10^{2}	-4.375	3×10^{-5}	9×10^{-10}	2.5×10^{-5}	4.79×10^{-4}	1.298
Pump channel width	w	$4 \times 10^{-2} \pm 6 \times 10^{-4}$	+2.86 x 10	+1.142	2×10^{-4}	4×10^{-8}	2.5×10^{-5}	3.27×10^{-5}	0.08864
Electrode length	L	$2.08 \times 10^{-2} \pm 3.12 \times 10^{-4}$	-1.925 x 10	-0.4	1.04×10^{-4}	1.08×10^{-8}	2.5×10^{-5}	4×10^{-6}	0.01084
Amplifier output impedance	R_g	$1 \times 10^{-2} \pm 1 \times 10^{-3}$	-2.4×10^{2}	-2.4	3.33×10^{-4}	1.11×10^{-7}	1.11×10^{-5}	6.38×10^{-3}	17.29
Friction factor constant	F	$3.1 \times 10^{-2} \pm 1.55 \times 10^{-3}$	-5.53 x 10	-1.715	5.17×10^{-4}	2.67×10^{-7}	2.78×10^{-4}	8.15×10^{-4}	2.209
								$\sigma_E^2 = 369 \times 10^{-4}$	
								$\sigma_E = 0.192$	

A worst-case analysis showed that the peak efficiency would be 1.85 percent.

The reliability estimate is as follows, where a lower limit of 3 percent is arbitrarily assigned for peak efficiency and no upper limit is assigned:

$$n_L = \frac{4.27 - 3}{0.192} = \frac{1.27}{1.92} = 6.62 \qquad n_U = \frac{\infty - 4.27}{0.192} = \infty$$

Percent $P_{n_L = 6.62} \approx 50$ Percent $P_{n_U = \infty} = 50$

Total ≈ 100

The reliability estimate is 1.0.

At system lifetime t = 500 hours, the peak efficiency was 3.98 percent. Figure 27 gives the characteristic curves for the flywheel. Table V gives the same information as Table II, but considers peak efficiency. The tolerance value for peak efficiency is 0.708 percent. The peak efficiency can be expressed as $E_{500\ hours} = 3.98 \pm 0.708$ percent. The parameters to which peak efficiency is most sensitive are tubing diameter, D_2, magnetic-flux density, B, and pump channel height, h; of equal consequence are amplifier gain, K_V, and amplifier output impedance. The breakdown of the variance shows that the greatest effect on peak efficiency is caused by amplifier gain, K_V, amplifier output impedance, R_S, and magnetic-flux density.

A worst-case analysis showed that the peak efficiency would be 1.65 percent.

The reliability estimate is as follows:

$$n_L = \frac{3.98 - 3}{0.235} = \frac{0.98}{0.235} = 4.17 \qquad n_U = \frac{\infty - 3.98}{0.235} = \infty$$

Percent $P_{n_L = 4.17} \approx 50$ Percent $P_{n_U = \infty} = 50$

Total ≈ 100 percent.

The reliability estimate is 1.00.

At system lifetime t = 5 years, the peak efficiency was 3.25 percent. The characteristic curves for the flywheel are shown in Figure 28. Table VI gives the same information as Table III, but considers peak efficiency. The tolerance value for peak efficiency is ±1.314 percent. The peak efficiency can be expressed as $E_{5\ years} = 3.25 \pm 1.314$ percent. The parameters to which the peak efficiency is most sensitive are tubing diameter, D_2, pump channel height, h, magnetic-flux density, B, and the amplifier gain, K_V. The variance breakdown shows that the effect of amplifier gain, K_V, completely swamps the effect from all the other parameters.

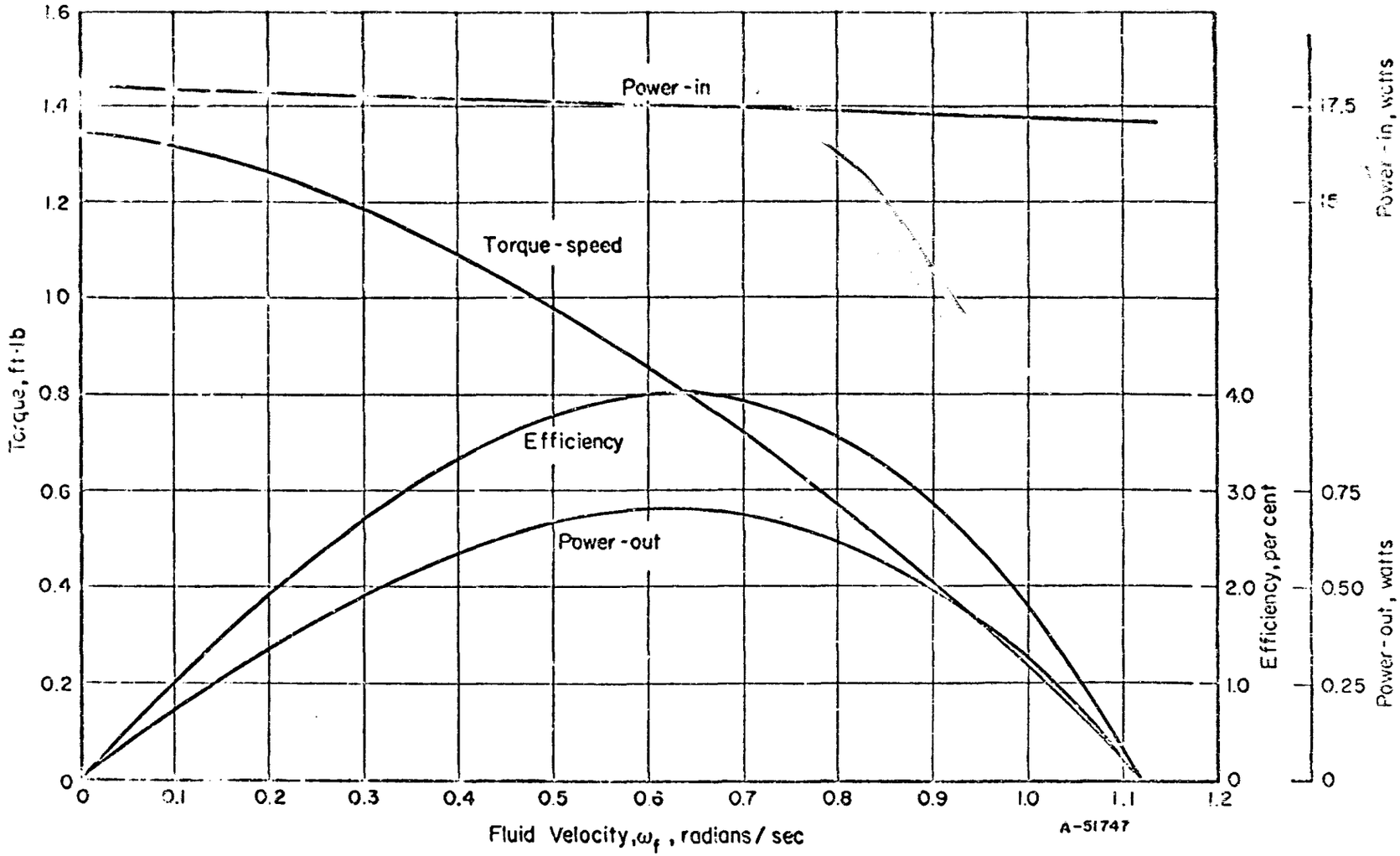

FIGURE 27. SYSTEM CHARACTERISTICS CURVES, SYSTEM LIFETIME 500 HOURS

TABLE V. FOR SYSTEM LIFETIME OF 500 HOURS, THE PARAMETER PARTIAL DERIVATIVES AND VARIANCES FOR THE PERFORMANCE CHARACTERISTIC OF OPEN-LOOP PEAK EFFICIENCY

Evaluation of the Open-Loop Peak Efficiency Variance, σ_E^2, and a Breakdown of σ_E in the Percent Contribution From Each Parameter

Parameter P_j	Symbol	Parameter Value and Tolerance	$\frac{\partial E}{\partial P_j}$	$\frac{\partial E}{\partial P_j}\bar{P}_j$	σ_{P_j}	$\sigma_{P_j}^2$	$\sigma_{P_j}^2 / \bar{P}_j^2$	$\left(\frac{\partial E}{\partial P_j}\right)^2 \sigma_{P_j}^2$	Breakdown of σ_E, %
Sensor dead band	D_s	$1 \times 10^{-2} \pm 3 \times 10^{-4}$	0	0	1×10^{-4}	1×10^{-8}	1×10^{-4}	0	0
Amplifier gain	K_v	$3.23 \times 10^{-1} \pm 7.26 \times 10^{-2}$	+8.55	+2.76	2.42×10^{-2}	5.88×10^{-4}	5.62×10^{-3}	4.3×10^{-2}	77.75
Magnetic-flux density	B	$1.38 \times 10^4 \pm 5.64 \times 10^2$	$+2.66 \times 10^{-4}$	+5	1.88×10^2	3.54×10^4	1×10^{-4}	2.505×10^{-3}	4.529
Loop diameter	L_1	$4 \pm 8 \times 10^{-3}$	-3.84×10^{-1}	-1.5	2.67×10^{-2}	7.13×10^{-4}	4.46×10^{-5}	1.05×10^{-4}	0.1898
Tubing diameter	D_2	$3 \times 10^{-2} \pm 8.33 \quad 10^{-5}$	$+2.135 \times 10^2$	+6.4	2.773×10^{-5}	7.71×10^{-10}	8.58×10^{-7}	3×10^{-5}	0.06365
Pump channel height	h	$6 \times 10^{-3} \pm 9 \times 10^{-5}$	-8.35×10^2	-5	3×10^{-5}	9×10^{-10}	2.5×10^{-5}	6.27×10^{-4}	1.133
Pump channel width	w	$4 \times 10^{-2} \pm 6 \times 10^{-4}$	$+2 \times 10$	+0.8	2×10^{-5}	4×10^{-8}	2.5×10^{-5}	1.6×10^{-5}	0.02893
Electrode length	L	$2.08 \times 10^{-2} \pm 3.12 \times 10^{-4}$	-2.14×10	-0.455	1.04×10^{-4}	1.08×10^{-8}	2.5×10^{-5}	4.95×10^{-6}	0.00895
Amplifier output impedance	R_s	$1 \times 10^{-2} \pm 1 \times 10^{-3}$	-2.77×10^2	-2.77	3.33×10^{-4}	1.11×10^{-7}	1.11×10^{-3}	8.52×10^{-3}	15.40
Friction factor constant	F	$3.14 \times 10^{-2} \pm 1.55 \times 10^{-3}$	-4.24×10	-1.33	5.23×10^{-4}	2.74×10^{-7}	2.78×10^{-4}	4.93×10^{-4}	0.8915
								$\sigma_E^2 = 55 \times 10^{-3}$	
								$\sigma_E = 0.236$	

A worst-case analysis showed that the peak efficiency would be 1.07 percent.

The reliability estimate is as follows:

$$n_L = \frac{3.25 - 3}{0.438} = \frac{0.25}{0.438} = 0.572 \qquad n_N = \frac{\infty - 3.25}{0.438} = \infty$$

$$\text{Percent } P_{n_L = 0.572} = 21.64 \qquad \text{Percent } P_{n_U = \infty} = 50.$$

Total = 71.64 percent.

The reliability estimate is 0.7164.

The distribution curves for each of the three peak efficiencies are shown in Figure 29. A plot of the peak-efficiency distribution curves and the line of nominal peak efficiency versus time is shown in Figure 30. It can be noted from Figure 30 that the nominal peak efficiency decreases continuously over time, with no fluctuations or sharp breaks. The path followed by the line of nominal peak efficiency indicates a decrease in efficiency at a rate that decreases with time. The decreasing rate results from exponential changes in the friction-factor constant, f_c. While the nominal value for peak efficiency does not fall below the specification limit in 5 years, the spread of the distribution increases so that approximately 30 percent of the systems built could be expected to be operating below the 3 percent specification.

Comparison of Results. It is possible that, when more than one system performance characteristic is used to define proper system operation, a change in one or more parameters will improve system operation when one performance characteristic is considered, and will degrade operation when one or more of the other performance characteristics are considered. The situation of a parameter conflict between performance characteristics occurred in this investigation. By comparing settling-time and peak-performance partial derivative values in Tables I through VI, it can be noted that changes in the loop diameter, D_1, pump channel width, w, electrode length, L, and the friction factor constant, f_c, that reduce (increase) settling time correspondingly reduce (increase) peak efficiency. The fixing of the design values, when parameter conflict exists, would have to be made on some basis other than the two system characteristics considered in this investigation.

Table VII gives the results of the moment method for system lifetimes considered, and includes the worst-case analysis values.

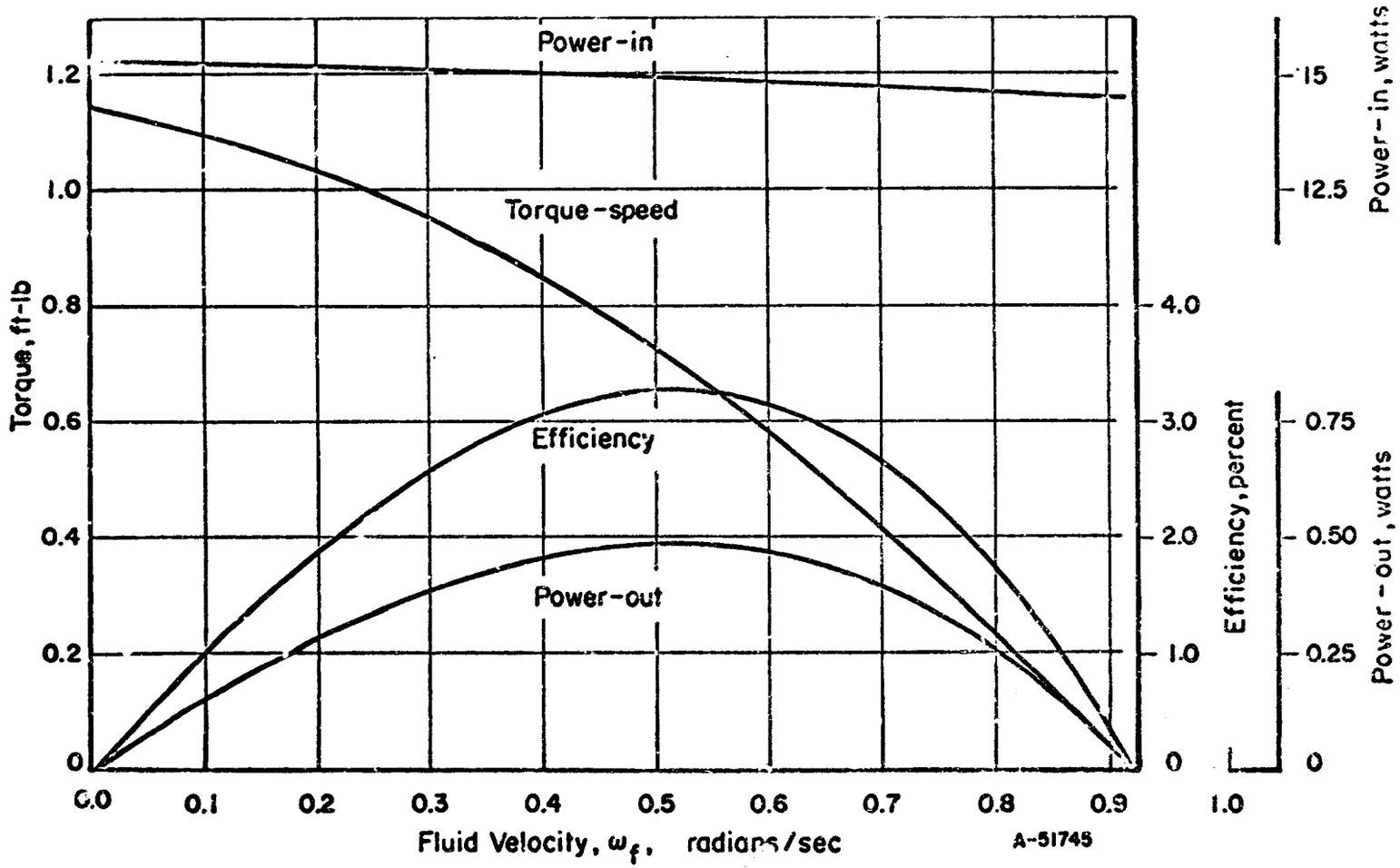

FIGURE 28. SYSTEM CHARACTERISTICS CURVES, SYSTEM LIFETIME 5 YEARS

TABLE VI. FOR SYSTEM LIFETIME OF 5 YEARS, THE PARAMETER PARTIAL DERIVATIVES AND VARIANCES FOR THE PERFORMANCE CHARACTERISTIC OF OPEN-LOOP PEAK EFFICIENCY

Evaluation of the Open-Loop Peak Efficiency Variance, σ_E^2, and a Breakdown of σ_E in the Percent Contribution From Each Parameter

Parameter P_j	Symbol	Parameter Value and Tolerance	$\frac{\partial E}{\partial P_j}$	$\frac{\partial E}{\partial P_j}\overline{P}_j$	σ_{P_j}	$\sigma_{P_j}^2$	$\sigma_{P_j}^2/\overline{P}_j^2$	$\left(\frac{\partial E}{\partial P_j}\right)^2 \sigma_{P_j}^2$	Breakdown of σ_E, %
Sensor dead band	D_S	$1 \times 10^{-2} \pm 3 \times 10^{-4}$	0	0	1×10^{-4}	1×10^{-8}	1×10^{-4}	0	0
Amplifier gain	K_V	$2.735 \times 10^{-1} \pm 1.173 \times 10^{-1}$	$+1.098 \times 10$	+3	3.92×10^{-2}	1.535×10^{-3}	2.06×10^{-2}	1.85×10^{-1}	96.65
Magnetic-flux density	B	$1.88 \times 10^{4} \pm 5.64 \times 10^{2}$	-2.29×10^{-4}	+4.3	1.88×10^{2}	3.54×10^{4}	1×10^{-4}	1.86×10^{-3}	0.9717
Loop diameter	D_1	$4 \pm 8 \times 10^{-2}$	-3.12×10^{-1}	-1.25	2.67×10^{-2}	7.13×10^{-4}	4.46×10^{-5}	6.94×10^{-5}	0.03625
Tubing diameter	D_2	$3 \times 10^{-2} \pm 8.33 \times 10^{-5}$	$+2.67 \times 10^{2}$	+8	2.775×10^{-5}	7.71×10^{-10}	8.58×10^{-7}	5.5×10^{-5}	0.02873
Pump channel height	h	$6 \times 10^{-3} \pm 9 \times 10^{-5}$	-7.42×10^{2}	-4.45	3×10^{-5}	9×10^{-10}	2.5×10^{-5}	4.96×10^{-4}	0.2591
Pump channel width	w	$4 \times 10^{-2} \pm 6 \times 10^{-4}$	$+2.125 \times 10$	+0.85	2×10^{-4}	4×10^{-8}	2.5×10^{-5}	1.81×10^{-5}	0.009456
Electrode length	L	$2.08 \times 10^{-2} \pm 3.12 \times 10^{-4}$	-1.685×10	-0.35	1.04×10^{-4}	1.08×10^{-8}	2.5×10^{-5}	3.07×10^{-6}	0.001603
Amplifier output impedance	R_S	$1 \times 10^{-2} \pm 1 \times 10^{-3}$	-1.77×10^{2}	-1.77	3.33×10^{-4}	1.11×10^{-7}	1.11×10^{-3}	3.475×10^{-3}	1.815
Friction factor constant	F	$3.984 \times 10^{-2} \pm 1.55 \times 10^{-3}$	-3.27×10	-1.3	6.64×10^{-4}	4.41×10^{-7}	2.78×10^{-4}	4.71×10^{-4}	0.2460
								$\sigma_E^2 = 192 \times 10^{-3}$	
								$\sigma_E = 0.438$	

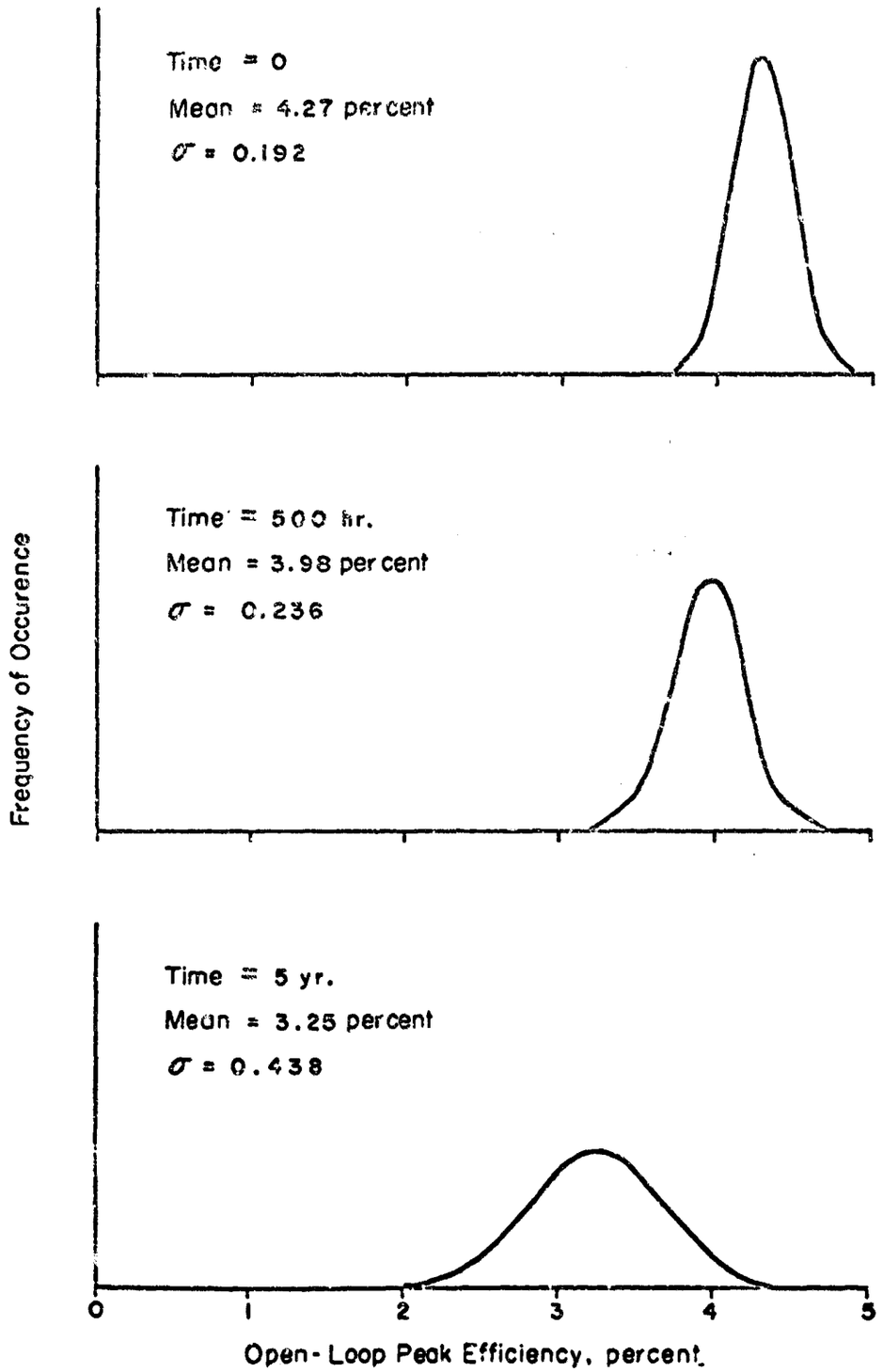

FIGURE 29. OPEN-LOOP PEAK-EFFICIENCY FREQUENCY DISTRIBUTIONS

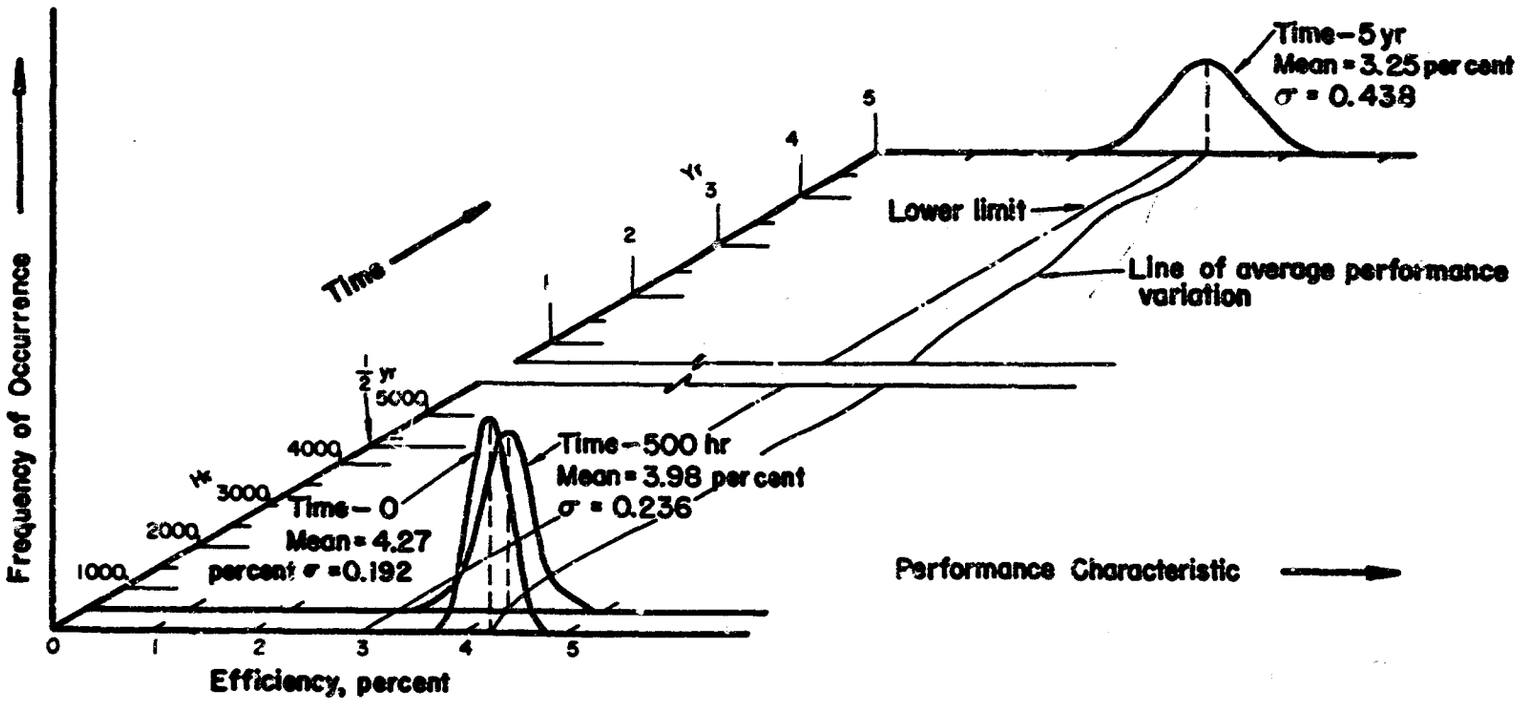

FIGURE 30. OPEN-LOOP PEAK-EFFICIENCY FREQUENCY DISTRIBUTIONS, TIME RELATIONSHIPS

TABLE VII. RESULTS OF MOMENT METHOD

Characteristic	System Lifetime	$\bar{A}_I$	σA_I^2	σA_I	n_L	n_U	Reliability	Worst Case
Settling time, t_S	0	13.25 sec	0.1297	0.360	∞	3.47	0.9999	7.5 sec
	500 hr	13.85 sec	0.1153	0.340	∞	1.91	0.9719	8.7 sec
	5 yr	11.75	0.7295	0.854	∞	3.22	0.9999	15.9 sec
Peak efficiency, E	0	4.27%	0.0369	0.192	6.62	∞	1.000	1.85%
	500 hr	3.98%	0.0553	0.235	4.17	∞	1.000	1.65%
	5 yr	3.25%	0.1914	0.438	0.572	∞	0.7164	1.07%

Conclusions

The Moment method for predicting drift-type failures in a system requires information about the system that was only qualitatively known about the fluid-flywheel attitude controller investigated. The lack of information concerning time degradation of parameters was particularly apparent. The qualitative information was sufficient, however, to make the educated assumptions needed for the analysis. The analysis showed that, for the system characteristics chosen and the arbitrarily assigned specification limits, the system has a high reliability.

This investigation demonstrates the ability of the Moment method to provide insights to a designer as to the behavior of the system characteristics being considered as measures of performance. It has been shown that the results of the Moment method depend greatly on whether the performance characteristic being considered is a continuous or discontinuous function of the system parameters. The knowledge of the functional relationship between performance characteristics and the system parameters is a great aid in design and prediction of future system operation.

The partial derivatives necessary for the evaluation of the Propagation of Variance formula, and which determine the performance characteristics sensitivity to the system parameters, also provide additional information when more than one performance characteristic is considered. The partial derivatives indicate which parameters are compatible, and which parameter changes cause improvement in some performance characteristics and degradation in others. That is, the partials indicate which parameters, when varied, will concurrently improve or degrade the performance characteristics (compatible parameters) and those parameters which, when varied, will improve some performance characteristics and degrade others (conflicting parameters).

The results of this investigation show that, with sufficient parameter information, the future performance can be predicted and reliability estimates made. If the information is not complete, but educated assumptions can be made, important insights into system performance can be obtained by use of the Moment method.

TASK II. LIQUID METAL NaK-77 SERVO-ACTUATING SUBSYSTEM

Introduction

The objective of this task was to develop a mathematical model of a high-temperature liquid-metal servoactuating subsystem and, using reliability prediction techniques, to make a prediction about the drift reliability of the system.

The hardware for the system, being developed by another contractor, was to consist of a centrifugal pump, a servo control valve, and an actuator driving a spring-loaded inertial load.

Development work on the system components, however, had not been completed at the time of initiation of the program, and was not completed during the program. The reliability analysis was limited, therefore, to a study of the actuator and pump since the servo-valve design and configuration had not been fully developed. The development of the system hardware concurrent with the reliability study posed a second limitation: there was no time to obtain degradation data on the components; only limited performance data were available.

Mathematical models of the pump and actuator were, however, developed and programmed on the analog computer, and partial derivatives and variances of the significant performance characteristics were calculated. A comparison of the sensitivity of the actuator performance to degradation in the actuator and in the pump also was included in the study. Supplemental material including the mathematical statements for modeling the system components and containing information on the physical characteristics of the components which may be considered proprietary by other contractors, has been delivered to the program Technical Monitor.

The next logical step in a reliability analysis is the prediction of time variation of system and component performance. Such an analysis is, however, based on a knowledge of the degradation rates of the critical parameters. Since information was not available during the current program, this phase of the analysis was limited to identification of the wear areas that most significantly affect the performance of the pump and actuator.

Engineering Activity

Development of the Mathematical Model of the Centrifugal Liquid-Metal Pump

The liquid-metal pump studied in this program was a ten-stage axially balanced centrifugal pump with 6-bladed radial vane impellers, designed for operation at 35,000 rpm and rated at 3000 psi at 10 gpm.

A cross section of the pump, showing the flow and leakage paths, is given in Figure 31. The liquid metal flows through the first five stages from right to left, and then is transferred to the rear of the pump where it flows through the last five stages from left to right. The axial forces on the impeller shaft are balanced by this reversal in flow direction. The main pump shaft is supported by three hydrostatically pressurized journal bearings and one radial thrust bearing. The pressurization for the forward bearing is taken from the flow path between the fifth and sixth stages (e and f) of the pump

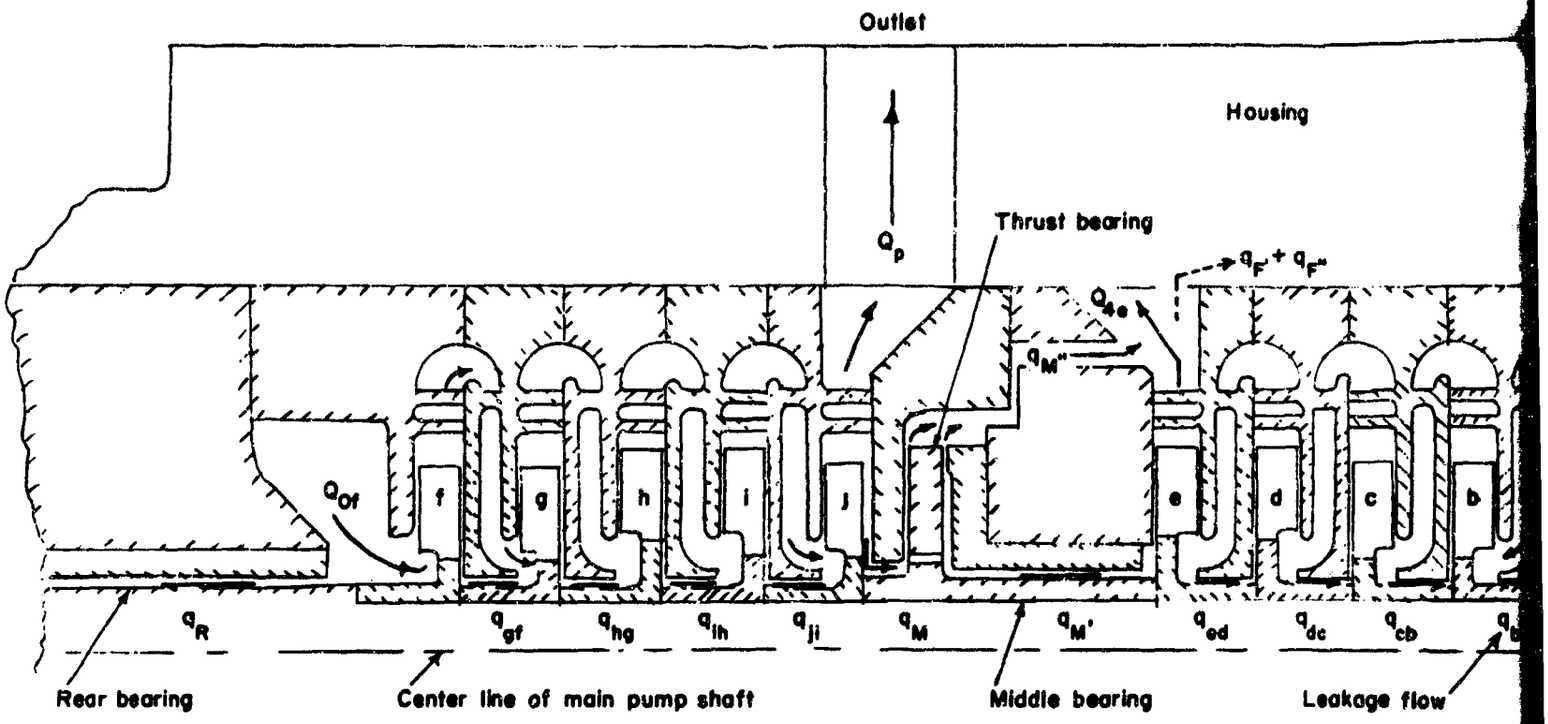

FIGURE 31. TEN-STAGE CENTRIFUGAL PUMP SHOWING FLOW AND LEAKAGE PATHS AND STAGE IDENTIFICATION

A

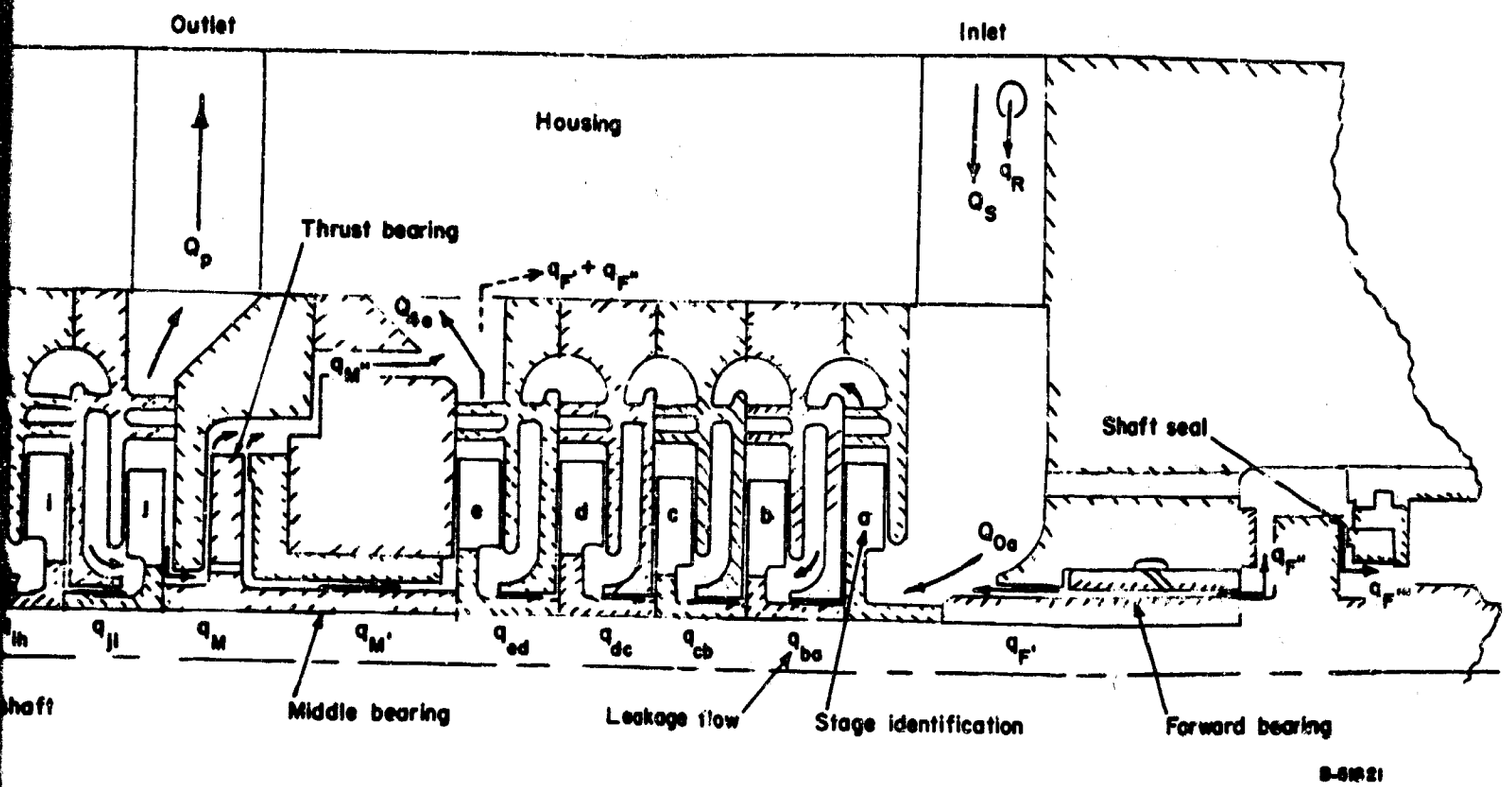

UMP SHOWING FLOW AND
IDENTIFICATION

B

and that for the rear bearing is obtained from the fluid which enters the sixth stage (f). The pressure for the middle bearing and for the radial thrust bearing is taken from the inlet to the tenth stage (j) of the pump.

Figure 32 shows a cross section of the impeller and diffuser. After fluid passes through the pump impeller (1-2)*, it enters a vane-type diffuser section (3-4) and then travels down the back side of the stage housing (4-5), through straightening vanes in the housing, which remove the rotary motion of the fluid in preparation for its entering the impeller of the next stage.

The mathematical model was designed to produce a curve of total pressure rise across the pump as a function of net pump flow. It was formulated on the assumption of steady-state operation and from the classical Euler equation for the total head rise developed across the impeller of a centrifugal machine.

Of course, a pump in a servo control system would not operate under steady-state conditions, unless a sufficiently responsive accumulator was included in the circuit. Although no such accumulator is indicated in the existing NaK control system, a steady-state analysis of the pump was performed because it enabled the engineering effort to be concentrated on the modeling of the various frictional, leakage, and impulse losses in the pump, which are difficult to predict because of complex flow patterns in the device. In addition, the steady-state analysis satisfactorily identifies parameters sensitive to degradation and predicts the effect of changes in these parameters on pump performance. A nonsteady-state analysis of the pump would involve the prediction of pressure and velocity distributions within the impeller and was therefore beyond the scope of this program. The loss equations developed for the steady-state analysis can be used, however, in developing a mathematical model of the centrifugal pump for nonsteady-state operation.

Development of Equations for Mathematical Model. The equations developed in this analysis are shown in supplemental material delivered to the program Technical Monitor, and are based in part on the work of O. E. Balje published in the ASME Transactions, 74 (1952), and entitled "A Contribution to the Problem of Designing Radial Turbomachines". The theoretical head developed across the pump impeller is expressed in Equation (43)** as a function of the flow through the impeller, Q_1, the angular velocity of the pump, ω, the degree of prerotation of the fluid as it enters the impeller, the geometry of the impeller, and a slip factor, m. It is seen from the nature of the pump flow and leakage paths, given in Figure 31, and from the flow summary in the supplemental material, that the flow through the impeller is net pump flow plus interstage leakage.

The slip factor accounts for the failure of the fluid to leave the impeller tip tangent to the impeller blades. The slip factor applies an average correction, greater than 1, and approaching a value of 1.0 for an infinite number of blades, to the direction of the relative velocity of the fluid with respect to the tip blade angle.

The prerotation factor, ψ, must be considered because, when the fluid enters the impeller blades, it may have some rotary motion due to its contact with the rotating shaft prior to its entry into the impeller or to the failure of the straightening vanes to remove the angular velocity imparted to the fluid by previous stages. This rotary motion reduces the total amount of energy that can be transferred to the fluid by the impeller.

*Numerical identification of key points in the flow path through the stage.
** Supplemental material.

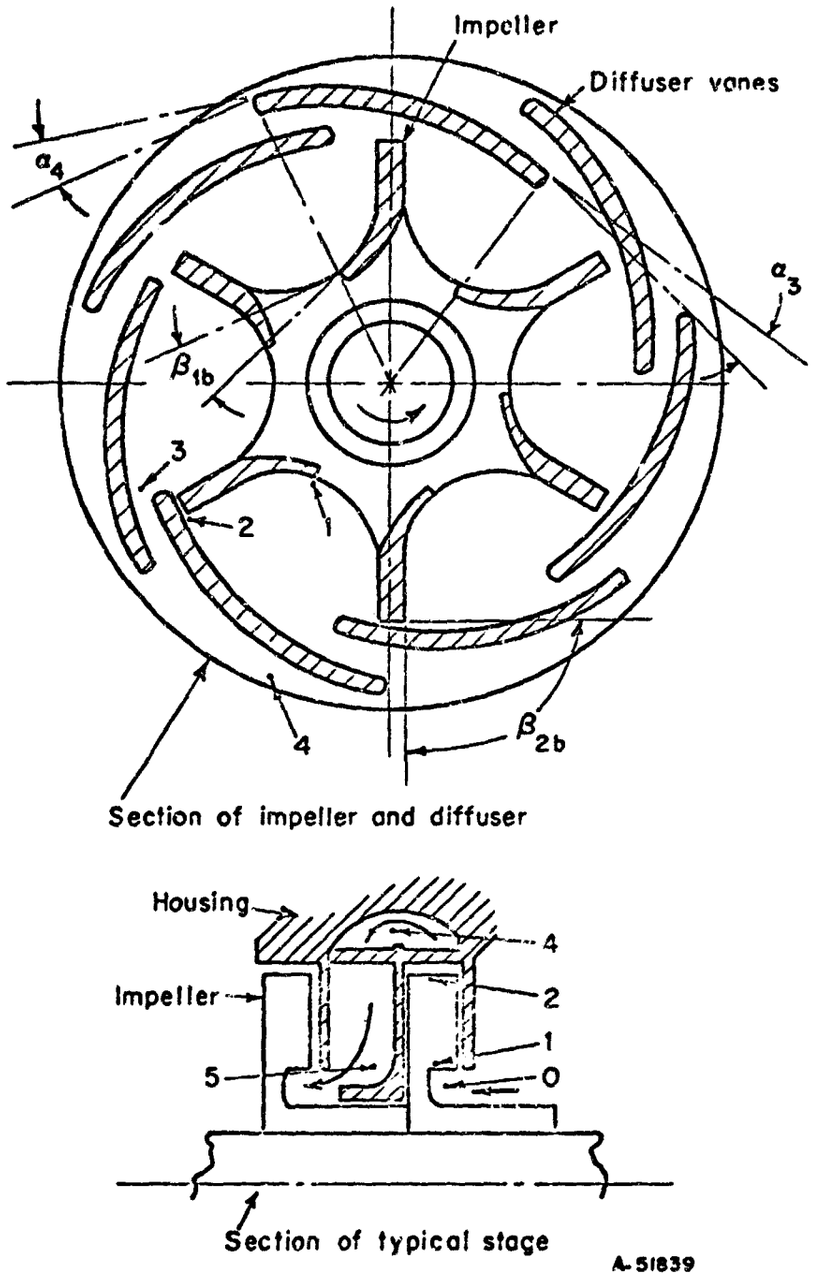

FIGURE 32. IMPELLER AND DIFFUSER CONFIGURATION, WITH IDENTIFICATION OF BLADE ANGLES AND FLOW LOCATIONS

The total output head from each stage of the pump is equal to the head at the inlet to the pump stage, plus the theoretical rise in total head across the impeller, less the various frictional and impulse losses discussed below.

There are several types of head losses in the centrifugal pump. The inlet entrance loss and the suction-head area loss [Equations (44) and (45)] are simply velocity-head losses that result from a change in the cross-sectional area of the fluid-flow path between the pump inlet port and the inlet to the impeller of the first stage.

For a given angular velocity, there is only one flow condition at which the inlet flow will enter tangent to the impeller vanes. At all other flow conditions, the impact of the fluid on blade surface causes shock and turbulance loss. This loss is given in Equation (46). It is expressed as a function of the flow conditions, the geometry of the pump, and a shock loss coefficient, X, which is experimentally determined.

Equation (48) gives the general form for frictional flow losses in the pump. The flow path through the nonshrouded impeller (L_{1-2}) is a logarithmic spiral form, and the friction occurs between the fluid and the surfaces of the stationary impeller housing. The frictional path length in the diffuser and return sections is taken as the mean path length through the diffuser and straightening vanes. The velocity through these sections is an average velocity equal to the square root of one-half the sum of the square of the magnitudes of the inlet and outlet velocities at each section.

Equations for calculating the absolute fluid velocities in the diffuser and the return sections are given in Equations (49), (50), and (51).

The diffuser mixing loss, as expressed by Equation (50), is a turbulance and momentum-exchange loss that occurs because of the difference in the direction of the absolute velocities of adjacent stream lines leaving the impeller tip.

The diffuser inlet impulse loss, shown in Equation (51), is a shock loss, and is similar to the impulse loss that occurs at the entrance to the impeller. At the diffuser inlet, there is only one flow condition under which the fluid enters the diffuser section tangent to the diffuser vanes. At all other flow conditions, shock and turbulance losses result. An empirical shock loss factor, X', is used to match the analog performance with experimentally determined pressure capacity curves.

The interstage leakage flow path consists of axial laminar flow around the pump shaft and then a small length of outward radial flow between the end of the impeller hub and the pump housing. Some viscous pumping action takes place in this latter area; however, the contribution of this action to the total leakage is much smaller than that due to the net pressure drop across the total flow path, and was therefore neglected in the calculations. The magnitude of the interstage leakage flow is given by Equation (54).

Equations (55) through (59) give the leakage flow through the three journal bearings and the thrust bearing. The pressures used in calculating these leakages and bearing flow rates are obtained by subtracting the velocity head, ($V^2/2g$), from the total head at the point in question. Front seal leakage, q'''_F, was assumed to be zero in this study.

Consideration of Pump Efficiency. A second important aspect of pump performance is efficiency, which is defined as the ratio of the net increase in hydraulic horsepower across the pump to the mechanical power put into the pump shaft. Although this aspect

of pump performance was not specifically modeled in this study, the various factors that contribute to efficiency losses in the current pump design are of significance and are, therefore, discussed in this section.

Shaft input power is required to:

(1) Impart energy to the fluid in the impeller of each state
(2) Overcome viscous and frictional losses in bearings, impeller, and seal
(3) Overcome recirculating flow losses around the ends of the impeller blades.

The fluid receives all of its energy while passing through the pump impeller, and the total shaft power imparted to the fluid is equal to the theoretical power requirements derived from the Euler equation as given in Equation (81). An equation for determining the power requirements for nonsteady-state flow operation is derived. The power delivered to the fluid is not completely recovered at the output of the pump. A portion of it is lost in overcoming frictional and shock losses in the impeller and pump passages and in throttling losses, which occur in the interstage leakage and bearing flow paths.

The power required to overcome viscous drag losses in the journal bearings and interstage clearance spaces and the viscous losses in the radial thrust bearing can be calculated from Equations (82) and (83).

The third type of power loss results from the leakage that occurs around the ends of the impeller blades. The pressure on the forward surface of the blade is always greater than that on the back surface, and the resulting pressure differential creates a tangential leakage flow through the clearance space between the edges of the blade and the stationary housing. This flow produces a viscous drag on the ends of the blade and also a throttling loss as the fluid passes from a region of high to low pressure.

The magnitude of this flow is difficult to calculate because a knowledge of the pressure velocity distributions within the impeller is required. Several methods for obtaining approximations of this distribution are contained in the literature and can be used as a basis for predicting the pressure drop across the faces of the impeller.*

A simpler method for obtaining a first approximation of the pressure differential across the blade surfaces is given in the supplemental material. This approach is based on a knowledge of the general shape of the pressure differential along the blade.

The operating efficiency of the centrifugal pump is equal to the net increase in hydraulic horsepower across the pump divided by the total input power requirements discussed above. The net hydraulic-pump horsepower is given by the expression: $(H_p - H_S)Q_p\gamma$.

Programming and Operation of the Analog Computer Simulation of the Liquid-Metal Pump

As a first attempt to program the mathematical model of the centrifugal pump on the analog computer, a wiring or "patch" diagram was designed directly from the equations. The program was designed to solve for the pressure-capacity performance of all

*"Method for Design of Pump Impellers Using a High-Speed Digital Computer", NASA Technical Note D-1562.

ten stages and to account for the dissimilarities among the stages due to differences in leakage flows. The result of this first effort was a program approximately four times too large to be programmed on the Battelle analog computer. The primary difficulty was the very large number of variable multipliers needed (about 80 channels) to simulate the entire pump.

Subsequent hand calculations, however, showed that the differences in the prestage pressure rises that are caused by the leakage flow variations among the stages are negligible compared to the very high static pressures present. Interstage leakage is, therefore, identical for all ten stages. It was thus possible to closely simulate the performance of the entire pump by modeling only the first four stages on the computer. This required only 20 channels of variable multiplication. In addition, the first four stages are identical in all respects, so that the final model amounted to a simulation of only one stage.

The wiring diagram and potentiometer setting sheets are presented in the supplemental material. The potentiometer settings shown are for the nominal "design point" dimensions and performance of the pump. When the operation of the program on the computer was started, reasonable values of the shock loss coefficient and slip factor, X and m, were arbitrarily chosen.

There were initially no integrators in the program, because there were no dynamic effects modeled and the calculations involved only algebraic operations. Often, when closed-loop algebraic circuitry such as this is programmed on the analog computer, instability occurs. This was true for the pump model, and an integrator was therefore added to the circuit. The integrator provided sufficient filtering effect and was successful in maintaining stability of the model without affecting the accuracy or performance of the simulation.

Simulation of Experimental Data. In a contractor's Technical Proposal, "A Study of Liquid Metal, NaK-77 for Application in Flight Control Systems", predicted pump performance data for several impeller speeds were supplied. These data were duplicated on the computer by manipulating the values of X and m. The value of m required was very reasonable, and for 35,000-rpm operation corresponded exactly to the value calculated from Equation (43) in Appendix I. The value of X required for the diffuser inlet was, however, somewhat higher than anticipated. Figure 33 is a graph of computer performance at 35,500 rpm.

Experimental test data were supplied for operation of this pump at lower speeds. In order to simulate performance in these cases, m had to be reduced slightly and the interstage leakage had to be increased considerably. From discussions with other contractor's personnel, it was determined that the interstage clearances on the pump used in these tests had been larger than the drawings specified and that the clearances would be decreased in subsequent pump models for the higher speed operation. Therefore, the clearances specified in the drawings were used in the simulation program.

A curve of predicted net positive suction head (NPSH) was also given. During the initial runs on the analog computer, a very poor simulation of this was obtained. Upon inspection of the program equations, it was determined that the equation for impeller inlet shock loss as developed by Balje was not directly applicable to the pump design under consideration because it provided for the existence of an impeller inlet shock loss at no-flow conditions. The equation was therefore modified to have the shock loss

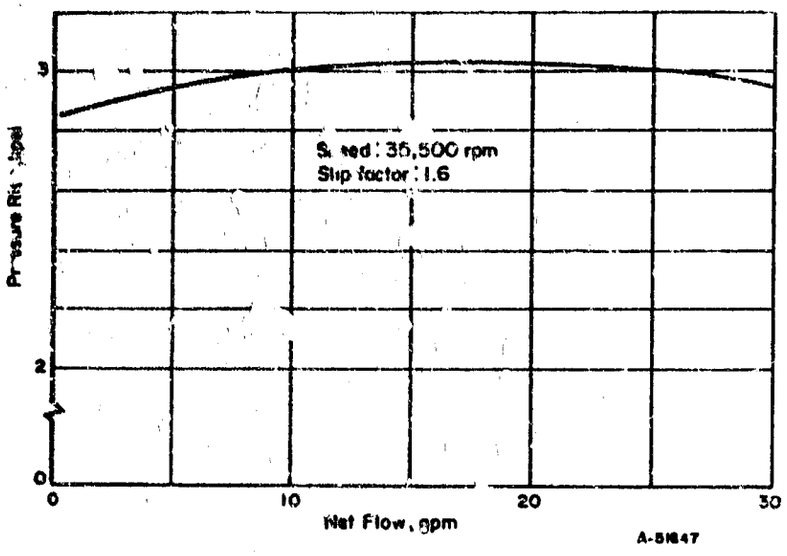

FIGURE 33. COMPUTED CENTRIFUGAL-PUMP PERFORMANCE AT 35,500 RPM

approach zero at no flow and to match the curve resulting from Balje's equations at higher flows. The equations for the diffuser inlet shock losses were satisfactory. Figure 34 is a graph of computed NPSH. This is lower than that predicted, but it is believed that the prediction was based on a general formula, which probably would not be as accurate as the specific program used for this project. However, the NPSH predicted may include some additional local turbulence, and therefore may be justifiably conservative. The partial derivatives of particular interest at this time are not, however, related to NPSH and, because a reasonably good simulation of predicted and experimental pressure-capacity performance had been obtained, it appeared that the simulation program could be used with confidence to compute partial derivatives of performance.

Analysis of Pump Reliability

A study of the configuration and mathematical model of the centrifugal pump reveals that pump performance, in terms of the pressure-capacity curve, is most dependent on the magnitude of (1) impeller tip radius, (2) impeller blade-tip angle, and (3) the interstage clearance.

The sensitivity of the pump performance to changes in these parameters, expressed as partial derivatives, forms the basis of the study of pump reliability by the Moment method of reliability analysis. These partial derivatives, when expressed in absolute terms (not normalized), are used in the Propagation of Variance formula to estimate the expected variation in performance due to tolerance variations introduced in the manufacturing process. The normalized partial derivatives (expressed as a change in performance per percent change in parameter) provide a measure of the sensitivity of performance to changes or degradation of the component parameters. These are useful for identifying critical degradation areas and for redesigning components to improve

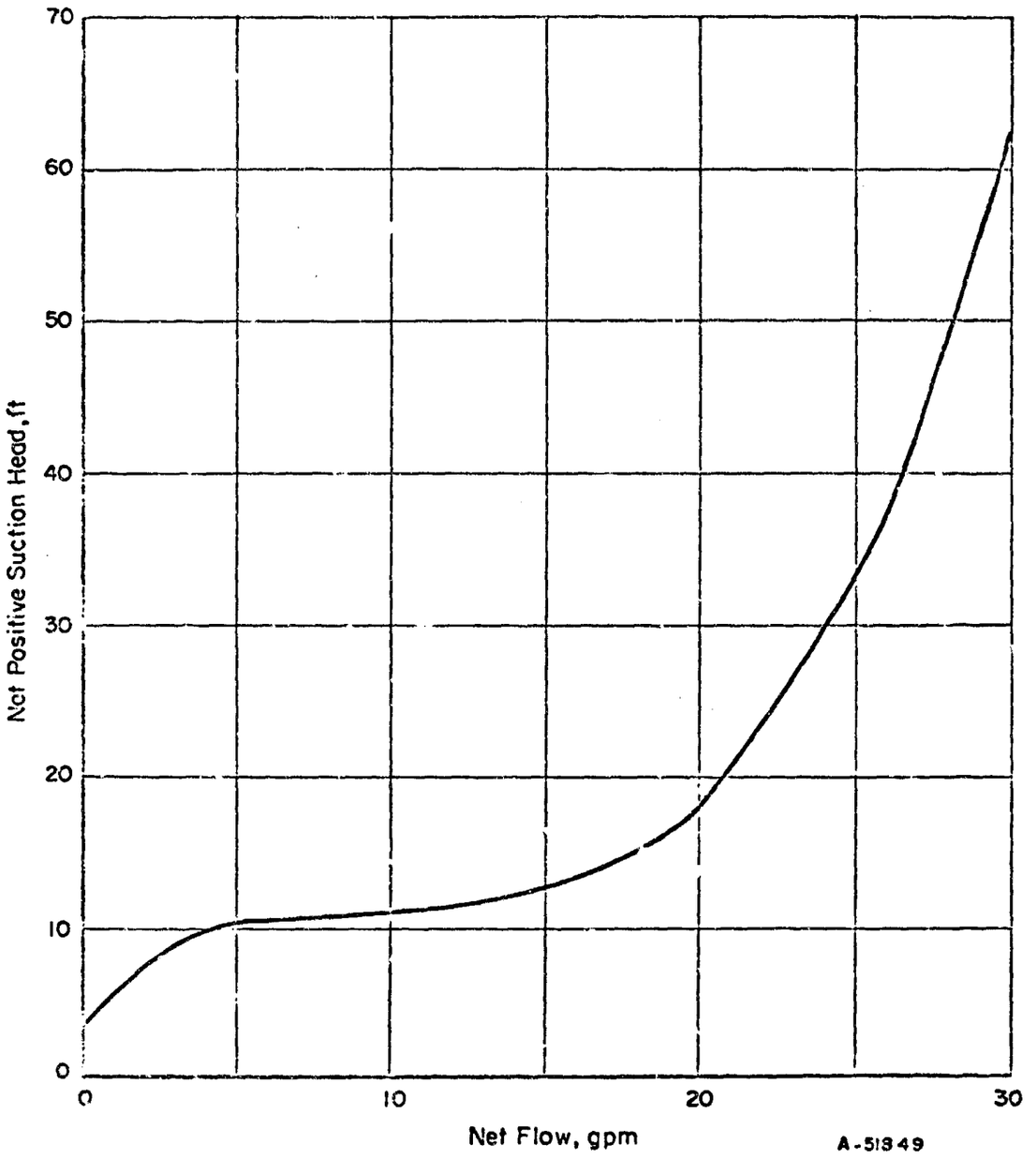

FIGURE 34. COMPUTED NET POSITIVE SUCTION HEAD

reliability and performance. When the time rate of degradation of the parameters is known, the absolute partial derivatives are used as weighting factors in predicting performance changes during operation.

Because quantitative data on the degradation of both the NaK system pump and actuator were not available, the analysis on these two components does not include a quantitative estimate of performance variation with time. However, Task III of this report does contain a detailed discussion of the use of the Moment method in predicting time-dependent performance changes on an electrohydraulic servo-control valve, and the basic methods used in this study could be applied to the NaK system when parameter degradation data become available.

Partial derivatives of pump performance are computed by varying the critical parameters of the analog model one at a time, and observing the variations that occur in pump performance. The variations were obtained by changing the necessary potentiometer settings on the analog computer. For each parameter variation, a new head-capacity curve was run on the computer and plotted on the X-Y plotter. Figure 35 shows the head-capacity curves for the range of parameter values investigated. Shown are (1) a normal curve, (2) curves for a 10 percent increase and decrease in impeller tip radius, (3) curves for a 10 percent increase and decrease in interstage diametral clearance, and (4) a curve for a 10 percent decrease in impeller blade-tip angle.

Partial derivatives were computed at capacities of 5, 15, and 25 gpm, and the curves of performance at 15 gpm from which the partial derivatives were calculated are shown in Figures 36, 37, and 38. Table VIII presents a summary of the partial derivatives of pressure at each of the flow capacities with respect to each of the parameters investigated. These are "normalized" partial derivatives, computed on a percentage basis.

TABLE VIII. SUMMARY OF NORMALIZED PARTIAL DERIVATIVES PREDICTED BY ANALOG COMPUTER

Partial Derivatives	Value, psi/%		
	5 gpm	15 gpm	25 gpm
$\partial P/\partial R_{2\%}$	23.4	28.7	35.0
$\partial P/\partial a_{ba\%}$	7.8	-1.5	-6.9
$\partial P/\partial \beta_{2b\%}$	31.5	40.0	45.0

The nominal values of the parameters are:

$R_2 = 0.764$ in.
$\beta_{2b} = 90$ deg
$a_{ba} = 0.002$ in

The standard deviations for the three critical pump parameters are obtained from the detailed drawing of the pump by assuming that the specified tolerance range represents a total of six standard deviations ($\pm 3\sigma$). The deviations obtained are:

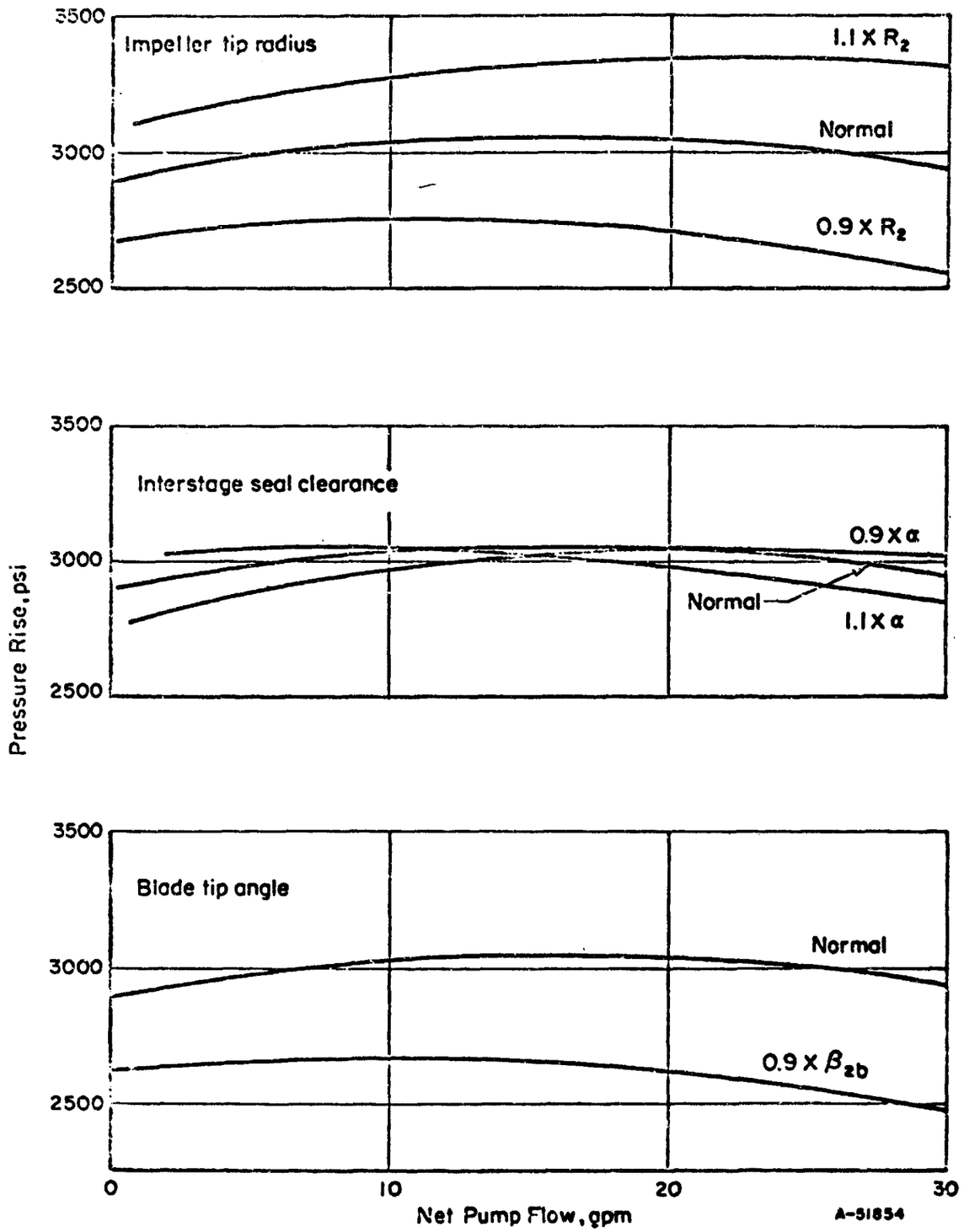

FIGURE 35. PRESSURE CAPACITY CURVES FOR PARAMETER VARIATION

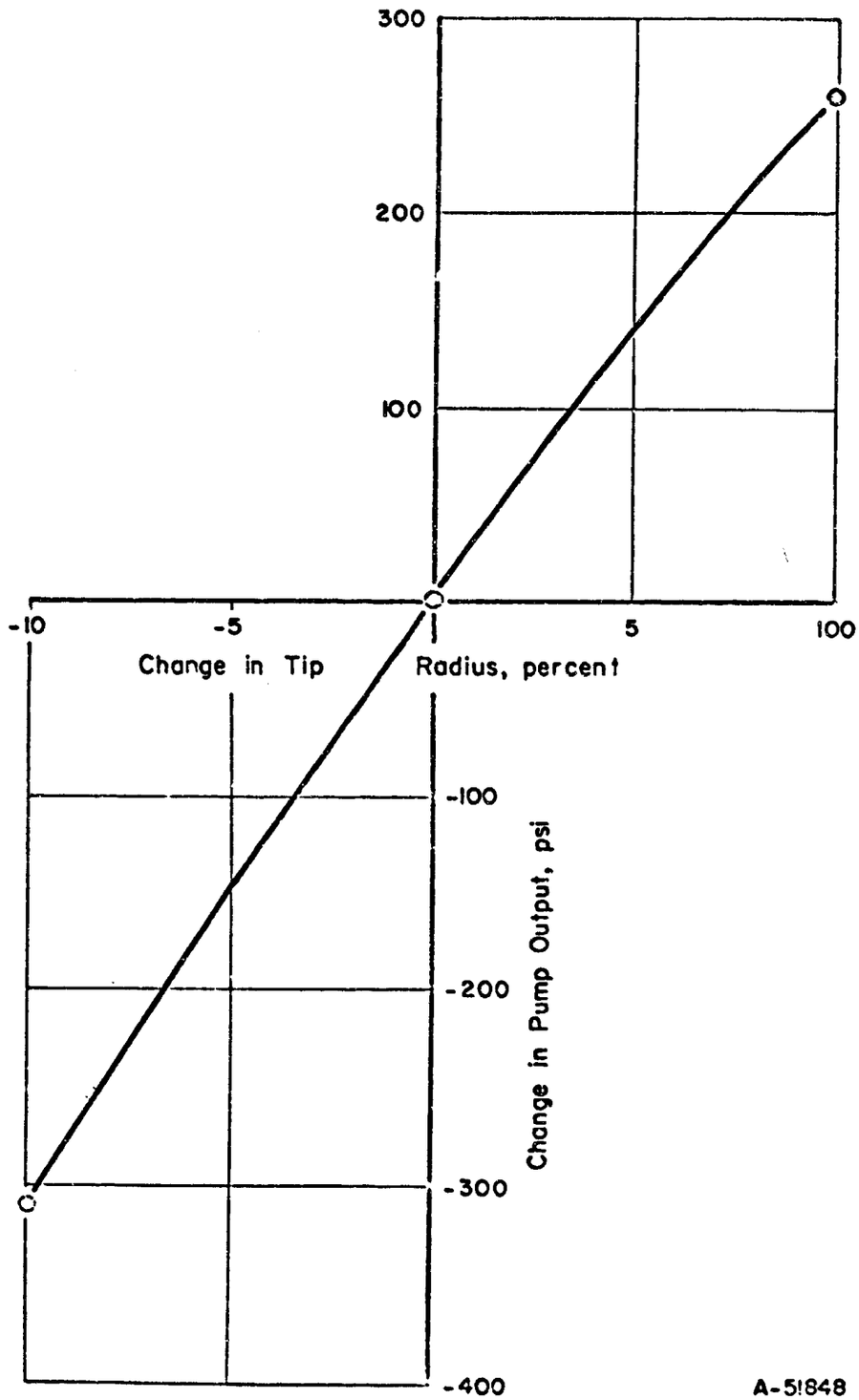

FIGURE 36. VARIATION IN PUMP PRESSURE RISE WITH RESPECT TO CHANGES IN IMPELLER TIP RADIUS AT A 15-GPM FLOW RATE

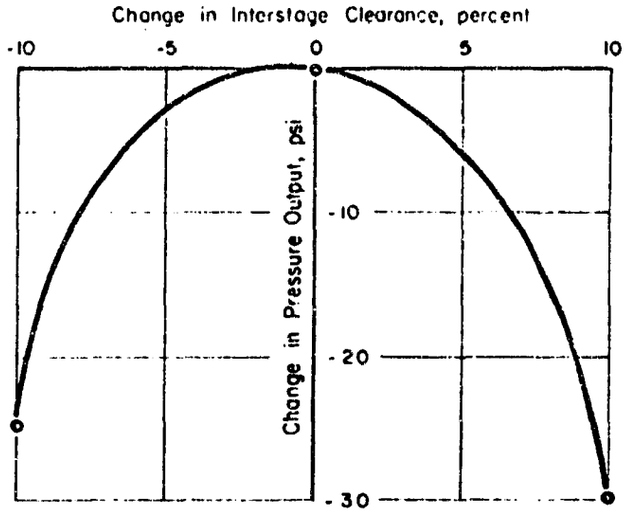

FIGURE 37. VARIATION IN PUMP PRESSURE WITH RESPECT TO CHANGES IN INTERSTAGE CLEARANCE AT A 15-GPM FLOW RATE

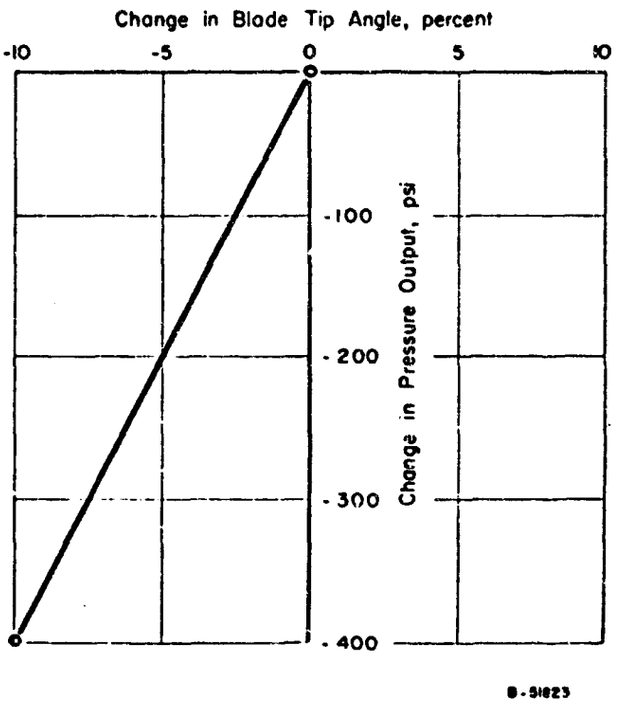

FIGURE 38. VARIATION IN PUMP PRESSURE RISE WITH RESPECT TO CHANGES IN BLADE TIP ANGLE AT A 15-GPM FLOW RATE

Tip diameter	0.00025 in.
Blade angle	0.109 deg
Interstage clearance	0.000033 in.

The resulting variance in output pressure at a nominal flow of 15 gpm is then obtained from the Propagation of Variance formula (Figure 1) and is computed to be 25.685 psi. The expected performance for ±3σ variation at 15 gpm is therefore:

3050 ± 15.2 psi.

Development of Mathematical Model of Liquid Metal Actuator

Figure 39 is a drawing of the liquid-metal actuator that was studied in the program. It uses a metallic-lip-type rod seal and metal piston rings. The rod is 422 stainless steel with a LW-1 flame-plated carbide coating. The pump housing is 422 stainless, and the liner and front bushings are carbide.

The performance and degradation studies of the actuator were run on the analog model of a flow-control servo valve and linear actuator, which were developed during Project 8225, Task No. 822502, and described in Technical Documentary Report No. FDL-TDR-64-30. The configuration of the NaK actuator differs from that of the actuator in this original system by having a single-ended, rather than a double-ended, connecting rod. The response and performance of the NaK system is therefore dependent on the direction of motion of the actuator. In order to study and compare the properties of the actuator in both directions, however, the double-ended actuator of the original system was utilized, and data were run with the pressurized area of the double-ended actuator equal to both the larger and the smaller areas of the NaK actuator. The larger area then represents motion to the left in Figure 39, and the smaller area represents motion to the right.

The performance of an actuator is tied to the performance of the entire system of which it is a part, and in the NaK system the actuator will ultimately be installed in a closed-loop control system with a 7-gpm flow-control valve with a spring-mass load as described in another contractor's proposal. The predicted performance of the system was described as "flat to 20 radians per second at 20 percent stroke amplitude". A frequency-response plot of predicted performance was also presented in the proposal. Comparison of this plot with other open-loop-type data indicates that it is an open-loop response of the actuator load only, without the control valve or fluid in the circuit.

To evaluate performance and degradation sensitivity, the modeled system was set up for closed-loop operation with proportional control. The gain was set reasonably below the marginal stability point, to provide good control without overshooting. Droop was 0.05 percent at 20 percent of maximum stroke from center position. No delay or other compensation circuitry was included, even though the system proposed uses a lag network in the control circuit. In addition, the parameters of the originally modeled servo valve were set to produce a saturation at 7 gpm.

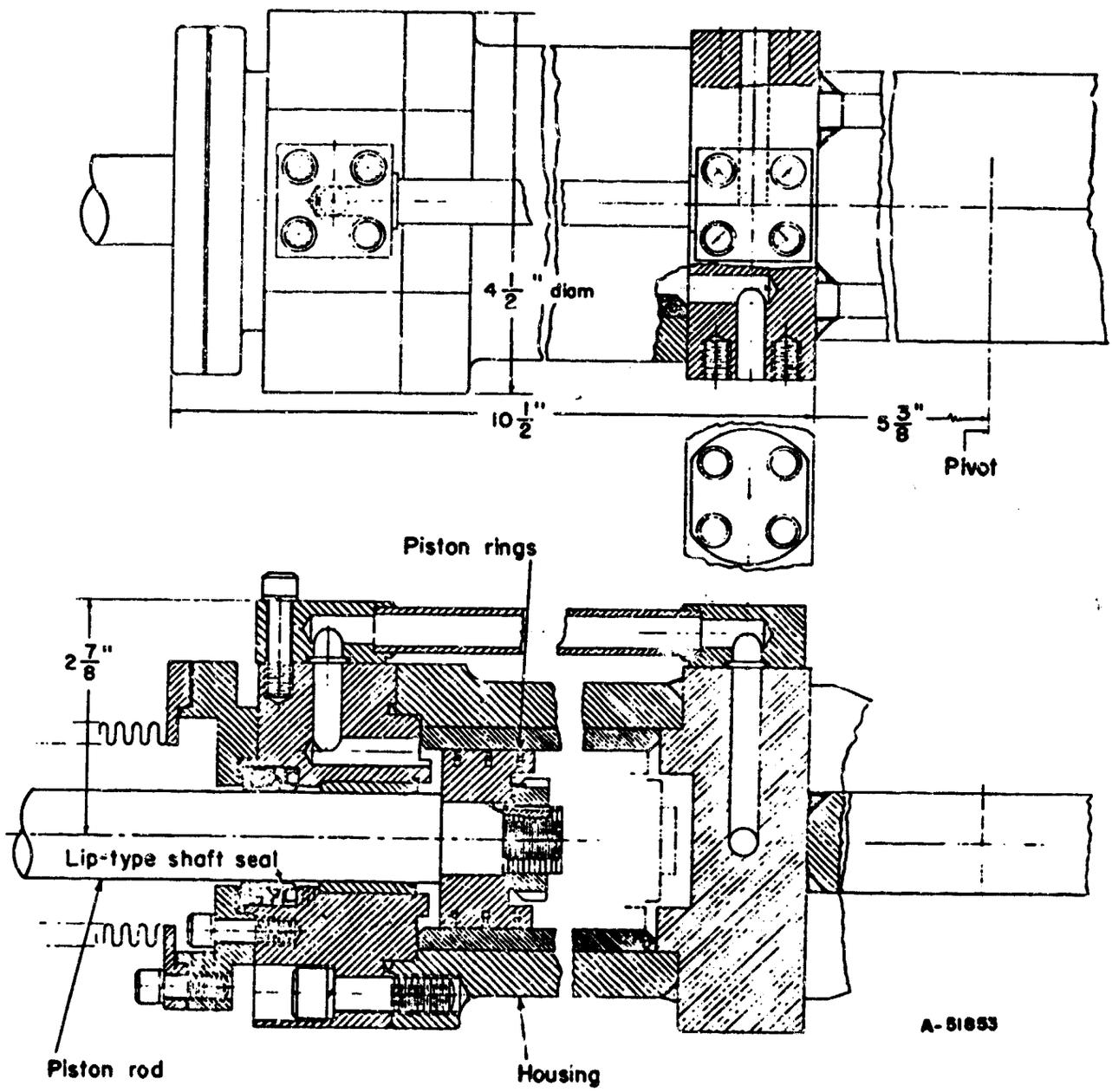

FIGURE 39. HIGH-TEMPERATURE LINEAR ACTUATOR

The system was cycled at 20 percent of maximum stroke amplitude, and the resulting frequency response plot expressed as a flow-amplitude ratio for both directions of motion is given in Figure 40. It was observed that the flow-control valve remained at full stroke during most of the cycle and that the actuator was therefore limited by the maximum flow capacity of the control valve. This effect occurs for large actuator motions when the response of the control valve is much higher than that of the actuator. The valve then acts as an on-off device, and the system performance is nonlinear. The effective system gain is also greatly reduced at the high error amplitudes.

Analysis of Actuator Reliability

The performance of the NaK actuator can degrade as a result of several types of failure. Friction can build up due to misalignment of seals or to bearing damage, or leakage can occur either through the end shaft seal or across the piston.

If the actuator is functioning properly, seal-end bearing friction and leakage of NaK from the end shaft seal will be small. If the shaft friction or end-seal leakage does begin to increase during operation, the rate of increase will generally be quite rapid and could be considered as a catastrophic failure. Wear in the piston rings, however, will normally progress at some relatively moderate rate and, as long as the seals and bearings are satisfactory, degradation can be considered as arising from piston-ring wear. If, however, the performance of the shaft seal or bearing begins to degenerate, this degradation will completely overshadow any effects of piston wear. Therefore, across-piston leakage was the only type of failure of interest in this drift reliability analysis.

An across-piston leakage rate of 1.5 cis at 500 psi and room temperature, as obtained from test data, was used as the "design point" nominal leakage and was used in determining the piston-ring clearance for the "design point" performance in Figure 40.

To compute the changes in performance that would result from across-piston leakage, frequency response was computed for the servoactuator system for each of three off-design-point conditions:

(1) Low leakage, 0.15 cis at 500 psi
(2) High leakage, 3 cis at 500 psi
(3) High leakage, 6 cis at 500 psi.

Normal leakage was assumed to be 1.5 cis at 500 psi, which was supplied from room-temperature tests. The leakage may be considerably higher at high temperature, thus providing a different design-point performance. However, partial derivatives taken for the room-temperature performance should be useful.

Figure 41 is a graph of the servoactuator-system frequency response for the large area and for the three off-design-point leakage rates previously discussed. By comparing these and data for the smaller area with the "normal" responses of Figure 40, the normalized partial-derivative data of Table IX were compiled. The partial derivatives were computed with respect to the diametral clearance, a, the effective value of which was computed to be 0.004 in. at room temperature.

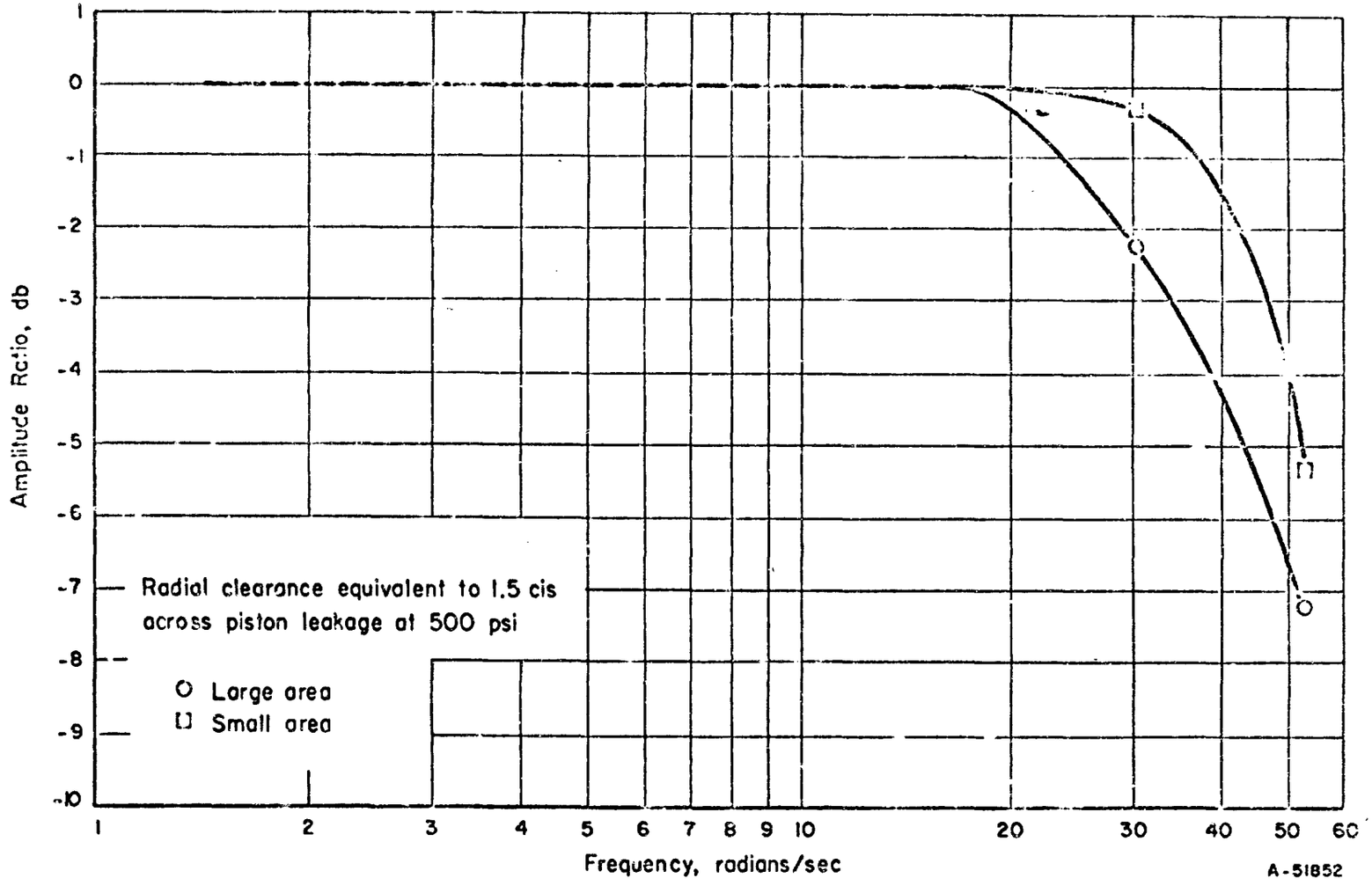

FIGURE 40. SYSTEM FREQUENCY RESPONSE

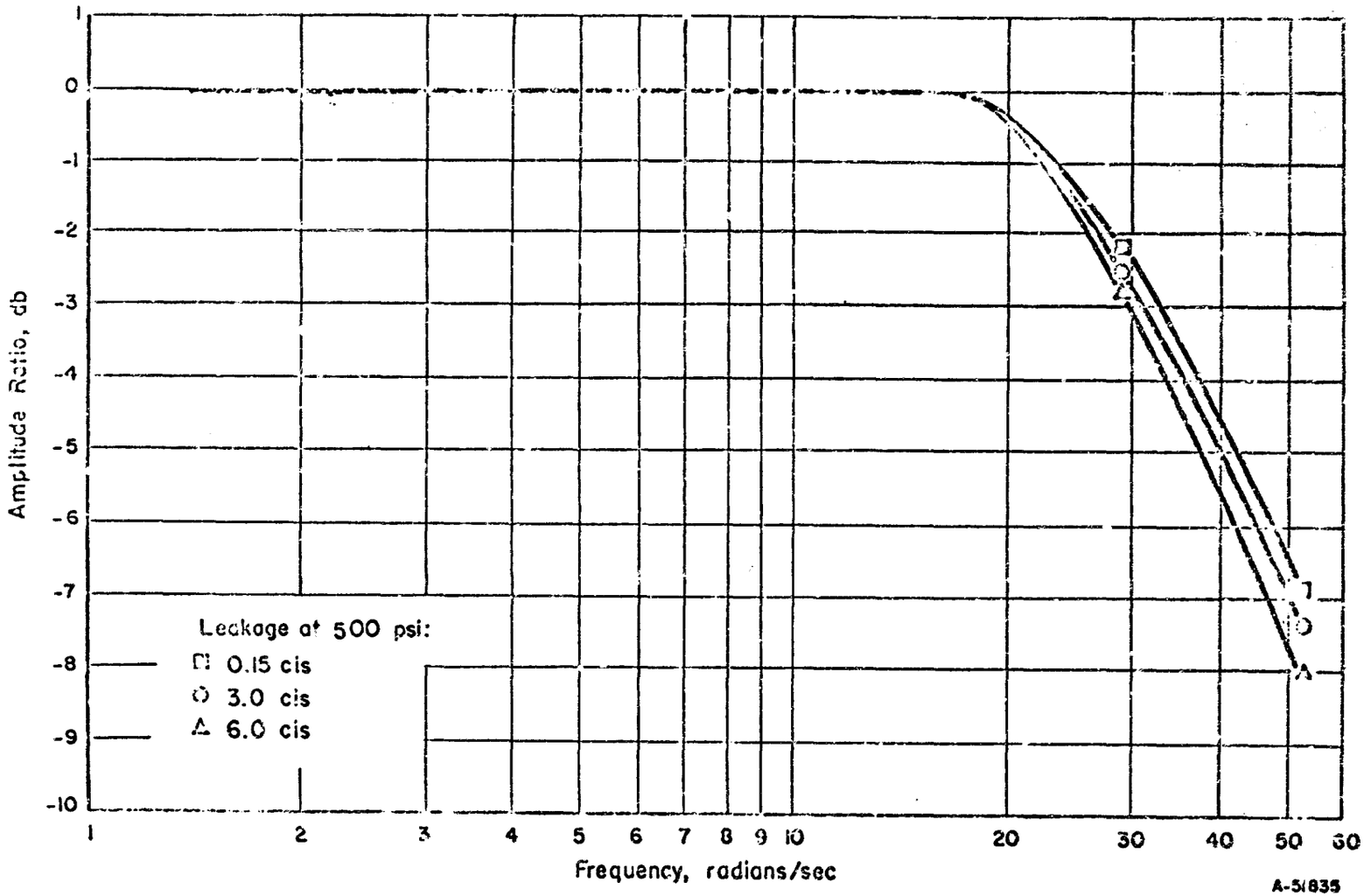

FIGURE 41. EFFECT OF PISTON-RING LEAKAGE ON ACTUATOR FREQUENCY RESPONSE (LARGE AREA)

TABLE IX. SUMMARY OF NORMALIZED DERIVATIVE DATA OF ACTUATOR PERFORMANCE, $\frac{\partial FR}{\partial a_{ba}\%}$

	20 Radians/ Sec	29.3 Radians/ Sec	52.1 Radians/ Sec
Large area	0.0 db/%	-0.0081 db/%	-0.014 db/%
Small area	0.0 db/%	-0.0085 db/%	-0.023 db/%

Analysis of System Reliability

After the critical partial derivatives of the performance of each of the elements in a system have been obtained, it is then necessary to determine which of the elements are the most critical as far as degradation of total system performance is concerned. In this study the relative sensitivity of system performance (actuator frequency response) to degradation in the pump, as compared with that in the actuator, was investigated.

This was done by first determining the absolute partial derivatives of actuator frequency response with respect to system supply pressure, $\partial FR/\partial P$. The resulting partials for the areas indicated at a nominal across-piston leakage of 1.5 cis are as follows:

	20 Radians/ Sec	29.3 Radians/ Sec	52.1 Radians/ Sec
Large Area	-0.00072 db/psi	-0.00168 db/psi	-0.00168 db/psi
Small Area	0.0	-0.00112	-0.00276 db/psi

The normalized partial derivatives of actuator frequency response with respect to the critical pump parameters can then be calculated from the following equations:

$$\frac{\partial FR}{\partial R_2\%} = \frac{\partial FR}{\partial P} \frac{\partial P}{\partial R_2\%}$$

$$\frac{\partial FR}{\partial \beta\%} = \frac{\partial FR}{\partial P} \frac{\partial P}{\partial \beta\%}$$

$$\frac{\partial FR}{\partial a_{ba}\%} = \frac{\partial FR}{\partial P} \frac{\partial P}{\partial a_{ba}\%}$$

The resulting normalized partial derivatives of frequency response with respect to across-piston leakage, impeller-tip radius, blade-tip angle, and interstage clearance at 5-gpm valve flow, across-piston leakage of 1.5 cis, and frequency of 52.1 radians per second are:

	Large Area	Small Area
$\partial FR/\partial C_{RA}\%$	-0.022 db/%	-0.0562 db/%
$\partial FR/\partial R_2\%$	-0.0393 db/%	-0.0647 db/%
$\partial FR/\partial \rho\%$	-0.0530 db/%	-0.0871 db/%
$\partial FR/\partial a_{ba}\%$	-0.00131 db/%	-0.00214 db/%

It is seen from the above results that degradation of the pump parameters has a strong effect on system performance as well as the degradation in the actuator piston rings on a percentage basis. This once again holds true only as long as the front shaft seal and bearing on the actuator are operable.

For an estimate of the numerical effect of piston leakage on system frequency response, calculations are made for an assumed piston equivalent clearance tolerance. The system variance in actuator frequency response is obtained from the equation:

$$\sigma^2_{FR} = \left(\frac{\partial FR}{\partial P}\right)^2 \sigma^2_P + \left(\frac{\partial FR}{\partial C_{RA}}\right)^2 \sigma^2_{C_{RA}} \quad .$$

With a nominal piston-ring clearance tolerance of 0.0004 in., the standard deviation of the across-piston clearance is assumed to be 0.00013 in. and the system pressure standard deviation is assumed to be 25.68 psi. The resulting deviation of the system frequency response in terms of actuator and pump manufacturing tolerances is then 0.0436 db and 0.0728 db, and the expected tolerance in system performance is -7.2 ± 0.13 db and -5.4 ± 0.22 db for the large and small areas, respectively, at 52.1 radians/sec.

The calculations show also that the assumed tolerance in the actuator would contribute approximately 2.6 percent of the variance when the large area is active and 6.2 percent when the small area is active.

Conclusions

One obvious but important result of Task II of this program was a demonstration of the ability of the Moment method reliability analysis technique in conjunction with mathematical and analog models to predict the variation that can be expected in the performance of a servo control system and in the individual system components, and to aid in the evaluation of the sensitivity of these performance characteristics to gradual degradations in the physical parameters of the system.

The analysis has shown that the variance in system performance, which in this case is taken to be actuator frequency response, is due to tolerances in the effective clearance around the actuator piston rings and tolerances in pump parameters. System performance is sensitive to degradations in the tip radius of the pump impeller and in the angle of the blade tip; these parameters produce about twice the change in system performance as an equal percentage increase in the piston-ring clearance. Leakage between stages of the centrifugal pump has only a slight influence on the pump and system

performance. It would, however, have more significance if pump efficiency were being considered as the pump performance characteristic.

While there were no data available on the extent of parameter degradation, a study of the pump and actuator configurations leads to the conclusion that changes in blade-tip radius and angle due to liquid-metal erosion would be very slight. Also, since interstage leakage does not significantly affect frequency response, it could be expected that wear in the piston rings of the linear actuator would be the most critical in the system. This assumes that the design of the actuator rod seal and bearing is fully developed, so that their performance is satisfactory over the required life of the system. If the design is not fully developed, then this area may be the most critical because degradation in the bearing and seal can lead to a "catastrophic" type of failure.

The above reliability observations provide useful design guidance during the development stages of new equipment. Decisions to reduce or increase manufacturing tolerances on parts that affect the various system parameters can be made on the basis of the degree of contribution of parameter tolerances to the total variance in system performance. The normalized partial derivatives of system performance indicate the sensitivity of performance to changes in system parameters; when these partials are considered along with the relative degradation rates of the parameters, critical wear areas can be pinpointed. For improvements in reliability, these critical areas should be studied first to see where changes in design configuration or in material selection could produce longer component life.

TASK III. REDESIGN OF AN ELECTROHYDRAULIC SERVO VALVE

Introduction

This section of the report covers the application of the Moment method of reliability prediction to a two-stage electrohydraulic servo valve. Task III objectives were in two parts:

(1) The objective of the first part was to use the Moment method and the mathematical model previously developed for a two-stage servo valve to improve the design of the valve from the standpoint of reliability.

(2) The second part consisted of analytically predicting the drift reliability of the improved servo valve relative to that of the original design and conducting life tests to verify the predicted relative reliability.

Engineering Activity

The engineering activity for Task III consisted primarily of three subtasks. First, the Moment method of statistical analysis was applied to a two-stage servo valve. Second, two modified and two unmodified servo valves were life tested. The third part consisted of analysis of the data gathered during the life testing in order to show the degree of correlation between the predicted and actual improvements in reliability.

Valve Redesign

This section describes the procedure and results of the effort to identify parameter changes that would improve the reliability of an electrohydraulic servo valve. The methods used for this subtask were those associated with the Moment method of reliability prediction. The Moment method is a statistical technique used for theoretically predicting certain attributes of the distribution of performance characteristics of a device or system. Use of the Moment method requires a mathematical model of the device or system under consideration, and also requires data on the actual or assumed distributions of the parameters governing the performance characteristics for which the distribution attributes are to be derived.

The first step in the procedure was the recognition and description of possible mechanisms by which degradation can occur in the servo valve and the identification of those areas and the specific parameters in the valve that are subject to the effects of degradation. It was assumed, in this study, that the valve design is at an advanced stage of development where gradual, drift-type failures — not sudden, catastrophic failures — are of concern.

Mechanics of Degradation. A list of the degradation modes and the affected parameters considered in the analysis is given in Table X.

TABLE X. MODES OF DEGRADATION AND AFFECTED PARAMETERS

I. Modes of Degradation

- A. Wear
- B. Dimensional Instability
- C. Parameter Instability
- D. Component Shift
- E. Human Error

II. Identification of Affected Parameters

A. Wear

1. Metering Edge Rounding and Port Coefficient
2. Spool-Bushing Clearance
3. Flapper Wear
4. Nozzle Coefficient
5. Orifice Coefficient
6. Feedback-Spring Ball
7. Spool Drag Coefficient

B. Dimensional Instability

1. Spool and Bushing Diameters
2. Nozzle Diameter
3. Orifice Diameter
4. Armature Thickness and Pole-Piece Height
5. Flapper Thickness
6. Spool Length
7. Nozzle Location
8. Armature-Assembly Location
9. Bushing Location
10. Magnet and Pole-Piece Location

C. Electromagnetic Instability

1. Magnet and Pole-Piece Permeability
2. Coil Resistance
3. Magnet Strength
4. Coil Inductance

D. Component Shift

1. Nozzle Location
2. Armature-Assembly Location
3. Bushing Location
4. Magnet and Pole-Piece Location

E. Human Error

1. Affects the Degree of Severity of A, B, C, and D, Above

Wear is defined as the change in the shape of a valve component due to erosion by contaminants in the hydraulic fluid, and as a change in the surface condition of a component due to abrasion, scoring, or impingement by solid contaminant particles.

Dimensional instability is defined as the change in physical dimensions that occurs as a function of time, stress, and temperature and is usually associated with creep or grain growth.

Electromagnetic instability is defined as the change that takes place in the electrical and magnetic characteristics of the valve over a period of time as a result of the thermal and magnetic environment in which the valve is located.

Component shift is defined as the changes that occur in the relative positions of valve components due to differences in thermal-expansion rates and to acceleration forces produced by mechanical shock or vibration.

Human error is an indirect mechanism of degradation, as it describes the increases that can occur in the severity of the above four modes of degradation due to human errors introduced in the manufacturing or assembly process that go undetected in the final checkout.

Selection of Most Significant Mechanisms of Degradation. The next step in the program was a study of the modes of degradation and the identification of those modes with the corresponding parameters that significantly contribute to the degradation of valve performance. This evaluation was based on Battelle's knowledge and experience from past programs and on a study of applicable literature.

The study revealed that wear is the primary cause of valve-performance degradation and that this manifests itself in:

(1) An increase in the discharge flow coefficient of the orifices and nozzles
(2) Deformation and pitting of the flapper surface
(3) Rounding of the spool metering edge
(4) An increase in the radial spool clearance
(5) An increase in the coulomb friction force on the spool due to scoring.

The rounding of the spool metering edge was modeled as an increase in valve underlap and in spool radial clearance.

Experimental and analytical work to date indicates that serious problems are not to be expected in the valve because of electromagnetic and dimensional instability. Valve materials, especially those machined to close tolerances, are chosen for their high stability. The normal environment in which these valves are used is generally not severe enough to cause excessive degradation of the electromagnetic or mechanical properties.

It was also concluded that there are no serious effects from thermal cycling and mechanical and thermal shock, because the valve is stabilized for mechanical vibrations and thermal cycling during the final stages of manufacture. In addition, the valves in normal service are not subjected to extreme shock or vibration.

The problem of human error is, of course, always present, but it was concluded that the occurrence of this in a highly developed and carefully inspected valve-manufacturing process is small, and that it would be difficult and beyond the scope of this program to attempt to define the rate of occurrence and the effects of human error in any quantitative way.

The objective of Task III included the investigation of effects of design changes in the critical parameters on the reliability of the servo valve. Because very little information is available on the time rate of degradation of these parameters, the technique is limited to predicting relative rather than absolute reliability. It is noted that this restriction on the application of the technique is set, not by limitations in the mathematical and analog models, but rather by limitations in the ability to predict rates of degradation. A parameter as it appears in the model can be manipulated if there is some knowledge of how it should be manipulated, i.e., if the rate of change of the parameter with, say, flow, is available, this information can be corrected to a time basis and used in the reliability analysis.

Consideration of Possible Design Changes for Improved Reliability. Improvement in reliability can generally be achieved in three ways. The first is to reduce the sensitivity of the valve-performance characteristics to degradation of the parameters and to variations introduced in manufacture, i.e., to reduce the partial derivatives. The second is to improve the nominal valve performance to create a greater tolerance for degradation, and the third is to make design and material changes that would reduce the rate of parameter degradation. Table XI shows the critical valve parameters and the valve-performance characteristics that are affected by changes in these parameters. While most of the characteristics are described in conventional terms, an explanation of some of the terms is helpful.

The blocked-spool pressure gain is a measure of the ability of the valve to overcome frictional forces on the spool when the spool is blocked. It is defined as the net axial force on the spool, created by the differential control pressure, per milliampere of differential current input per inch of spool circumference, i.e.,

$$\text{Blocked-spool pressure gain} = \frac{\Delta P_N}{i} \; \frac{d_s}{4} \; \frac{\text{lb}}{\text{ma in.}} \quad ,$$

(See list of symbols).

It is assumed that the frictional force on the spool is created by particles that have been forced into the spool clearance space and that the magnitude of this force is proportional to the number of particles entrapped around the spool. For any clearance, the number of entrapped particles is a function of the spool circumference.

The threshold current is the amount of input current required to initiate spool motion, and is related to the blocked-spool pressure gain.

Null bias is the amount of input current required to center the valve spool. A change in bias, or a shift in the null, develops if the orifice or nozzle on one side of the spool wears at a different rate from that on the other side.

TABLE VI. INFLUENCE OF CRITICAL PERFORMANCE CHARACTERISTICS ON VALVE PERFORMANCE

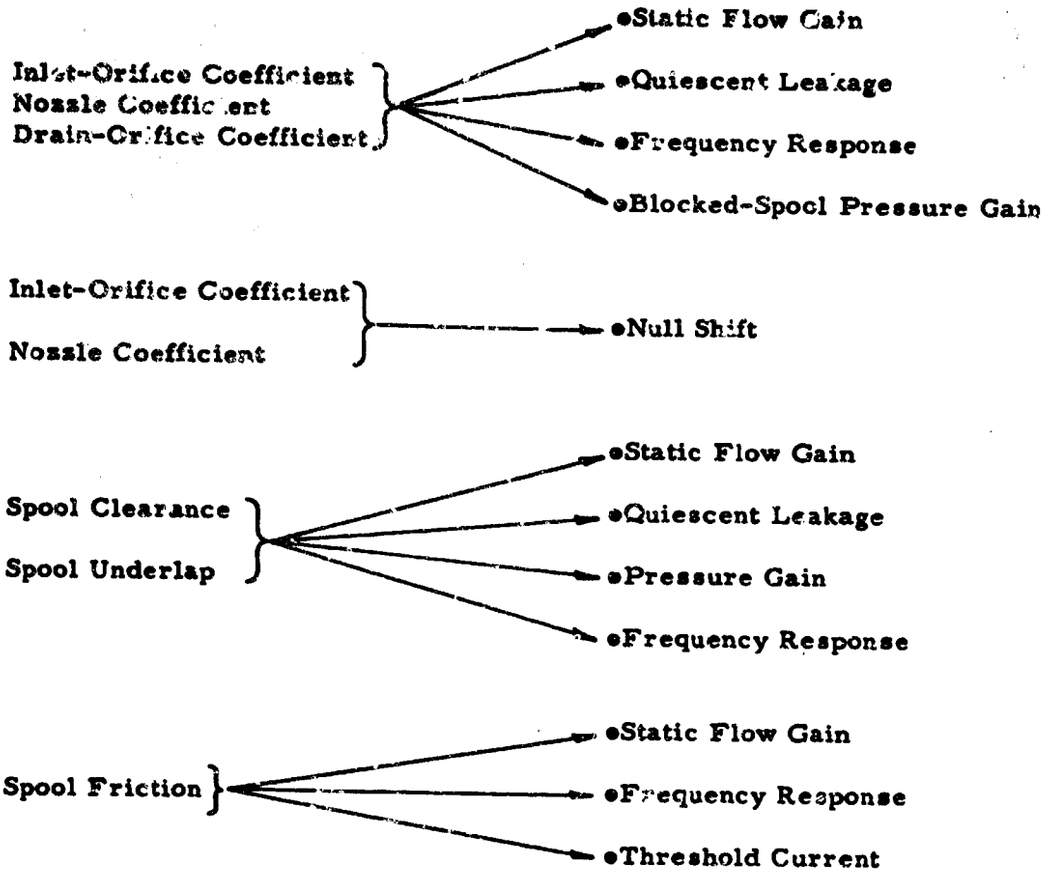

After initial study of the existing valve design, it was concluded that reductions in sensitivity to degradation and improvements in the nominal value of performance characteristics might best be achieved by:

(1) Changing the relative size of the nozzle and orifice diameters

(2) Decreasing the slot width and spool diameter, and decreasing the spring rate of the feedback wire to increase the spool stroke.

The relative size of the nozzle and orifice diameters is expressed as a ratio of nozzle diameter to orifice diameter, $\frac{D}{d}$.

Figures 42 through 45 show the effect of a design change in the $\frac{D}{d}$ ratio on the significant valve performance characteristics and on the normalized partial derivates of quiescent leakage, static flow gain, and control pressure gain with respect to changes in the nozzle, orifice, and discharge coefficients. Figure 46 shows the change in the input current required to bring the spool to the null position for a given percentage change in the orifice and nozzle coefficients on one side of the valve. The nozzle discharge area is equal to πDh; to facilitate manipulating this quantity on the analog computer model, the parameter h was chosen as the variable to represent discharge area. Thus, the partials are expressed relative to the parameter h. The data for these curves were obtained from the analog model of the servo valve developed during Project 8225, Task 822502, and described in FDL-TDR-64-30.

The existing design condition is represented by a $\frac{D}{d}$ ratio of 2.02. New values of this ratio were obtained by increasing the area of the orifice and decreasing the discharge area of the nozzle (the circumferential orifice between the nozzle tip and the flapper) by the same factor and vice versa.

In Figure 42, frequency response is represented as the decrease in flow (or spool travel) between 5 cycles per second and 150 cycles per second expressed in decibels. An additional dynamic characteristic, maximum armature deflection, is shown on the curves. This characteristic is the observed maximum armature deflection at 150 cycles per second and ±4-ma differential-current input, and represents the tendency of the flapper to hit the nozzle tip under dynamic conditions. The possible design alternatives were determined, in part, on the basis that the armature deflection in the new design would be no greater than that in the original design. This assumes, therefore, that the rate of degradation of the nozzle discharge orifice in the new design, due to impingement against the nozzle tip, is no greater than in the original design.

The results of design changes in the second stage of the valve are shown in Figures 47 through 52. All the curves were obtained with the $\frac{D}{d}$ ratio at the existing value of 2.02. Figure 47 shows the effect on the performance characteristics of a design change in the spool diameter. Figures 48 and 49 show the effect of a decrease in slot width and feedback-wire spring rate (to keep flow gain constant) on the performance characteristics at a given spool diameter. Figures 50 and 51 show the effect of a change in slot width on the normalized partial derivative of quiescent leakage with respect to the valve underlap and spool radial clearance. Computer runs made at two different spool diameters show that these partials are not affected by changes in spool diameter. Figure 52 shows the effect of changes in spool diameter and feedback-wire spring rate on the blocked-spool pressure gain.

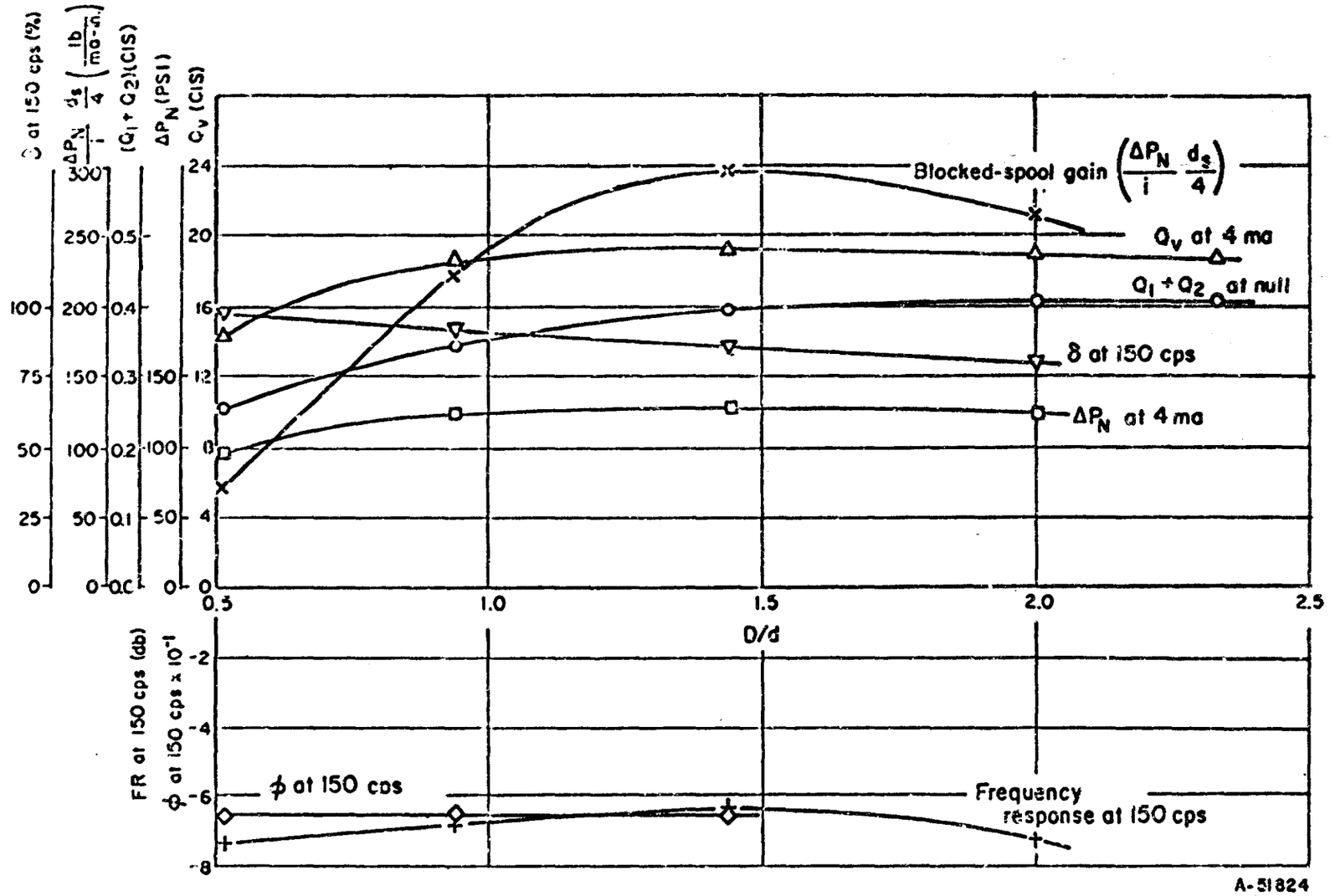

FIGURE 42. EFFECT OF D/d RATIO ON PERFORMANCE CHARACTERISTICS OF ELECTROHYDRAULIC SERVO VALVE

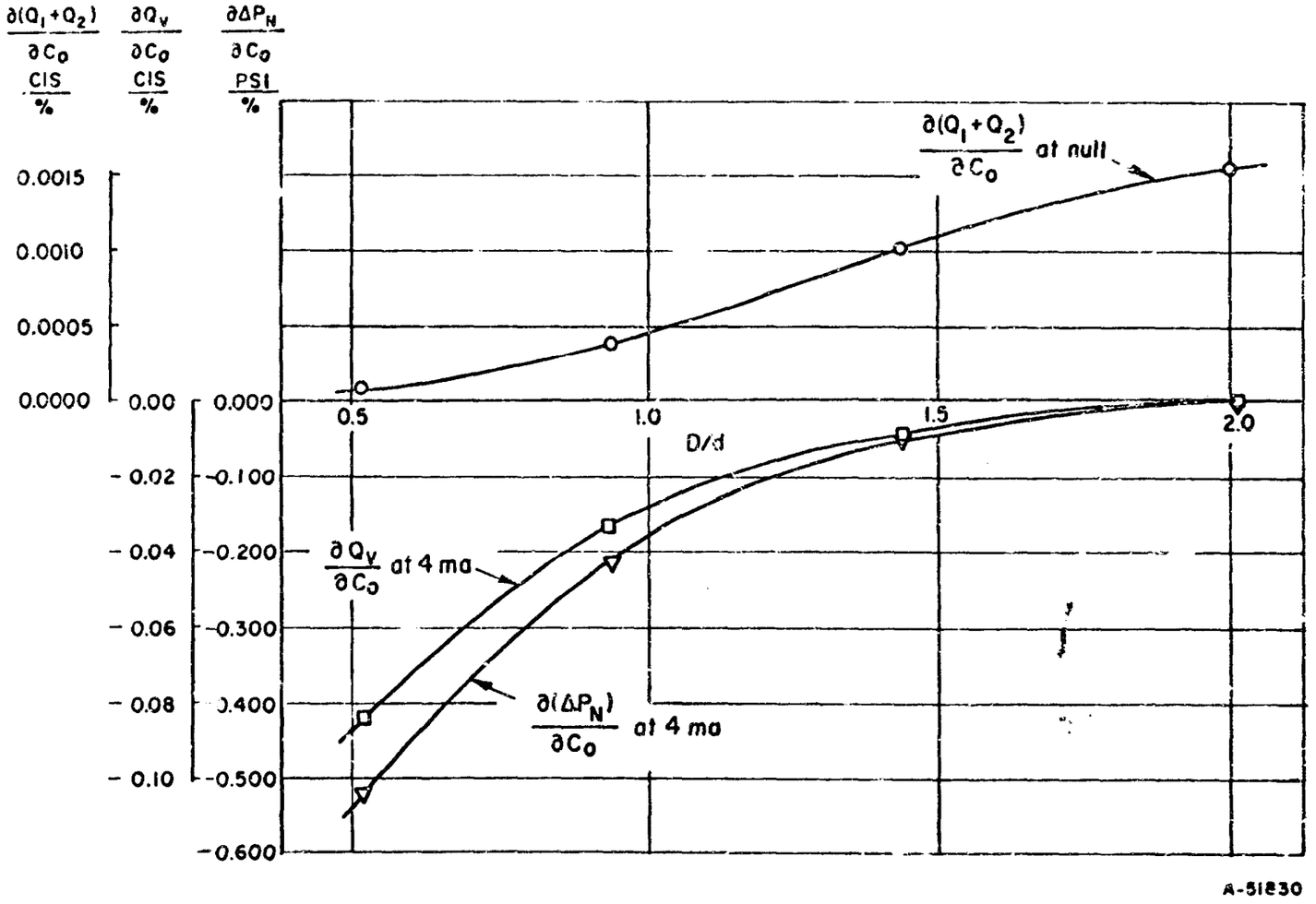

FIGURE 43. EFFECT OF D/d RATIO ON NORMALIZED PARTIAL DERIVATIVES OF PERFORMANCE WITH RESPECT TO ORIFICE DISCHARGE COEFFICIENT

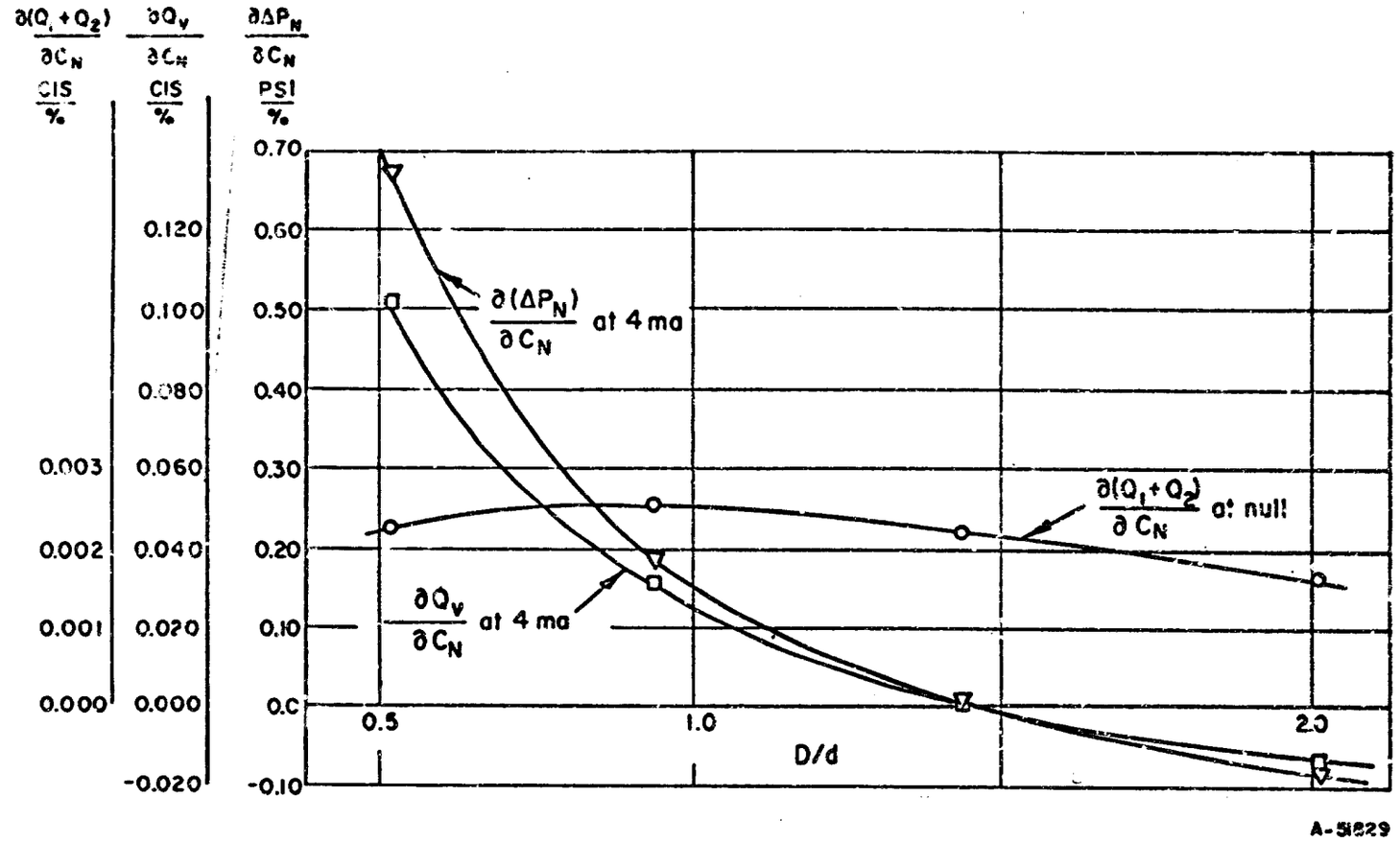

FIGURE 44. EFFECT OF D/d RATIO ON NORMALIZED PARTIAL DERIVATIVES OF PERFORMANCE WITH RESPECT TO NOZZLE DISCHARGE COEFFICIENT

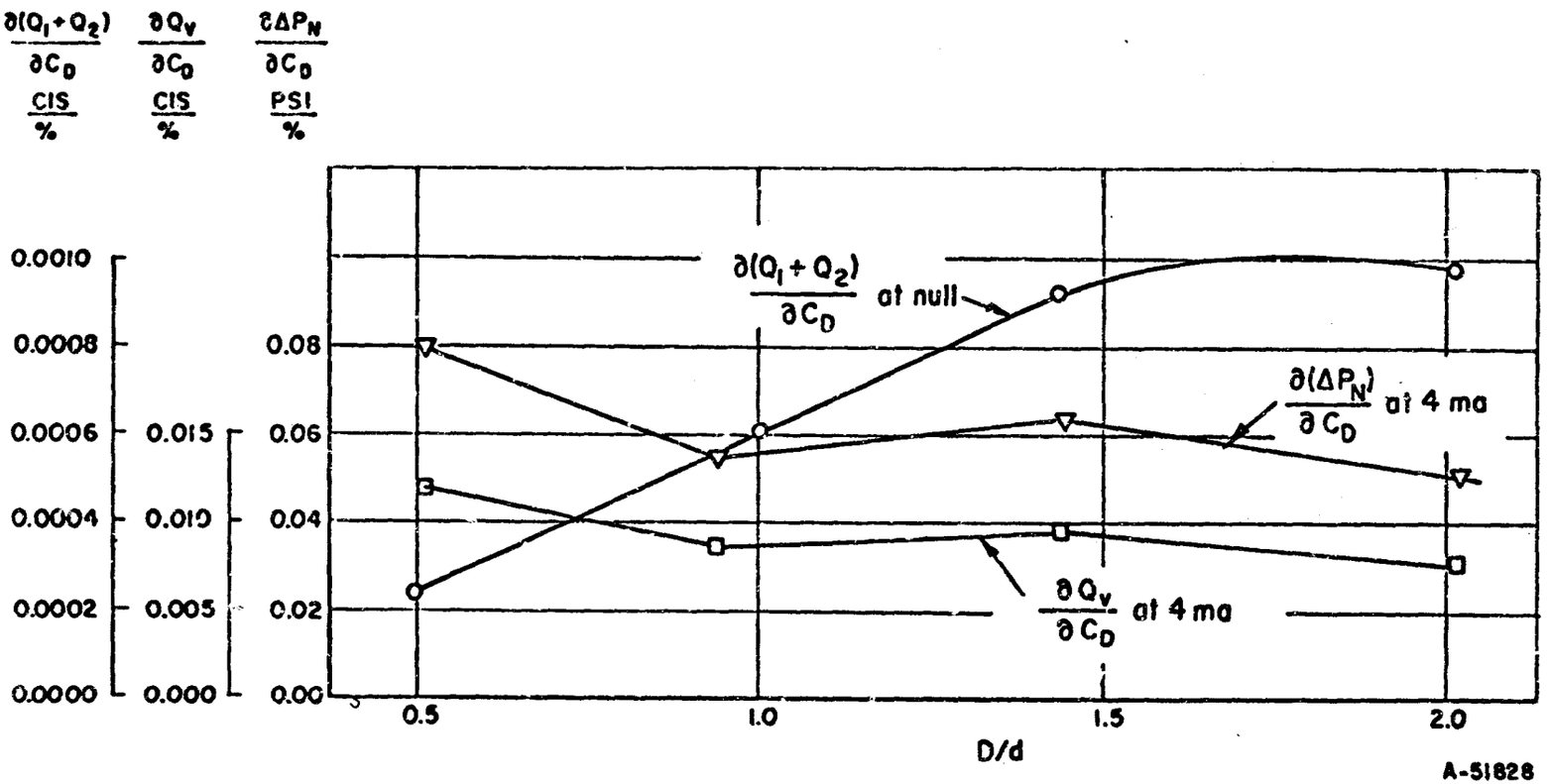

FIGURE 45. EFFECT OF D/d RATIO ON NORMALIZED PARTIAL DERIVATIVES OF PERFORMANCE WITH RESPECT TO DRAIN-ORIFICE DISCHARGE COEFFICIENT

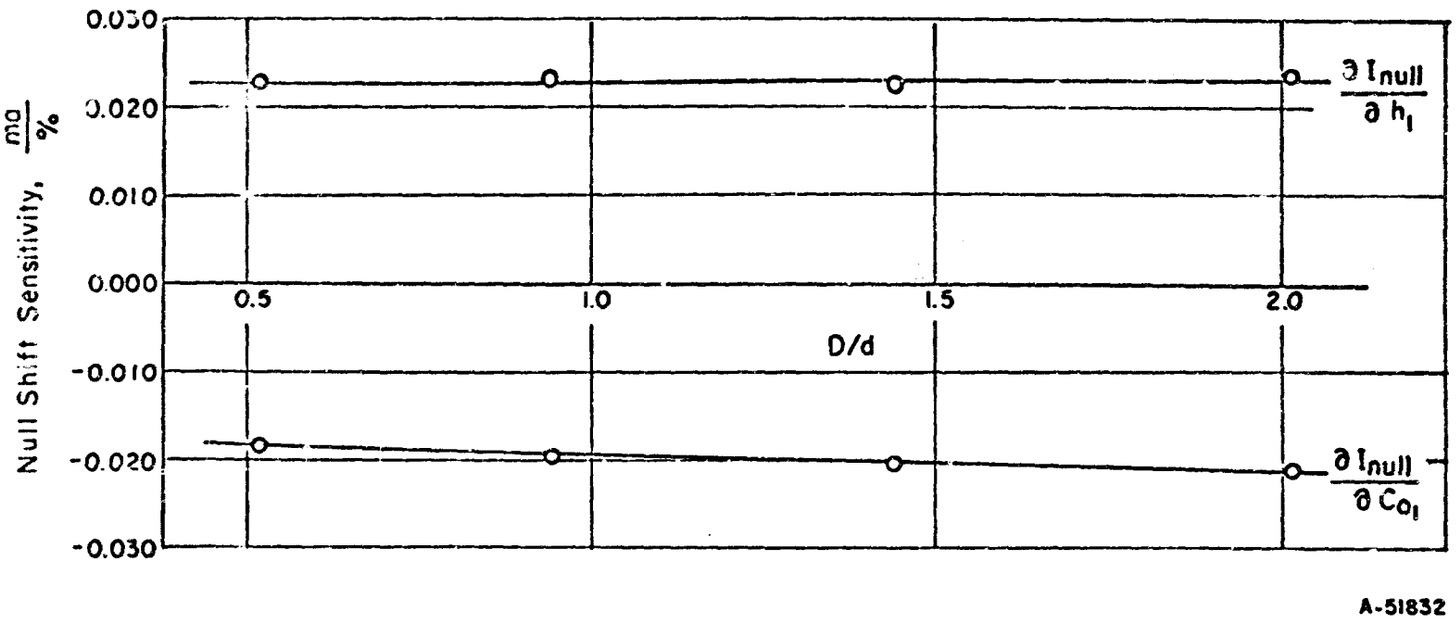

FIGURE 46. EFFECT OF D/d RATIO ON NORMALIZED NULL SHIFT SENSITIVITY FOR ± 20 % CHANGE IN h_1 AND C_{O_1}

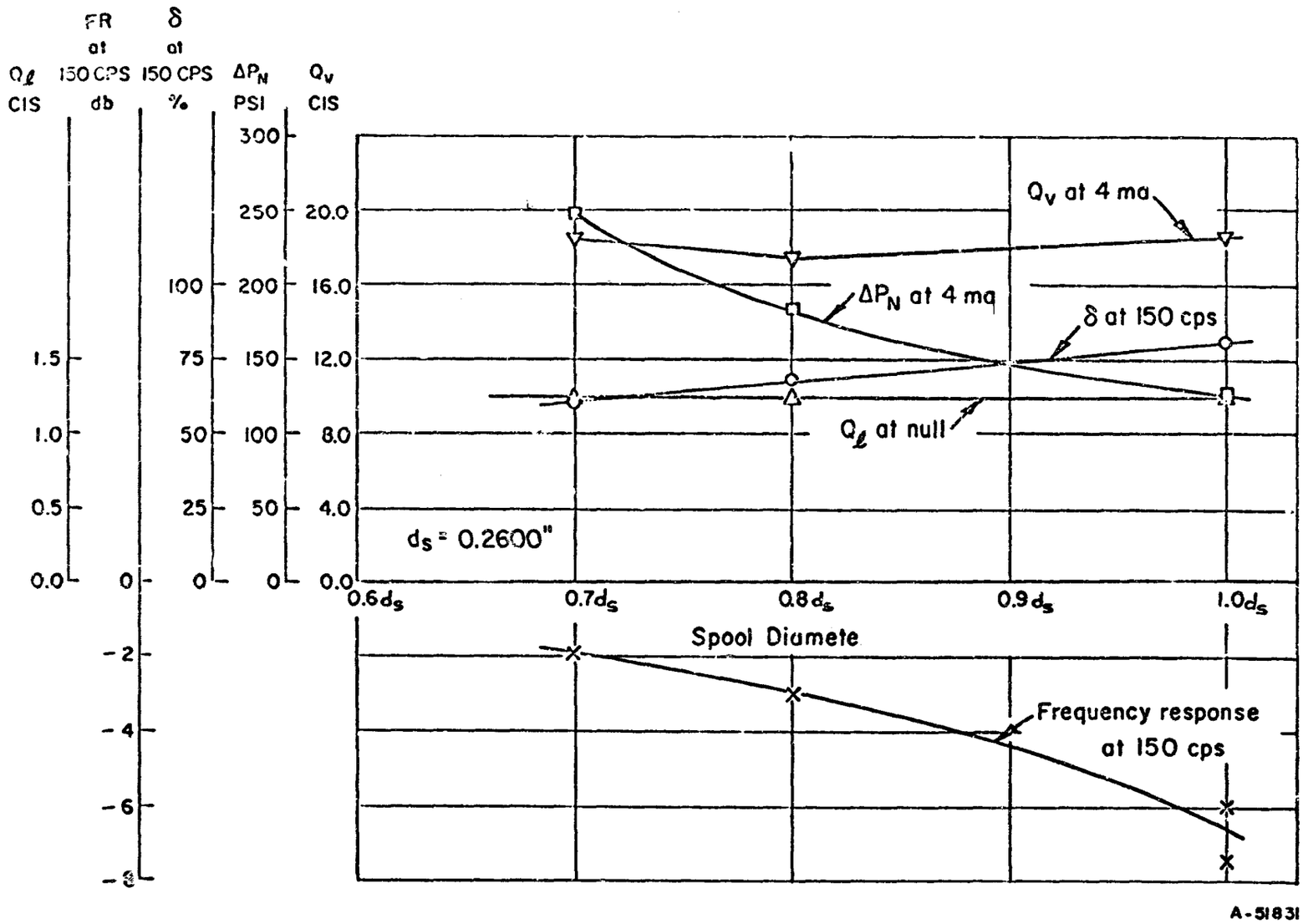

FIGURE 47. EFFECT OF SPOOL DIAMETER ON PERFORMANCE CHARACTERISTICS OF ELECTRO-HYDRAULIC SERVO-VALVE FOR A SLOT WIDTH OF 1.0 ω

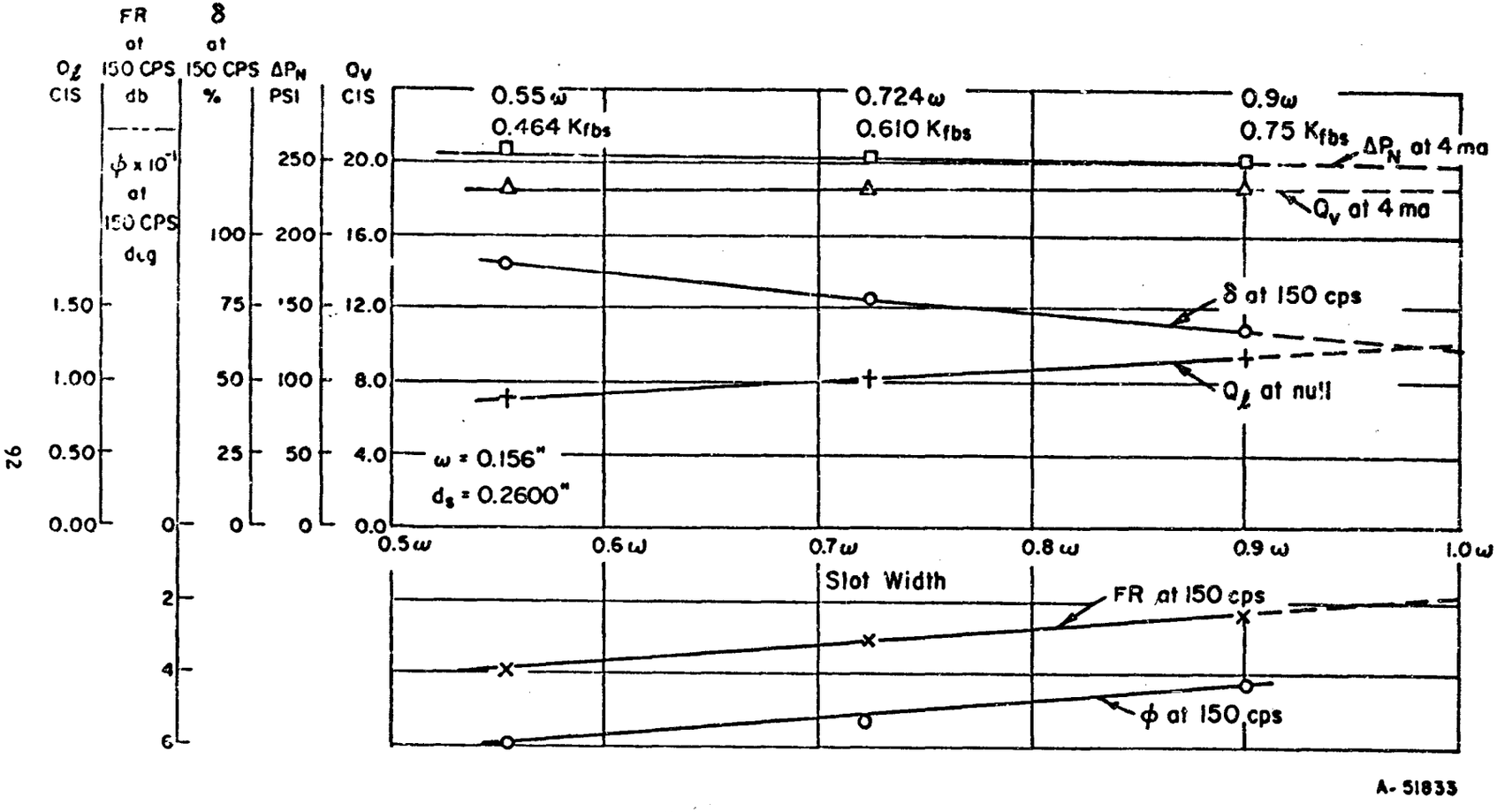

FIGURE 48. EFFECT OF SLOT WIDTH ON PERFORMANCE CHARACTERISTICS FOR CONSTANT FLOW GAIN (SPOOL DIAM, 0.7 d_s; D/d RATIO, 2.02)

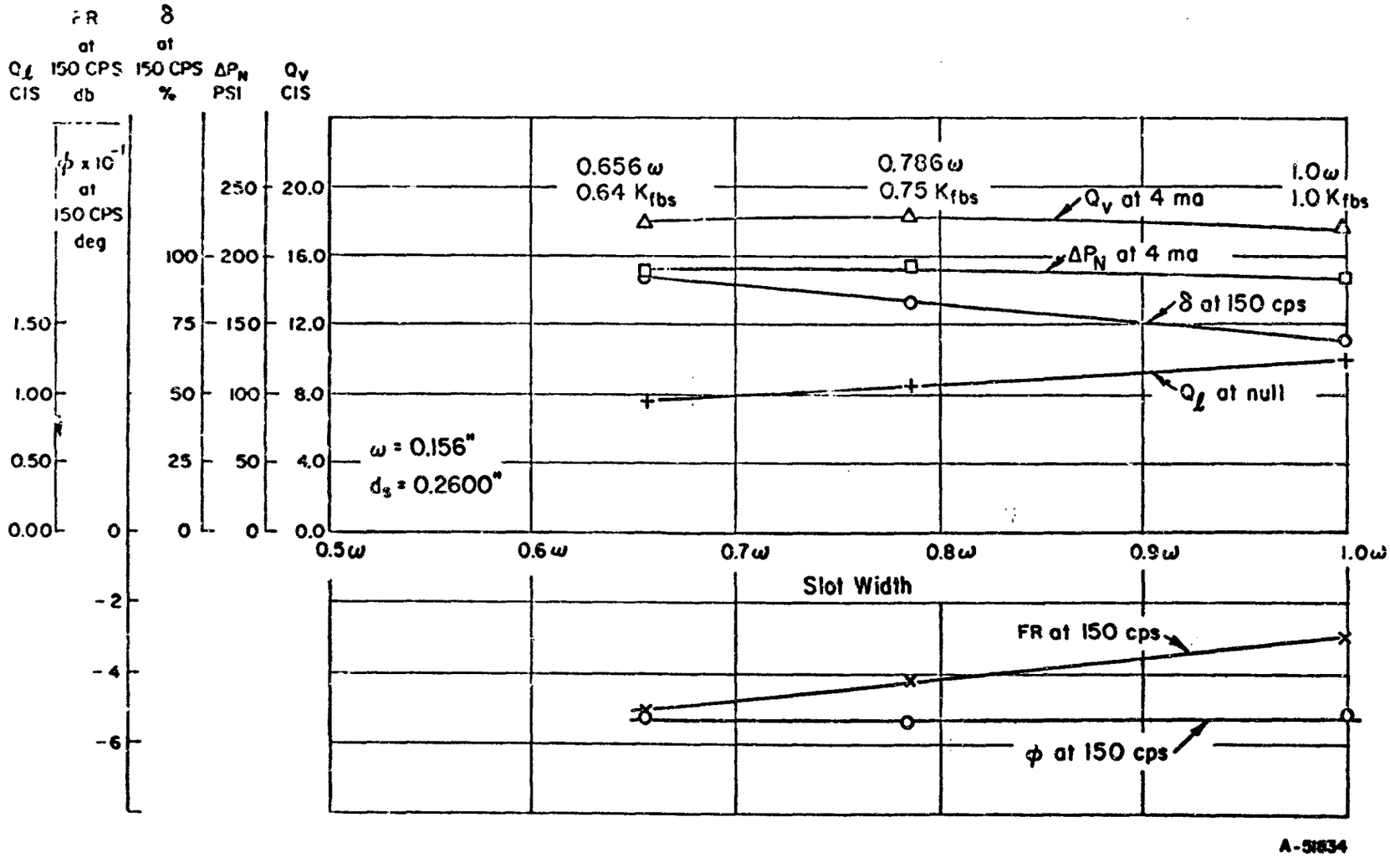

FIGURE 49. EFFECT OF SLOT WIDTH ON PERFORMANCE CHARACTERISTICS FOR CONSTANT FLOW GAIN (SPOOL DIAM, 0.8 d_s; D/d RATIO, 2.02)

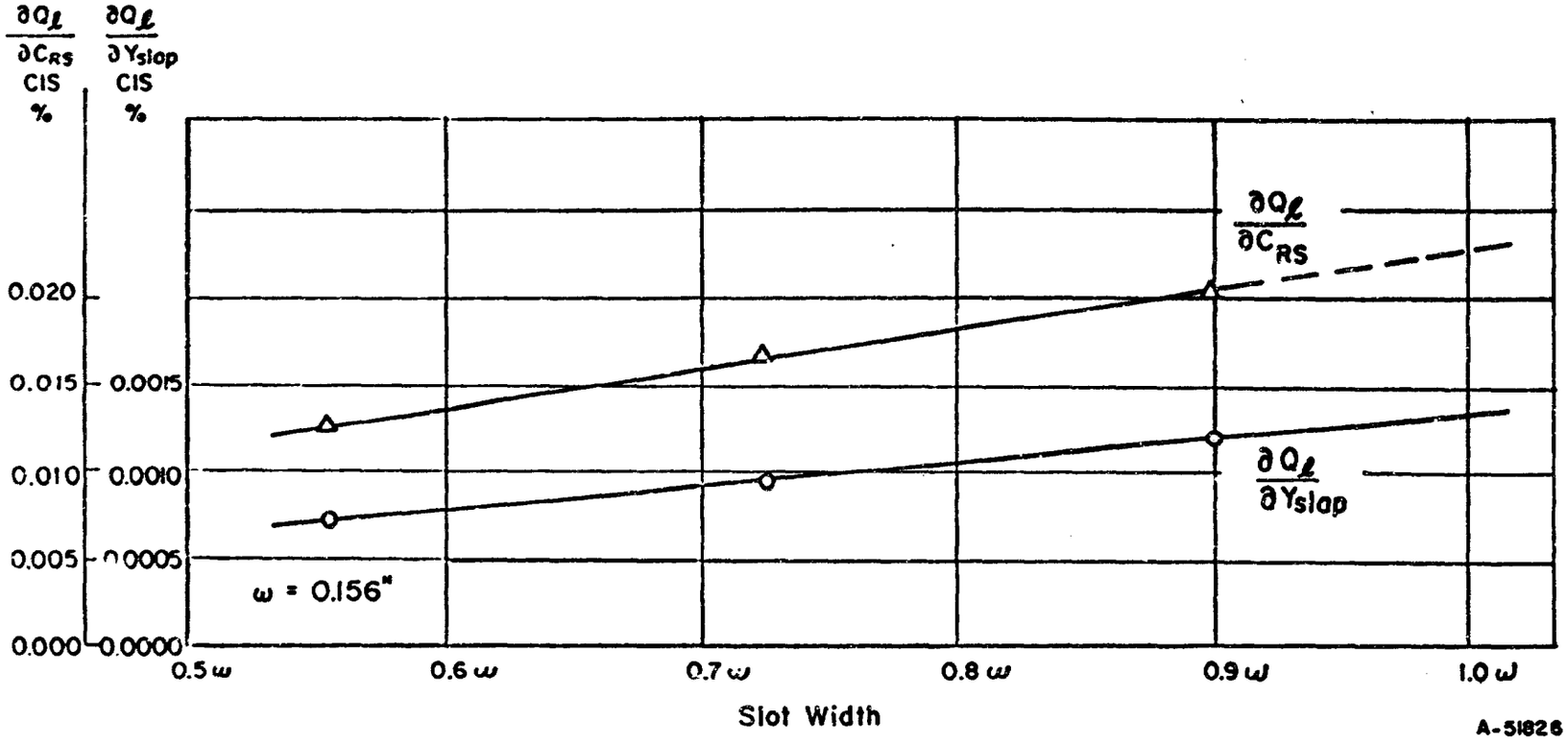

FIGURE 50. EFFECT OF SLOT WIDTH ON NORMALIZED QUIESCENT LEAKAGE PARTIALS WITH RESPECT TO Y_{SLAP} AND C_{RS} (SPOOL DIAM, 0.7 d_s)

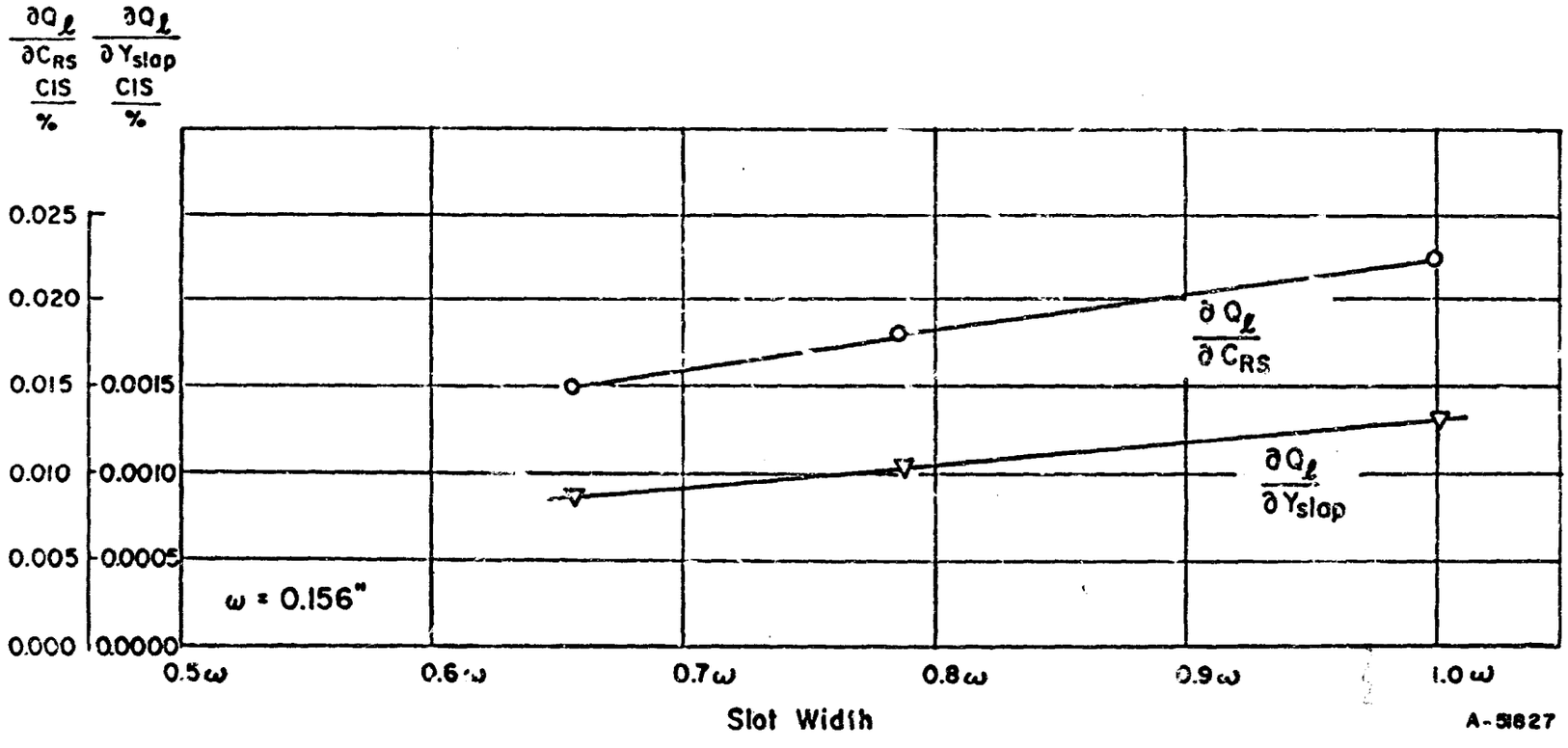

FIGURE 51. EFFECT OF SLOT WIDTH ON NORMALIZED QUIESCENT LEAKAGE PARTIALS WITH RESPECT TO Y_{SLAP} AND C_{RS} (SPOOL DIAM, 0.8 d_s)

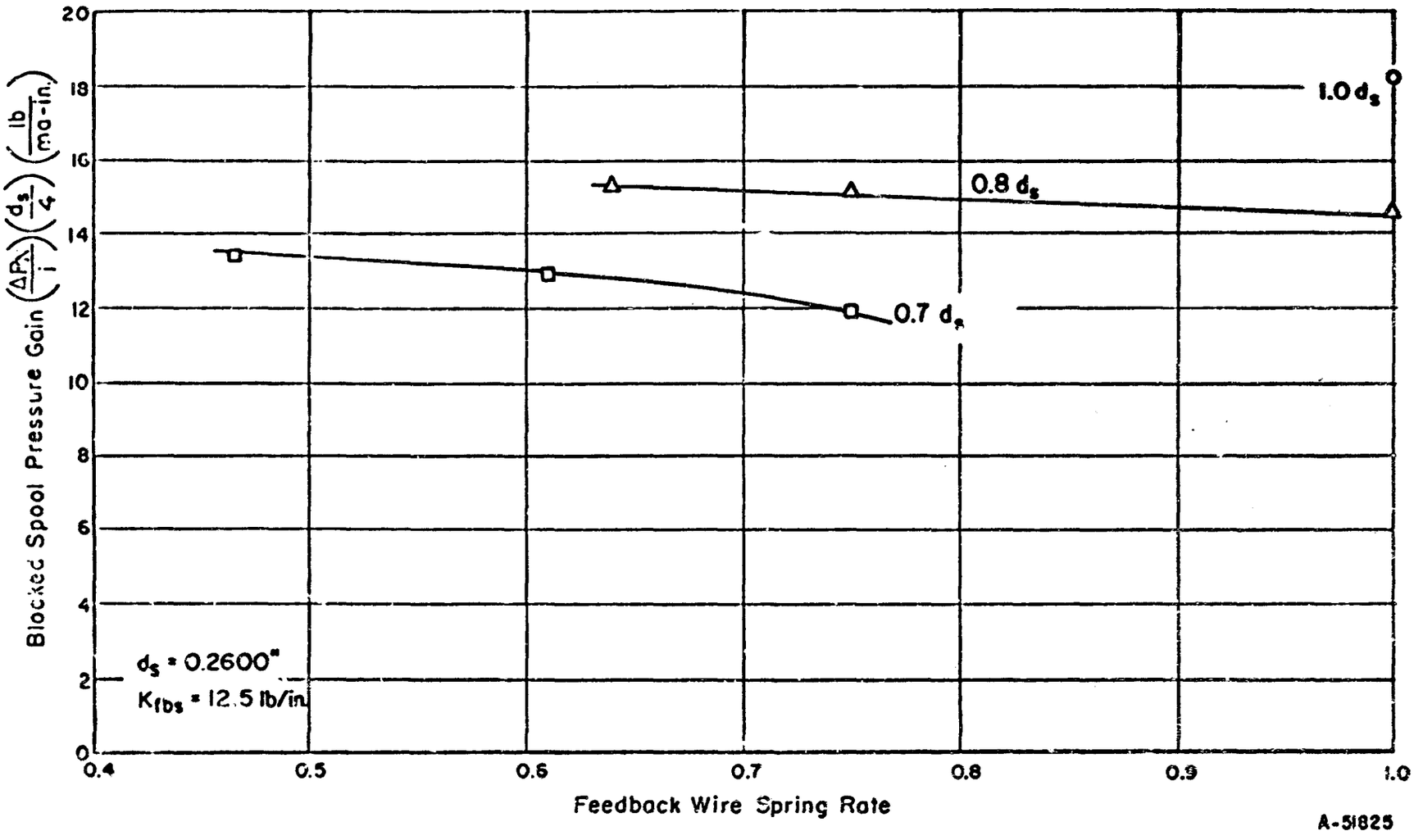

FIGURE 52. EFFECT OF SPOOL DIAMETER AND FEEDBACK-WIRE STIFFNESS ON BLOCKED-SPOOL PRESSURE GAIN FOR CONSTANT FLOW GAIN

Since the valve is rated according to its flow gain, all design changes in the second stage were made with the limitation that the static flow gain of the valve remain the same. If the slot width is reduced, the spool must travel further to provide the same output flow, and this is obtained by a proportionate reduction in the stiffness of the feedback wire. Thus, a direct relationship exists between changes in slot width and required changes in feedback-wire stiffness.

From the curves, it can be seen that quiescent leakage and the partial derivative of this leakage with respect to underlap and spool clearance can be reduced if the slot width (and correspondingly, the feedback-wire spring rate) is reduced. From the investigation of the first stage, it is seen that a reduction in the $\frac{D}{d}$ ratio can produce a net reduction in the normalized partial of flow gain with respect to nozzle and orifice degradation (the decrease in the partial derivative with respect to a change in nozzle coefficient is greater than the increase in the derivative with respect to change in orifice coefficient). The other effects produced by a decrease in slot width and in $\frac{D}{d}$ ratio must, however, be correlated to arrive at possible design alternatives.

Table XII summarizes the effects produced by the various possible design changes.

Determination of Characteristics of Improved Design. A decrease in the $\frac{D}{d}$ ratio and in the slot width must be accompanied by a decrease in the spool diameter in order to keep the maximum armature deflection within the specified limitation and the frequency response as flat as in the existing valve. A decrease in spool diameter is accompanied, however, by a decrease in blocked-spool pressure gain, and this must be balanced by the increase that results from the decrease in the $\frac{D}{d}$ ratio.

Figure 53 shows the method by which allowable combinations of $\frac{D}{d}$ ratio, spool diameter, and slot width for constant flow gain were determined. It is based on Figure 52 but with slot width rather than feedback-wire spring rate as the abscissa. Loci are drawn that locate the minimum allowable slot width at any spool diameter and $\frac{D}{d}$ ratio to keep the maximum armature deflection below 80 percent at 150 cycles per second (this is the value achieved in the present design). These loci are based on the data in Figures 42, 48, and 49, and on the assumption that the minimum allowable slot width is that value below which the decrease in maximum armature deflection due to the decrease in spool diameter no longer compensates for the increase in armature deflection due to the change in slot width and $\frac{D}{d}$ ratio. Thus, for any $\frac{D}{d}$ ratio, the allowable slot width must lie to the right of the corresponding locus line.

The consideration of allowable blocked-spool pressure gain establishes a second limitation on the design alternatives. The decrease in the blocked spool pressure gain resulting from a decrease in spool diameter must be balanced, essentially, by the increase that results from a decrease in the $\frac{D}{d}$ ratio. Thus, a new set of loci can be shown to locate the minimum allowable blocked-spool pressure gain for any combination of spool diameter, slot width, and $\frac{D}{d}$ ratio. In this case, the allowable combinations of slot width and spool diameter for any $\frac{D}{d}$ ratio must lie above the corresponding locus line. These two limitations now establish the possible new design combinations since, for any $\frac{D}{d}$ ratio, the combination of spool diameter, slot width, and the corresponding feedback-wire spring rate must lie to the right and above the intersection of the two appropriate loci. The set of intersections establishes an envelope of possible designs, and the most desirable point on this envelope is that which results in a minimum slot width. This point on the envelope is represented by the following parameters, which describe a new valve design:

TABLE XII. SUMMARY OF EFFECTS OF POSSIBLE DESIGN CHANGES ON VALVE CHARACTERISTICS

Valve Characteristic	Design Change[a]		
	Decrease in $\frac{D}{d}$	Decrease in Slot Width	Decrease in Spool Diameter
Static flow gain	+	Constant	Constant
Quiescent leakage	+	+	0
Frequency response (db)	-	-	+
Maximum armature deflection	-	-	+
Blocked-spool pressure gain	+	+	-
Quiescent leakage partial with respect to C_O and C_N	+	Not applicable	Not applicable
Quiescent leakage partial with respect to Y_{SLAP} and C_{RS}	Not applicable	+	0
Null shift current	0	Not applicable	Not applicable
Flow gain partial with respect to C_O and C_N	+	Not applicable	Not applicable

(a) + indicates desirable change.
- indicates undesirable change.
0 indicates insignificant change.

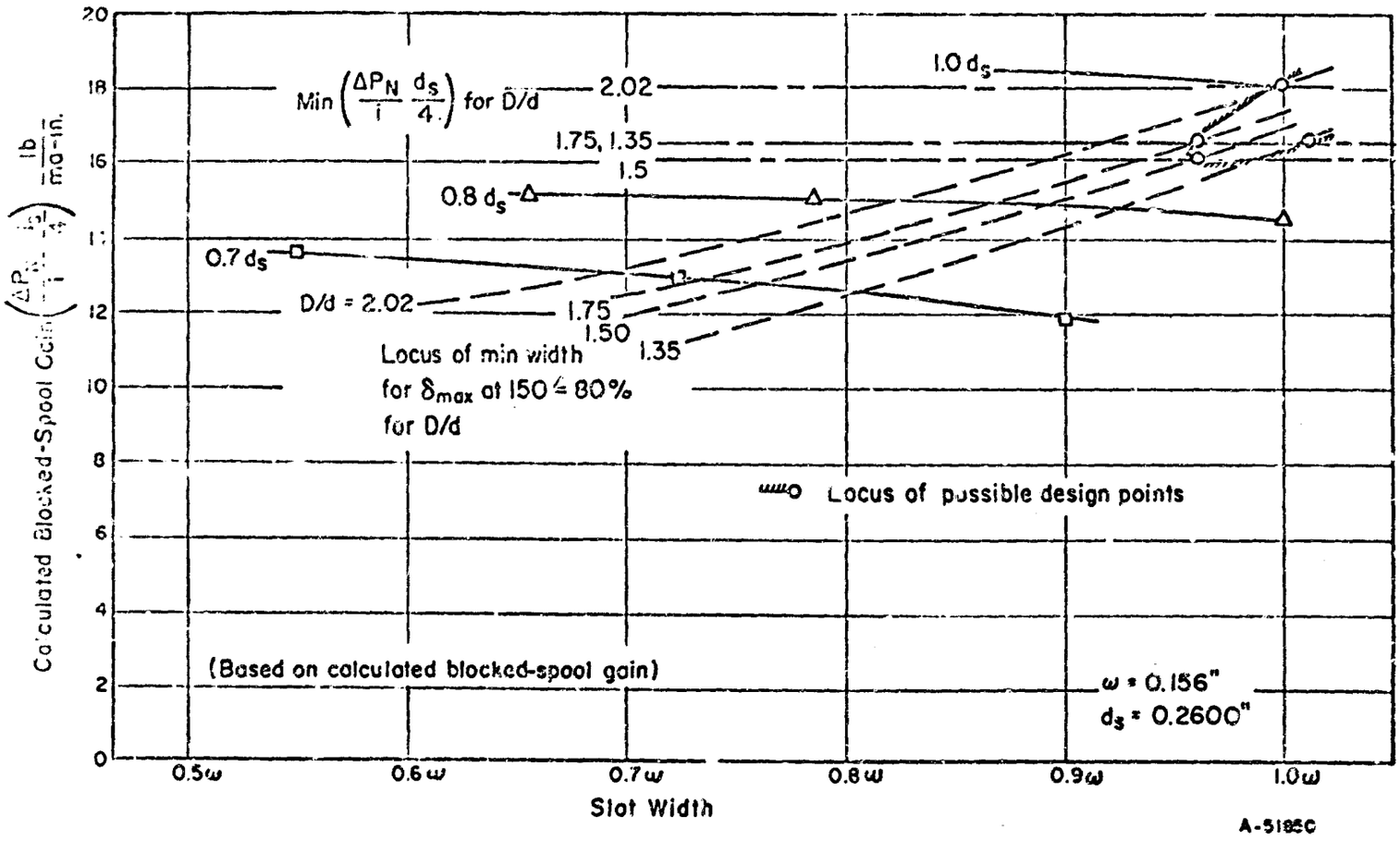

FIGURE 53. DETERMINATION OF ALLOWABLE DESIGN PARAMETER

$\frac{D}{d}$ = 1.57

D = 0.0135 in.

d = 0.00862 in.

d_s = 0.2250 in.

ω = 0.150 in.

K_{fbs} = 11.5 lb/in.

Table XIII gives a summary comparison of the performance characteristics and normalized partial derivatives of the new design with the existing design. The Per Cent Change column shows the improvement in the sum of the normalized partial derivatives, assuming an equal per cent change in each parameter.

For comparable flow gains and blocked-spool pressure gain, the nominal quiescent leakage and valve attenuation have been decreased, and the sensitivity of the flow gain, blocked-spool pressure gain, quiescent leakage, and frequency response to parameter degradation have been reduced.

Measurements of differential-load pressure gain were not made for all design conditions, because the high ratio of this gain makes it difficult to get an accurate measurement on the analog computer. The strut pressure gain is, however, inversely proportional to quiescent leakage at small values of input current, and it can be assumed that the changes in pressure gain are related directly to changes in quiescent leakage.

The reduction in the $\frac{D}{d}$ ratio to 1.57 was accomplished by increasing the inlet-orifice diameter and decreasing the nozzle diameter. This has the additional benefit of reducing the tendency of the orifice to be blocked by contaminant particles. Since the orifice is the smaller of the two diameters and has, therefore, a greater susceptibility to being blocked, an increase in this diameter produces an increase in reliability.

It is clear from the results of this design investigation that, while some improvement in valve reliability can be achieved, the parameters selected by the manufacturer in the present design configuration are very close to their optimum values.

Predicting Relative Reliability

The next subtask of project activity was to estimate quantitatively the improvement in valve reliability that could be anticipated from the new valve design. The analysis was based on the performance characteristic of quiescent leakage at null. The relative reliability was expressed as the ratio of the expected number of cycles of operation of the new valve design for the quiescent leakage to reach a specified limit to the number of cycles of the original valve design to reach the same limit. Quiescent leakage was chosen as the focus of study because past laboratory experience had shown that this valve characteristic was most susceptible to degradation, and that the change in performance over the period of the life test could be readily observed.

TABLE XIII. COMPARISON OF ORIGINAL AND NEW DESIGN

Value	Original Design	New Design	Change, %
Q_v at 4ma	18.64 cis	18.59 cis	
δ at 4ma	5.06%	7.52%	
Y_S at 4ma	28.74%	29.82%	
ΔP_N at 4ma	125.2 psi	165.8 psi	
P_{N1} at 4ma	1844 psi	2240 psi	
Q_ℓ at null	1.240 cis	1.135 cis	-8.6
$\Delta P_N(ds)/(4i)$	17.2 lb/ma in.	16.7 lb/ma in.	
FR at 150 cps	-5.98 db	-4.38 db	-26.7
Φ at 150 cps	-64.2 deg	-54.5 deg	
δ at 150 cps	80%	80%	
$\partial I_{Null}/\partial h_1$	0.024 ma/%	-0.0241 ma/%	0
$\partial I_{Null}/\partial C_{O1}$	-0.021 ma/%	-0.0195 ma/%	
$\partial Q_v/\partial C_O$	-0.001 cis/%	-0.0083 cis/%	-28
$\partial Q_v/\partial C_N$	-0.014 cis/%	-0.0025 cis/%	
$\frac{\partial(\Delta P_N d_s/4i)}{\partial C_O}$	-0.013 lb/ma in.	-0.058 lb/ma in.	-32
$\frac{\partial(\Delta P_N d_s/4i)}{\partial C_N}$	-0.093 lb/ma in.	-0.016 lb/ma in.	
$\partial Q_\ell/\partial C_O$	+0.0015 cis/%	+0.0012 cis/%	-7
$\partial Q_\ell/\partial C_N$	+0.0016 cis/%	+0.002 cis/%	
$\partial Q_\ell/\partial Y_{SLAP}$	+0.0013 cis/%	0.00125 cis/%	
$\partial Q_\ell/\partial C_{RS}$	+0.0223 cis/%	0.0203 cis/%	
$\partial FR/\partial C_O$ at 150	-0.033 db/%	-0.022 db/%	-38
$\partial FR/\partial C_N$ at 150	-0.056 db/%	-0.033 db/%	

The prediction of reliability involves:

(1) Calculating the variance that can be expected in the performance characteristics under study as a function of the manufacturing tolerances of the critical parameters

(2) Deriving a mathematical expression for the change in the mean performance characteristics resulting from degradation in the critical valve parameters during operation

(3) Combining the variance and average degradation equation to determine the range of cycles of operation during which the performance specifications will be exceeded.

The parameters that have the most significant influence on the quiescent leakage and are subject to degradation during operation are:

(1) Nozzle flow coefficient (C_N)

(2) Orifice flow coefficient (C_O)

(3) Clearance between spool and bushing (C_{RS})

(4) Magnitude of spool underlap (Y_{SLAP}).

The quiescent leakage at null is expressed by the equation:

$$Q_\ell = Q_1 + Q_2 + 2(C_{SLL1\text{-}DP} + C_{BLL1\text{-}DP})(P_{L1} - P_{DP}) + 2(C_{PSL}/Y_{S2})(P_{L1} - P_{DP}) + 2\left(\frac{1}{K_P}\right)^{1/2}\left(P_{L1} - P_{DP}\right)^{1/2} Y_{SLAP} ,$$

where

$$Q_1 = \pi D C_N (2/\rho)^{1/2} h (P_{N1} - P_D)^{1/2}$$

$$Q_2 = \pi D C_N (2/\rho)^{1/2} h (P_{N2} - P_D)^{1/2}$$

$$C_{SLL1\text{-}DP} = (\pi d_s - 4\omega) C_{RS}^3/12\mu_\ell$$

$$C_{BLL1\text{-}DP} = \pi d_B C_{RB}^3/12\mu_\ell$$

$$C_{PSL} = n \omega C_{RS}^3/12\mu X_{SMAX}$$

$$Y_{S2} = 1.47$$

$$1/K_p = \frac{2(C_q n \omega X_{SMAX})^2}{\rho \times 104}$$

In the original design, $Q_\ell = 1.240$ cis and in the new design it is reduced to 1.198 cis.

Calculation of Leakage Variance. The variance that can be expected for the above leakage values is calculated from the partial derivatives developed from the analog model and from the variance in the valve parameters by means of the Propagation of Variance formula as given in Figure 1.

It is assumed that the nozzle and orifice flow coefficients have zero variance and that the leakage from the end of the spool through the spool clearance is small, so that the variance in the nozzle flow at null is due only to the manufacturing tolerances in the nozzle and orifice diameters. The laminar spool end leakage, Q_{END}, is calculated from the equation:

$$Q_{END} = \frac{2\pi d_S}{12\mu\ell} C_{RS}^{\ 3} (P_S - P_N)$$

Values for Q_{END} were calculated to be 0.00372 cis and 0.00223 cis for the original and new designs, respectively. P_{N1} = 1783 psi in the original design and 2160 psi in the new design, as obtained from the analog model.

The partial derivitaves with respect to flow area can be obtained from the partials with respect to flow coefficient by noting that the normalized values of these partials are equal. This results from the fact that the flow coefficient is simply an area correction factor.

We can thus write that:

$$\frac{\frac{\partial Q_\ell}{\partial C_O}}{C_O} = \frac{\frac{\partial Q_\ell}{\partial A_O}}{A_O} \quad \text{and} \quad \frac{\frac{\partial Q_\ell}{\partial C_N}}{C_N} = \frac{\frac{\partial Q}{\partial A_N}}{A_N} \quad ,$$

and that:

$$\frac{\partial Q_\ell}{\partial A_O} = \frac{C_O}{A_O} \cdot \frac{\partial Q_\ell}{\partial C_O} \quad \text{and} \quad \frac{\partial Q_\ell}{\partial A_N} = \frac{C_N}{A_N} \cdot \frac{\partial Q_\ell}{\partial C_N}$$

$\frac{\partial Q_\ell}{\partial C_O}$ and $\frac{\partial Q_\ell}{\partial C_N}$ are the absolute values of the partial derivatives as obtained from the analog model.

It can further be assumed that the dimensional tolerances in the nozzle and orifice diameters represent the range of ±3 standard deviations or 99.9 percent of all parts manufactured. The nozzle-diameter tolerances of ±0.0005 in. and the orifice tolerance of ±0.0001 in. then give the standard deviations in the respective flow areas, as listed in Table XIV.

TABLE XIV. STANDARD DEVIATIONS IN NOZZLE AND ORIFICE AREAS

	Original Design	New Design
Nozzle area	0.042×10^{-4} in.^{2}	0.036×10^{-4} in.^{2}
Orifice area	0.0042×10^{-4} in.^{2}	0.0045×10^{-4} in.^{2}

The spool clearance and underlap are the same in both designs, and the standard deviations in these values, due to manufacturing tolerances, are as given in FDL-TDR-64-50, page 52:

Spool Clearance Deviation = 1.67×10^{-6} in.
Spool Underlap Deviation = 0.29×10^{-2} percent.

These variances taken with the computed partial derivatives then result in quiescent leakage standard deviations of 0.0676 cis for the original design and 0.0618 cis for the new design.

If a tolerance range of ±3 standard deviations is assumed, the expected quiescent leakage from the servo valves is:

Original Design: 1.24 ± 0.20 cis or 0.322 ± 0.053 gpm.
New Design: 1.198 ± 0.19 cis or 0.309 ± 0.048 gpm.

The quiescent leakage will be affected by two types of wear degradation. The first is due to erosion of metal surfaces by the impact of solid particles contained in the fluid, and the second is abrasive wear due to the sliding action between contacting metal surfaces. The leakage that is affected by erosive degradation will be identified as $Q_{\ell e}$, and is equal to the nozzle flow ($Q_1 + Q_2$) less the laminar flow out the ends of the spool, plus the flow through the lap space. The abrasive wear will affect the radial spool clearance, and the leakage through this clearance will be identified as $Q_{\ell a}$. The total quiescent leakage is then $Q_\ell = Q_{\ell a} + Q_{\ell e}$ + bushing leakage.

The standard deviations for the degradable leakage components is as follows:

	Original Design	New Design
$Q_{\ell e}$	0.0054 cis	0.00626 cis
$Q_{\ell a}$	0.0675 cis	0.0616 cis

Leakage Degradation Equation. The expression for the change in leakage as a function of time or of cycles of operation is based on the differential equations of the form:

$$\frac{dA_i}{dN} = \sum_{J=1}^{m} \frac{\partial A_i}{\partial P_J} \frac{dP_J}{dV} \frac{dV}{dN} \quad \text{for erosive wear} \tag{32a}$$

and

$$\frac{dA_i}{dN} = \sum_{J=1}^{m} \frac{\partial A_i}{\partial P_J} \frac{dP_J}{dN} \quad \text{for abrasive wear,} \tag{32b}$$

where

$\frac{dA_i}{dN}$ is the change in performance characteristic, A_i, per cycle of operation.

$\frac{\partial A_i}{\partial P_J}$ is the partial derivative of the performance characteristic with respect to the parameter P_J, as obtained from the mathematical model.

$\frac{dP_J}{dV}$ is the change in the value of the parameter P_J per unit volume of material removed and is obtained from the geometrical configuration of the valve component in question.

$\frac{dV}{dN}$ is the total volume removed V, per cycle. For erosive wear, this differential is the product of the volume of material removed per particle (v), number of particles per unit volume of fluid (K_2), and the volume of fluid passing through the region per cycle.

The volume of material removed per particle v can be expressed as*

$v = K_1 u$, where K_1 is a constant that depends on:

(1) The mass of the particle, or the average particle mass
(2) The angle of incidence of the particle on the surface being eroded
(3) The plastic flow stress of the material,

and u is the average fluid velocity in the region of erosion.

The number of particles per unit volume of fluid is determined from a fluid contamination count.

The fluid flow per cycle is a function of the flow at null (q) and is expressed as $K_3 q$, where K_3 is a constant.

Then, $\frac{dV}{dN} = K_1 u \times K_2 \times K_3 q.$

Since $V = 0$ when $N = 0$, $V = KuqN$,

where $K = K_1 K_2 K_3$.

$\frac{dP_J}{dN}$ is the rate of change of parameter, P_J, per cycle, N. For abrasive wear in the servo valve, this parameter is the radial clearance. Degradation is assumed to be a function of the distance traveled by the spool per cycle and is expressed as:

$\frac{dC_{rs}}{dN} = My$, where M is a constant that depends on:

(1) The material characteristics
(2) The magnitude of the input signal in ma
(3) An arbitrary maximum spool displacement, and

y is a measure of the amplitude of spool motion and is expressed as a percentage of the arbitrary maximum spool amplitude per milliampere of input current. Equations (32a) and (32b) can now be rewritten for quiescent leakage as:

*"Erosion of Surfaces by Solid Particles", Wear, March, 1960.

$$\frac{dQ_{\ell e}}{dN} = \frac{\partial Q_\ell}{\partial C_O}\ \frac{dC_O}{dV_O}\ K_O u_O q_O + \frac{\partial Q_\ell}{\partial C_N}\ \frac{dC_N}{dV_N}\ K_N u_N q_N + \frac{\partial Q_\ell}{\partial Y_{SLAP}}\ \frac{dY_{SLAP}}{dV_Y}\ K_Y u_Y q_Y \quad , (33)$$

where the subscripts O, N, and Y refer to the parameter values of the orifice nozzle and lap space, respectively.

$$\frac{dQ_{\ell a}}{d_N} = \frac{\partial Q_\ell}{\partial C_{RS}}\ My \quad . \tag{34}$$

The values of $\frac{dC_O}{dV_O}$, $\frac{dC_N}{dV_N}$, and $\frac{dY_{SLAP}}{dV_Y}$ are derived from the geometry of the valve elements. If one now considers the factors affecting the magnitudes of K_O, K_N, and K_Y, above, it could be assumed that these constants are to some first order of approximation almost equal, or that they at least are of the same order of magnitude. If it is initially assumed that they are equal, it is possible to further simplify Equation (33); in doing so, it can be shown that the assumption that K_O, K_N, and K_Y be of the same order of magnitude is sufficient for the simplification.

If we let $K_O \approx K_N \approx K_Y \approx K$ and divide by K, we can write Equation (33) as:

$$\frac{dQ_{\ell e}}{dK_N} = \frac{\partial Q_\ell}{\partial C_O}\ \frac{dC_O}{dV_O}\ u_O q_O + \frac{\partial Q_\ell}{\partial C_N}\ \frac{dC_N}{dV_N}\ u_N q_N + \frac{\partial Q_\ell}{\partial Y_{SLAP}}\ \frac{dY_{SLAP}}{dV_Y}\ u_Y q_Y \quad .$$

Then, since $uq = \frac{V}{KN}$, we can rewrite this as:

$$\frac{dQ_{\ell e}}{dK_N} = \frac{\partial Q_\ell}{\partial C_O}\ \frac{dC_O}{dV_O}\ \frac{V_O}{KN} + \frac{\partial Q_\ell}{\partial C_N}\ \frac{dC_N}{dV_N}\ \frac{V_N}{KN} + \frac{\partial Q_\ell}{\partial Y_{SLAP}}\ \frac{dY_{SLAP}}{dV_Y}\ \frac{V_Y}{KN} \quad . (35)$$

By assuming that the partial derivatives remain constant, a curve of $\frac{dQ_{\ell e}}{dKN}$ versus KN can be plotted. The area under this curve between any two values of KN represents the change in $Q_{\ell e}$ between these values. It can be shown that the terms relating to wear in the orifice and nozzle are insignificant when compared with the terms involving Y_{SLAP}. Thus, as long as K_O, K_N, and K_Y are of the same order of magnitude, Equation (33) can be simplified by considering only the effect of changes in spool underlap. The same conclusion can be drawn for the new design.

Equation (35) then becomes:

$$\frac{dQ_{\ell e}}{dK_N} \approx \frac{\partial Q_\ell}{\partial Y_{SLAP}}\ \frac{dY_{SLAP}}{dV_Y}\ \frac{V_Y}{KN} \quad . \tag{36}$$

From the supplemental material:

$$\frac{dY_{SLAP}}{dV_Y} = 6840\sqrt{\frac{1}{V_Y}} = \frac{6840}{\sqrt{u_Y q_Y KN}}$$

substituting this into Equation (36) and integrating gives:

$$Q\ell_e = 6840 \frac{\partial Q_\ell}{\partial Y_{SLAP}} - \sqrt{u_Y q_Y KN} + Q_{\ell e}' \quad , \text{ where:} \tag{37}$$

$Q_{\ell e}'$ is the initial value of $Q_{\ell e}$.

Now by integrating Equation (34), the abrasive degradation equation is obtained:

$$Q_{\ell a} = \frac{\partial Q_\ell}{\partial C_{RS}} \quad y\, M\, N + Q_{\ell a}' \quad . \tag{38}$$

Table 15 lists the calculated values of the parameters of Equations (37) and (38) as applied to the original and the new valve designs.

TABLE XV. VALUES OF QUIESCENT LEAKAGE DEGRADATION PARAMETERS

Parameter	Original Design	New Design
$\partial Q_\ell / \partial Y_{SLAP}$	1.33 cis/% max stroke	1.25 cis/% max stroke
$\partial Q_\ell / \partial C_{RS}$	0.0404×10^6 cis/in.	0.0369×10^6 cis/in.
u_Y	4520 in./sec	4520 in./sec
q_Y	0.0162 cis	0.0156 cis
$Q_{\ell e}$	0.5341	0.5222
$Q_{\ell a}$	0.6839	0.6441
y	7.18%/ma[a]	7.46%/ma[a]

(a) Based on data from analog model.

From the values in Table 15 and the consideration of a ±3 standard deviation tolerance, the final leakage degradation equations are:

Original Design

$$Q_{\ell e} = 0.1555 \times 10^6 \sqrt{KN} + 0.5341 \pm 0.0162 \text{ cis} \tag{39}$$

$$Q_{\ell a} = 0.29 \times 10^6\, M\, N + 0.684 \pm 0.2025 \text{ cis} \tag{40}$$

New Design

$$\bar{Q}_{\ell e} = 0.1488 \times 10^6 \sqrt{K\, \bar{N}} + 0.5222 \pm 0.0188 \text{ cis}^* \tag{41}$$

$$\bar{Q}_{\ell a} = 0.275 \times 10^6\, M\, \bar{N} + 0.644 \pm 0.1848 \text{ cis} \quad . \tag{42}$$

The bushing leakage is calculated from the equation $C_{BLL1\text{-}DP}(P_{L1} - P_{DP})$ and has a value of 0.022 cis for both designs.

* A bar over a symbol indicates the new design.

Relative Reliability. If the limiting value of quiescent leakage is taken as 2 cis, and since $Q_l = Q_{l_a} + Q_{l_e}$ + bushing leakage, then, using Equations (39) through (42), expressions for numbers of cycles to failure for the two designs are:

$$0.1555 \times 10^6 \sqrt{K N_1} + 0.29 \times 10^6 M N_1 = 0.760 \pm 0.219 \text{/for the original design}$$

$$0.1488 \times 10^6 \sqrt{K \bar{N}_1} + 0.275 \times 10^6 M \bar{N}_1 = 0.812 \pm 0.204 \text{/for the new design,}$$

where N_1 and $\bar{N}_1$ represent the number of cycles to failure for the original and new designs respectively.

Depending on the values of K and M, we would expect, on the average, that the ratio $\bar{N}_1/N_1$, the relative reliability for the two designs, would be between 1.125 and 1.25. This indicates a net improvement in valve reliability. If K is much larger than M so that the abrasive degradation can be neglected, the higher ratio could be expected.

It should be noted, however, that the above ratios represent only mean values and that, in a direct comparison of a small sample of valves, the relative reliabilities will not necessarily fall on this average. In fact, if a sample of, say, two valves of each design is taken, one should consider that the valve performance could fall anywhere within a range of ±3 standard deviations from the average. Thus, at the extreme, if the leakage of the new design were at the high limit and that of the original design at the low limit, one could expect the relative reliability ratio to be about 0.65, which would indicate poorer reliability. If, on the other hand, the new design were at the low limit and the original design at the high limit, a 96 percent improvement in reliability could be expected.

Experimental Verification of Reliability Prediction

Construction of Modified Servo Valves. In order to examine experimentally the reliability resulting from an application of the Moment method analysis to a two-stage servo valve, a sample of four valves was ordered from a supplier. Two of the valves incorporated the design changes derived from the Moment method analysis. The other two were of conventional design for comparison.

Although the two modified valves formed a small sample, it was hoped that they would provide useful information concerning the effectiveness of the application of the Moment method to the reliability optimization of an actual device. As stated earlier, the servo valve design was found to be already close to optimum. However, some significant changes were evolved that would improve the predicted reliability. The sample valves were gradually degraded by life testing under continuous cycling. A record of the progress of degradation was kept by periodically removing the valves from the life-testing stand and placing them on an instrumented test stand to undergo a series of tests covering the major parameters contributing to the predicted reliability improvements.

Description of Testing Program. Initial tests (before life testing) were made in order to establish a standard against which degradation would be measured. The initial tests applied to each valve are listed below:

(1) Record Null
(2) Quiescent Flow Versus Differential Current
(3) Differential Load Pressure Versus Differential Current
(4) Short-Circuited Load Pressure Versus Differential Current
(5) Total Flow Versus Differential Current
(6) Load Flow Versus Differential Current
(7) Frequency Response With Blocked Load.

In later tests, this series was shortened to cover the characteristics most directly applicable to the results of the Moment method analysis:

(1) Record Null
(2) Quiescent Flow Versus Differential Current
(3) Differential Load Pressure Versus Differential Current
(4) Total Flow Versus Differential Current
(5) Frequency Response With Blocked Load.

After initial testing, the valves were placed on a life-testing stand and operated by continuously reversing the direction of flow. At intervals during the life testing, the valves were removed and the individual tests were repeated to record the progress of degradation in the operating characteristics of the valves. The test series was made a total of seven times at 0; 140,000; 300,000; 900,000; 1,600,000; 3,000,000; and 8,600,000 cycles.

The final step in the testing program was the plotting of trend curves to show the rate of degradation of the operating characteristics as a function of total cycles or total hours. The characteristics represented by the trend curves were null bias, peak quiescent flow, minimum quiescent flow, difference between maximum and minimum quiescent flow, pressure gain, and frequency response at 100 cycles per second.

Description of Test Equipment. The equipment used in testing the valves consisted primarily of two independent systems: an instrumented hydraulic test bench and a life testing stand.

Instrumented Test Bench. The test bench was originally designed for the monitoring of servo-valve characteristics. It includes a pump, reservoir, variable load, and instrumentation. A schematic diagram of the test bench is shown in Figure 54. Oil is delivered under pressure to the manifold block through a passage leading to the valve supply ports. It is then routed by the valve (depending on spool position) to either Load Line A or Load Line B. The variable-load device is not shown on the diagram. It consists of a main valve and a bypass valve for fine adjustments. The load may be adjusted anywhere from fully blocked to fully open, i.e, very low hydraulic resistance. A closed load valve is referred to as "blocked load", and a fully open load valve is called "short-circuited load". Except in the null or centered spool position, one load line is always connected to supply and the other to drain. The main flow leakage and nozzle flow are mixed inside the manifold at the manifold drain port.

The test bench instrumentation consists of a servo amplifier, flowmeters, pressure gages, and thermometers. A signal generator is used as an accessory during frequency response tests. The flowmeters are arranged in two parallel banks, each containing two

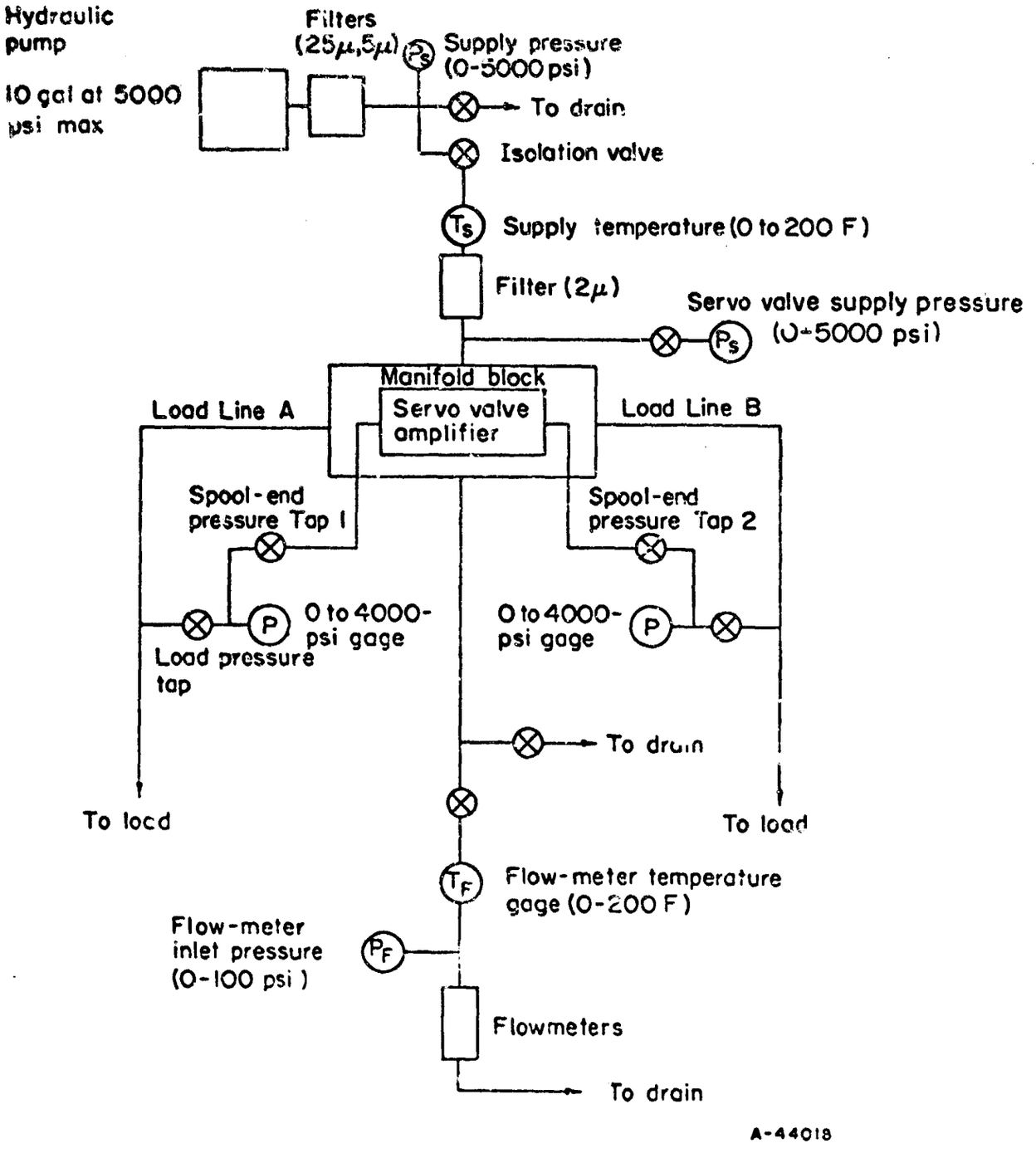

FIGURE 54. SERVO-VALVE HYDRAULIC-TEST-STAND SCHEMATIC

meters in series. One bank cover flows up to 1 gpm, and the other registers flows from 1 to 20 gpm. The flowmeters are of the variable-orifice type, using a metal float in a tapered glass tube. The meters may be read easily to three significant figures. Pressure gages are provided at the supply port, in both load lines, and in the drain line. The difference between the load-line pressure readings is governed by the setting of the load valve and spool position. Oil is supplied to the test bench circuit by a fixed displacement pump delivering 10 gpm at pressures up to 5000 psi. Tests are normally run with a supply pressure of 3000 psi, which is held constant under varying conditions by adjusting a bypass valve. Flow from the pump is smoothed by an accumulator in the supply line.

Objectives and Procedures for Tests. The following describes the objectives and summarizes the method used for the five tests that formed the series made at each of the seven testing points during the life tests.

Record Null. The purpose of this test is to determine the amount of differential current required to place the spool so that the pressures in Load Lines A and B are equal with the load valve completely shut off. The amount of current required to achieve this "hydraulic null" should be very small, and is a measure of the difference between electric null (zero differential current) and an actual pressure balance in the valve. Ideally, these conditions would coincide, though in a real valve it is only reasonable to expect a small offset between them. A plot of the "null bias" or current required to balance the valve, versus time, can be valuable in revealing changes in the behavior of the valve in the critical area around null. Scoring of the spool, bending of the feedback wire, wear of the feedback-wire tip, or damage to the flapper can result in changes in the value of the null bias current with time.

The record null, or null bias test, is run by bringing the spool slowly from full displacement to a pressure-balanced condition. This is done from both directions to cancel out the effect of spool friction. In the tests, the average of the null differential currents from both directions was taken as the null bias, expressed in milliamperes.

Quiescent Flow Versus Differential Current. This test is performed with the load valve shut off. The "quiescent flow" measured is the sum of the flow through the nozzles and the spool leakage flow. The quiescent flow characteristically reaches a peak near null and decreases to a relatively constant value in the 0.1 to 0.2-gpm range on either side of null. Since the spool leakage is very small away from null, and since the total nozzle flow remains essentially constant throughout the normal spool stroke, the quiescent leakage curve may be viewed as a portrait of variable spool leakage superimposed on constant nozzle flow, as a function of spool position (spool position is represented by differential current in the linear region of valve operation). The maximum value of quiescent leakage is a sensitive indicator of spool metering edge wear, and was a characteristic of primary importance in the modification of the valve for better reliability.

The quiescent flow test is run by stepping the differential current away from null in both directions ("positive" and "negative" differential current), and recording the total flow from the valve at each step. No load flow is permitted. A typical quiescent flow test curve is shown in Figure 55.

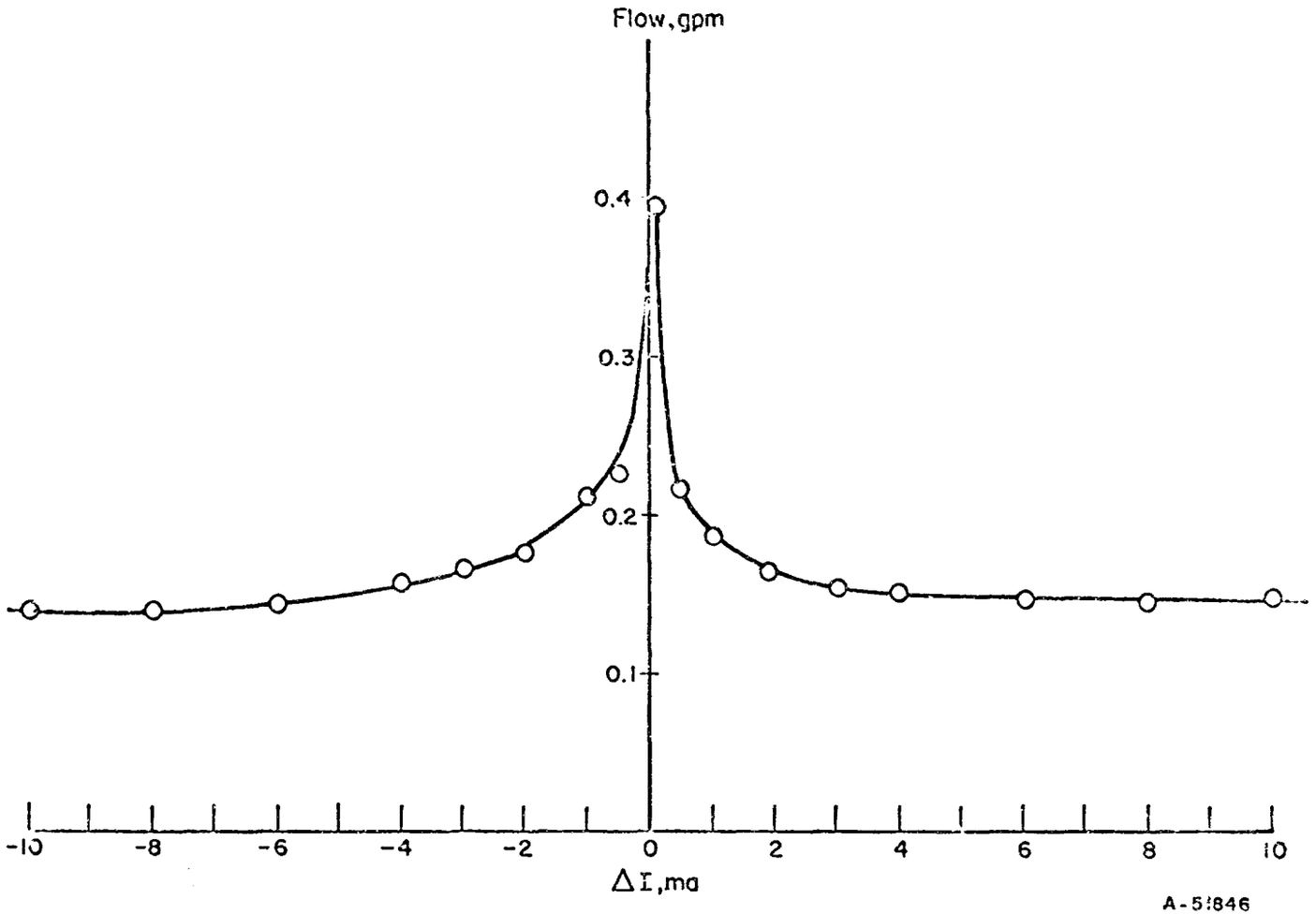

FIGURE 55. QUIESCENT FLOW VERSUS DIFFERENTIAL CURRENT

Differential Load Pressure Versus Differential Current. The differential load pressure test is a blocked-load procedure used to evaluate the "resolution" or proportionality of response of the valve near hydraulic null. The test is performed by closing the load valve and noting the difference between load-line pressure A and B as the spool is shifted slightly to either side from the pressure-balanced condition. The slope of the differential-pressure curve is known as "pressure gain", and is an index of nozzle, spool, and metering-port wear. The existence of a finite pressure gain is due primarily to the slight underlap built into the valve to improve its proportionality. Figure 56 shows a typical differential-load-pressure curve.

Total Flow Versus Differential Current. In this test the load valve is opened and adjusted so that, for any value of differential current, a specified constant pressure drop occurs from Load Line A to Load Line B, or vice versa. Supply pressure is also adjusted (as in all tests) to maintain 3000 psi. Differential current, i.e., spool displacement, is increased from null in steps under the above conditions, and total flow is recorded at each step. The resulting graph takes the characteristic form of two lines sloping upward in a vee from the origin, which represents zero differential current. The right leg of the vee shows an increase in flow with increasing spool motion in one direction through the simulated load resistance, and the left leg represents a similar flow increase in the opposite direction. At the vertex of the vee, only quiescent flow occurs. One of the objectives of the total-flow-versus-differential current test is to illustrate graphically the extent to which flow increases linearly with increasing differential current. The slope of the total-flow curve is called the "flow gain". The flow gain generally remains quite constant for differential currents from zero up to about 6 ma. It should be emphasized that, in order to obtain this linearity, both supply pressure and load-pressure drop must be held at fixed values by varying the supply bypass and load-valve settings after each change in differential current. This is, of course, a static or steady-state test, as are all those in this series except frequency response. Figure 57 shows a representative total-flow curve.

Frequency-Response Test. For this program, a form of frequency-response test was devised to conform to the available instrumentation on the static-test stand. The test was run with the load valve closed, and the spool was oscillated about hydraulic null with a sinusoidal torque-motor signal of 7 millivolts peak-to-peak magnitude, and frequencies ranging from 5 to 150 cps. A signal generator was connected to the regular test-stand d-c amplifier to provide the sinusoidal input. The output, or dependent variable, was the mean flow as read visually from the flowmeter. The response of the flowmeter was smooth above 5 cps, and provided an accurate and repeatable reading. The individual test curves were plotted directly as recorded, giving flow in gpm versus frequency in cps. For the trend curves representing changes from test to test, the ratio of flow at 100 cps to maximum flow was recorded, in decibels, as a function of total cycles on the valves. A representative frequency-response curve is shown in Figure 58.

Application of the Moment Method. Before reviewing the results of the life tests of the two modified and two unmodified servo valves, it will be helpful to review some of the general features of the Moment method of statistical inference.

The Moment method cannot, by itself, take time into account as a variable. It yields only the first and second moments (mean and variance) of a

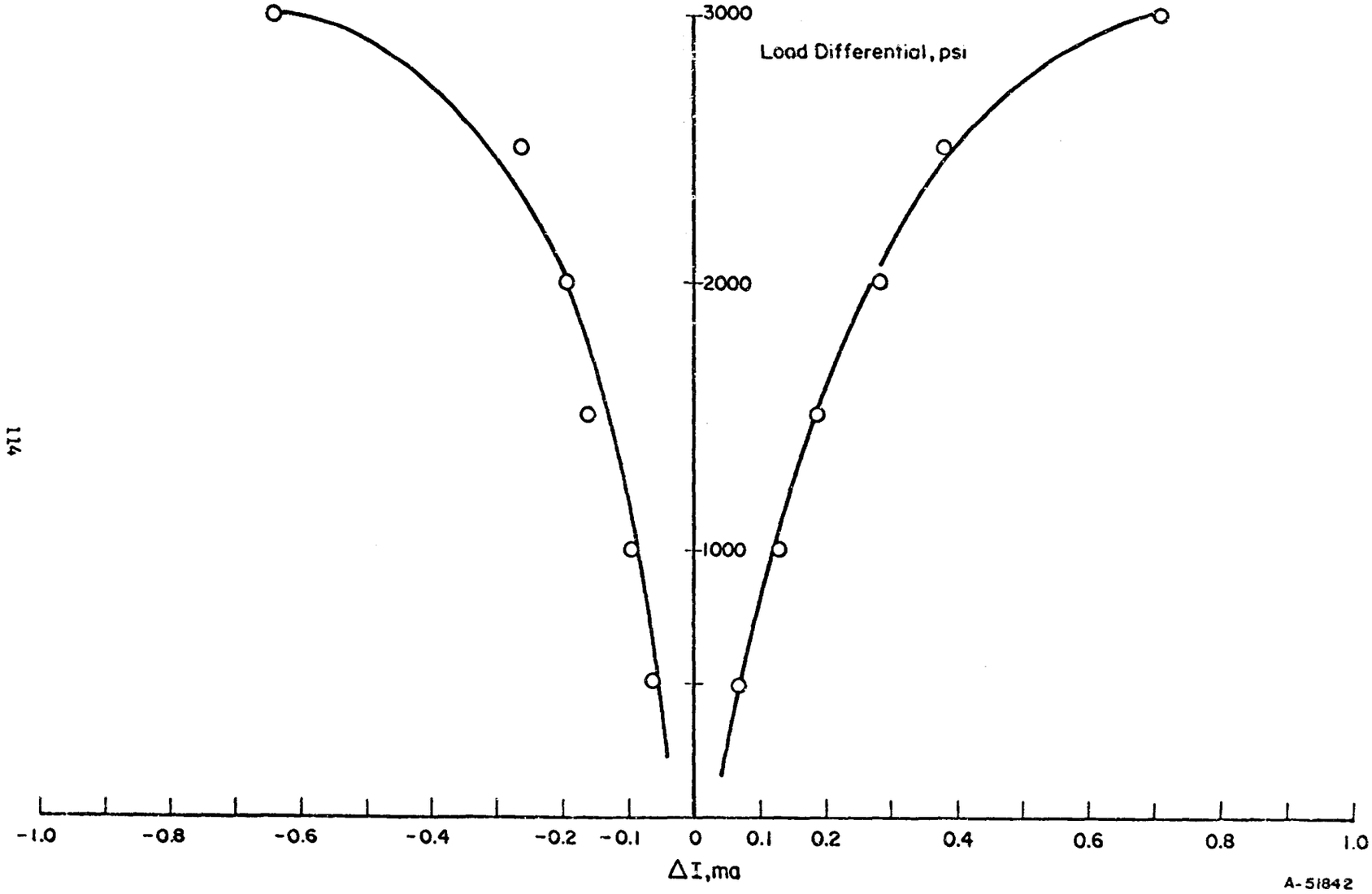

FIGURE 56. DIFFERENTIAL LOAD PRESSURE VERSUS DIFFERENTIAL CURRENT

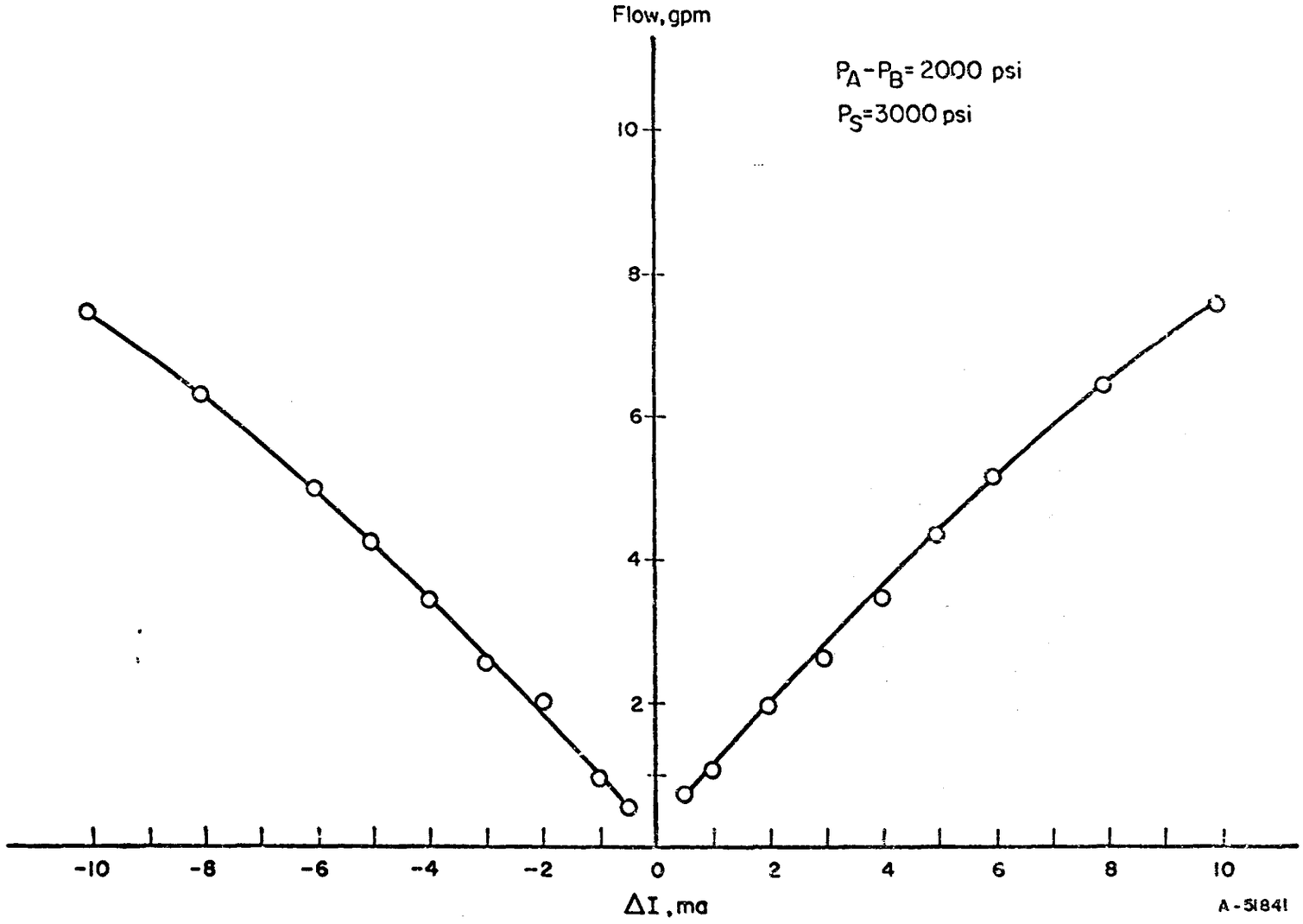

FIGURE 57. VALVE FLOW VERSUS DIFFERENTIAL CURRENT

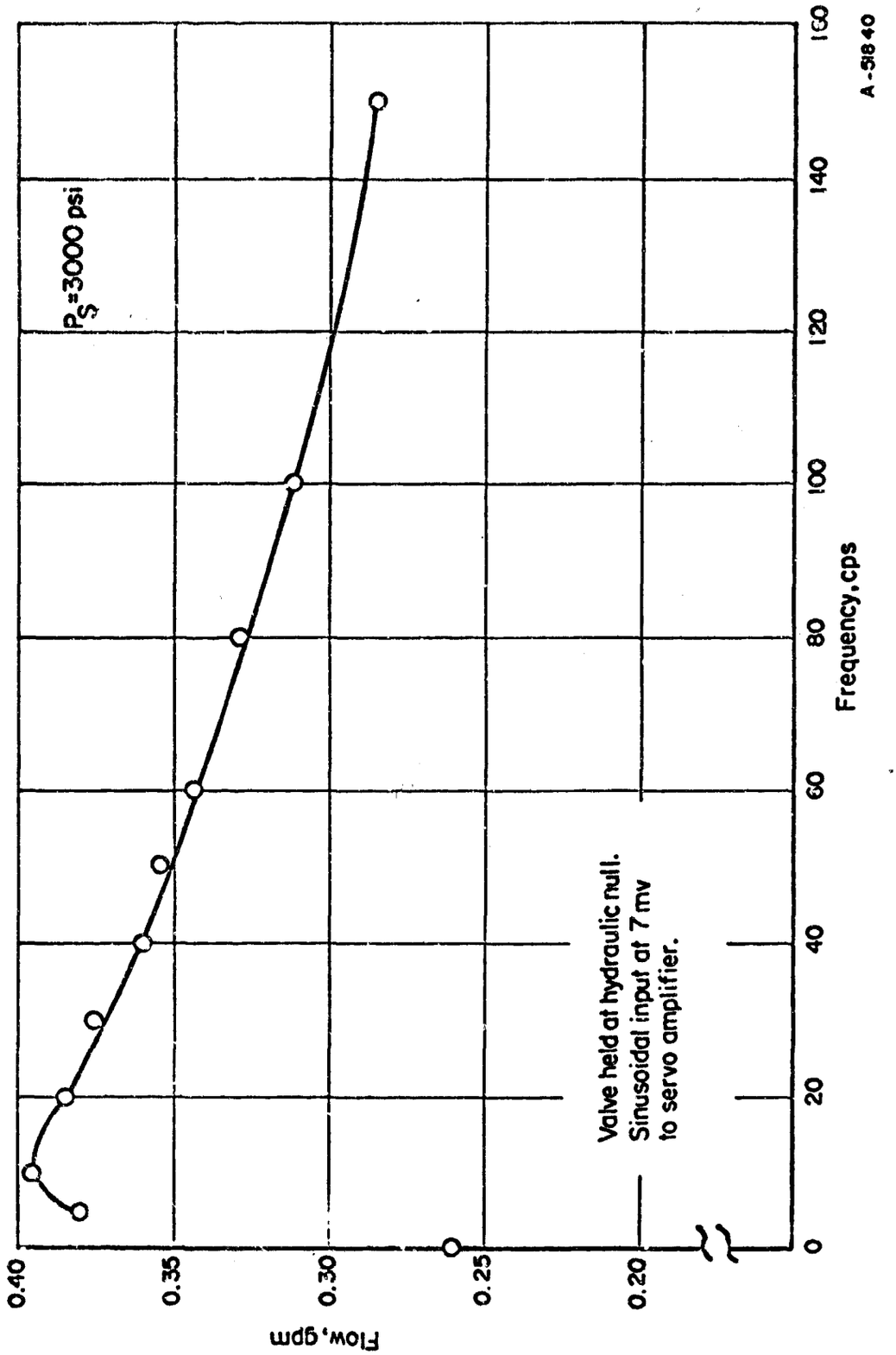

FIGURE 58. BLOCKED-LOAD FLOW VERSUS FREQUENCY

performance-characteristic distribution at a particular point in time. The full shape of the distribution is not known unless some specific form such as the normal is assumed. The success of the method depends on accurate knowledge of the form of the parameter distributions involved, and also on the validity and depth of the mathematical model used to represent the device or system under analysis. In order to extend the Moment method to take into account the passage of time, either experimental or theoretical estimates of time rates of parameter degradation must be secured. One of the objectives of the present life tests was to determine empirically the long-term rates of change of servo-valve parameters, such as quiescent leakage and frequency response. In addition, the comparative performances of the modified and unmodified valves were expected to allow inferences about the extent to which predicted and realized reliability improvements were matched in practice. In formulating the design changes incorporated in the two modified valves, ways to improve reliability were found by noting where in the design an application of one or more of three cardinal criteria could be applied. The first criterion was the reduction of the values of the partial derivatives representing the rate of change of a given performance characteristic with respect to a physical parameter of the valve. For instance, if the maximum quiescent leakage can be made less sensitive to spool metering edge location (without affecting other performance characteristics), then the design change producing this reduction of sensitivity may be said to increase the relative reliability of the valve with respect to statistical variations in the longitudinal spacing of the metering edges.

The second criterion for reliability improvement was the tightening of the nominal specifications of parameters, so that the probability of their being a given amount off ideal to begin with would be lessened. The variations in physical parameters may be thought of as operating on performance characteristics by means of a variable leverage factor — the leverage factor being the partial derivative of the characteristic with respect to the parameter. A reduction in either the original parameter variation or the partial derivative relating it to a performance characteristic can effect an improvement in reliability.

The third primary means for reliability improvement was the reduction of the time rate of change of physical parameters. This area of improvement is usually concerned with the wear and aging of parts. It may be considered an extension of the notion of initial parameter variation. Not only is the original spread or distribution of a tolerance dimension or property of concern, but also the further broadening of the range of possible values due to hours of operation or hours of shelf time.

Test Results. As the bench tests progressed, it was possible to estimate the relative repeatability of the tests by noting the scatter evident in the trend curves, and the geometric similarities between curves taken in adjacent series. The repeatability of all tests appeared to be good, with the exception of the differential-load-pressure test. During this test, apparent instabilities in valve operation often occurred, and control of the d-c servo amplifier to the required degree of precision was difficult. An example of instability in the differential-load-pressure test is shown in Figure 59. The vertical section of the curve represents a region in which continuous control of the valve was not possible because of a sudden shift of the spool. The shift occurred repeatedly and seemed independent of the rate at which the differential current was increased.

With the exception of pressure-gain curves, all the bench tests performed seemed sufficiently repeatable to justify confidence in using successive sets of curves to trace

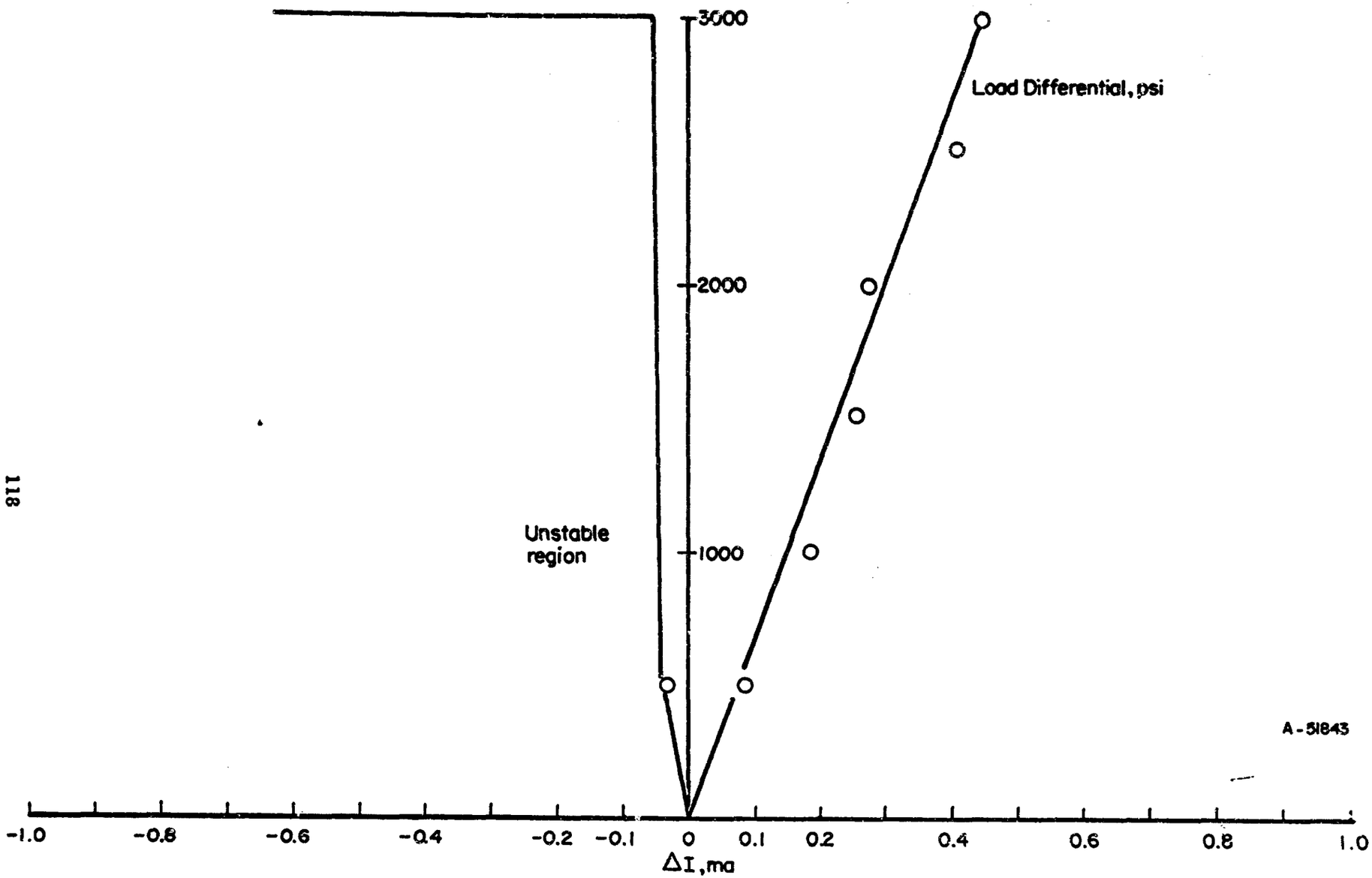

FIGURE 59. DIFFERENTIAL LOAD PRESSURE VERSUS DIFFERENTIAL CURRENT

parameter changes with time by means of trend curves. The trend curves were made by plotting some significant feature of each graph for a given valve against total cycles. For example, the trend curve for quiescent flow shows the peak value of this performance characteristic as found at each testing period. The testing periods occurred at 0; 150,000; 300,000; 900,000; 1,500,000; 3,000,000; and 8,600,000 cycles. A set of trend curves for a given test requires four graphs, one for each valve. Six sets of trend curves were plotted. They illustrate peak quiescent flow, quiescent spool leakage, quiescent nozzle flow, frequency response at 100 cps, pressure gain in the interval from 1000 to 2000-psi blocked-load differential, and null bias. The set of quiescent-flow-trend curves was expected to be most significant in efforts to relate actual to predicted reliability.

Quiescent Flow. The trend analysis of quiescent flow employed three types of curves. The first was a plot of peak quiescent flow for each test series. The second was a graph of the difference between the peak flow at null and the nearly constant flow beyond 4- or 5-ma differential current on either side of null. Following the reasoning given in the description of the quiescent flow test, this difference may be considered to represent the portion of the maximum quiescent flow accounted for by leakage past the underlapped-spool metering edges. It should be the most sensitive indicator of metering edge wear available, aside from direct measurement. The third quiescent-flow trend curve showed the flow at 8-ma differential current for each test series. Since the 8-ma point is quite far from null, it is on the constant portion of the quiescent-flow test curve, and may be taken to represent nozzle flow. The slope of nozzle-flow trend curve is an indicator of nozzle wear, and was used to check this parameter.

Figure 60 illustrates a typical peak quiescent-flow trend curve. It shows a period of rapid initial increase extending through the first 2 or 3 million cycles, and a gradual leveling off into a much lower long-term rate of increase. The rapidly increasing section probably represents an initial rounding of the spool metering edge. Because the rounded edge presents more and more area to the flow after each increment of erosion, it is to be expected that the rate of wear will decrease and produce a peak leakage that changes very little as the life testing progresses. Comparison of the curves for modified and unmodified valves showed that no definite conclusions may be drawn concerning relative reliabilities, at least on the basis of the small sample treated in this project. There were some marked differences in the degradation of the valves, but some of these differences were split among the valves so that they must be considered intrasample and not intersample phenomena. For instance, both unmodified valves showed an increase in total quiescent flow of about 0.1 gpm over the entire test program, while one modified valve increased by only 0.05 gpm, and the other by nearly 0.2 gpm. The final slopes of the quiescent-flow trend curves for three valves were similar, and a fourth, a modified valve, was somewhat steeper.

The second set of trend curves associated with quiescent flow was that of spool leakage. This quantity is the difference between nozzle flow and peak quiescent flow. Since it turned out that the nozzles degraded only a negligible amount, the spool-leakage curve was nearly equal to the total quiescent curve minus a constant value. Hence, the conclusions drawn from the total quiescent-flow curves also apply to the spool-leakage curves. Typical spool-leakage and nozzle-flow trend curves are shown in Figure 61 and 62. Spool leakage is plotted against total hours rather than total cycles, because it was felt that spool metering edge wear (the primary cause of spool leakage at null) would be dependent on total hours of flow rather accumulated cycles. Hours and cycles were not uniformly related throughout the life test, because the frequency of operation was

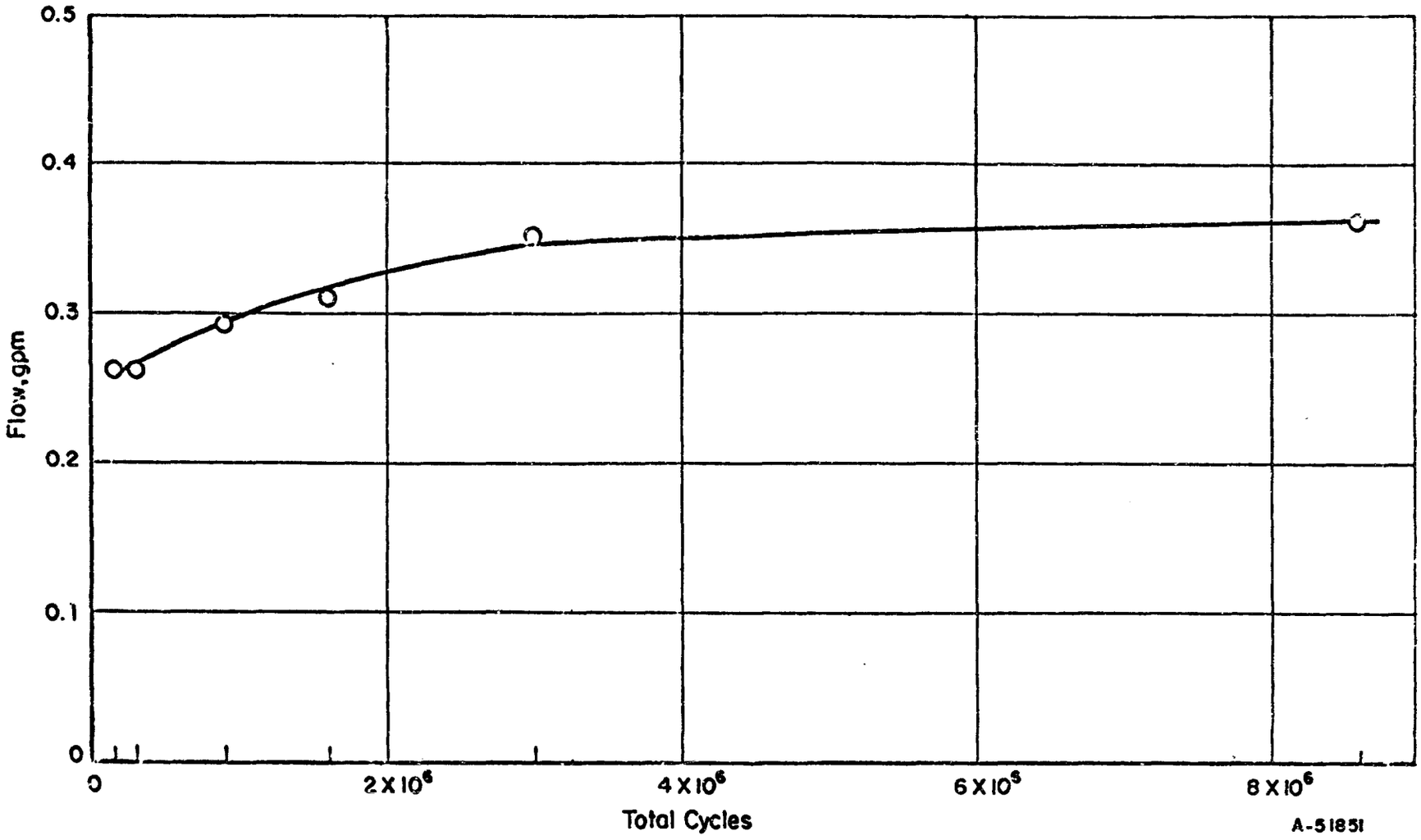

FIGURE 60. PEAK QUIESCENT FLOW VERSUS TOTAL CYCLES

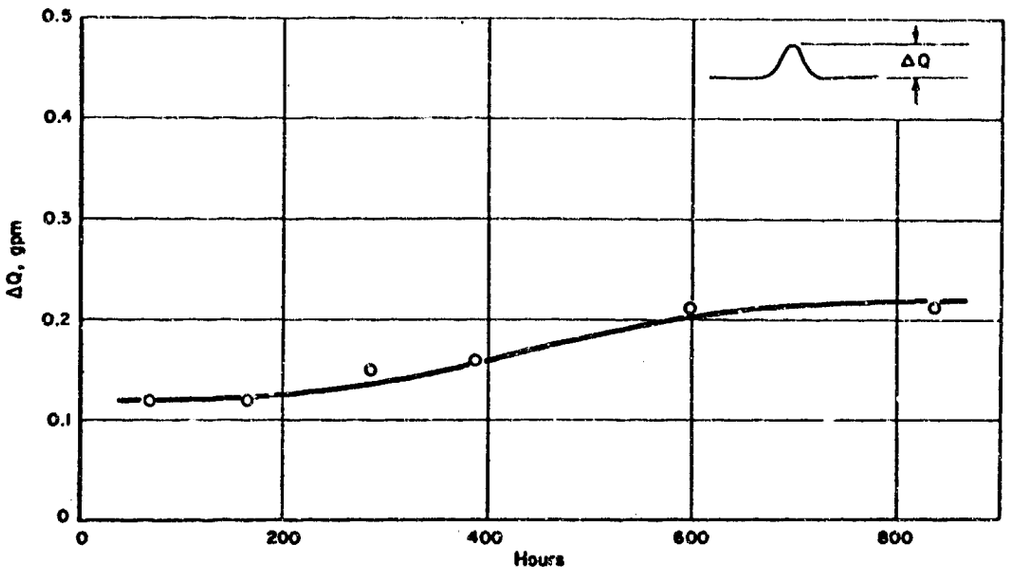

FIGURE 61. SPOOL LEAKAGE, ΔQ, VERSUS TOTAL HOURS

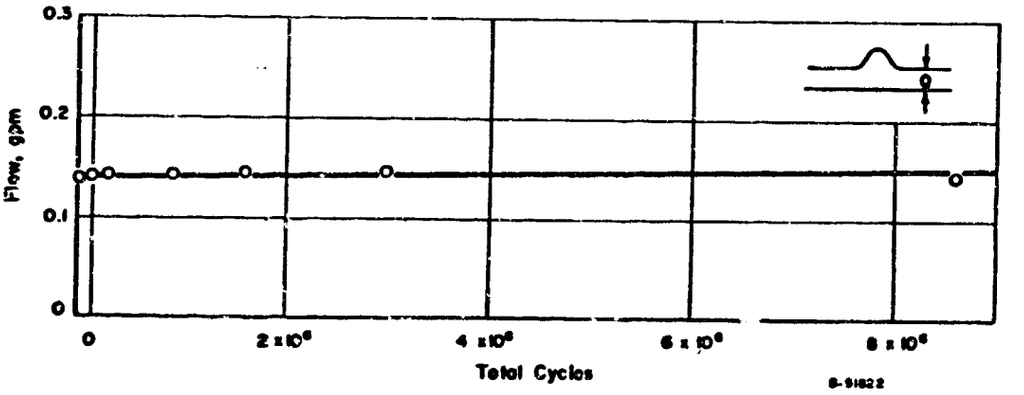

FIGURE 62. QUIESCENT NOZZLE FLOW AT 8mA VERSUS TOTAL CYCLES

increased during the latter portion. None of the valves exceeded the quiescent-flow specification limit during the test program.

Conclusions concerning the quiescent-flow trend curves are limited by the rather low final steady rate of spool-leakage degradation, and the extremely small rate of nozzle degradation. It was hoped that removal of the 2-micron filter from the life-testing circuit would increase contamination considerably beyond that experienced in previous tests. An increase by a factor of two did occur, but the degradation rate was still slower than originally hoped for. The possibility of adding contamination or switching to a contamination stand was considered, but it was decided that this type of forced general wear is not realistic when compared with the actual conditions of use for the valves, and in fact might not proceed with the same relative balance as the slow wear associated with systems as used in normal applications. In addition, time and cost considerations made it impractical to use a contamination-stand procedure in which only one or two valves could be run at a time. The cumulative-contamination-count curve for the present tests is shown in Figure 63. The contamination count was made on a Coultier counter. Although contamination counts obtained by this method are not as accurate as obtained by more laborious methods, the results appear to be consistent with the filter system that was used.

Frequency Response. The frequency-response trend curves showed that, generally speaking, the response of the modified valves at 100 cps was better than the response of the unmodified valves. At the conclusion of the life-testing period, the two unmodified valves were down 7 and 3 db, while the modified were down 1 and 2 db. Initially, both unmodified valves were down approximately 4 db, and both modified were down about 2 db. During the tests, then, the one unmodified lost 3 db of response and one gained 1 db; for the modified valves, one remained the same and one also gained 1 db. With samples as small as two units, it cannot necessarily be concluded that the modified valves are inherently better in frequency response, although such a conclusion was not contradicted by the actual valves tested. A typical frequency-response trend curve is shown in Figure 64. All valves demonstrated an initial dip in response, but for two of the valves (one modified and one unmodified) the dip was considerably more pronounced than that shown.

Pressure Gain. The pressure-gain trend curves were, unfortunately, indicative of the instabilities and other difficulties encountered during the differential-load-pressure versus differential-current tests. Only one valve (an unmodified) showed the initial increase and subsequent decrease that would be expected in the light of experience gained in a previous test program. Two of the valves, one modified and one unmodified, showed a long-term increase in pressure gain, which is difficult to explain in view of the slow but normal degradation evidenced by the other tests. It was felt that the pressure-gain trend curves must be regarded as inconclusive data for this test series.

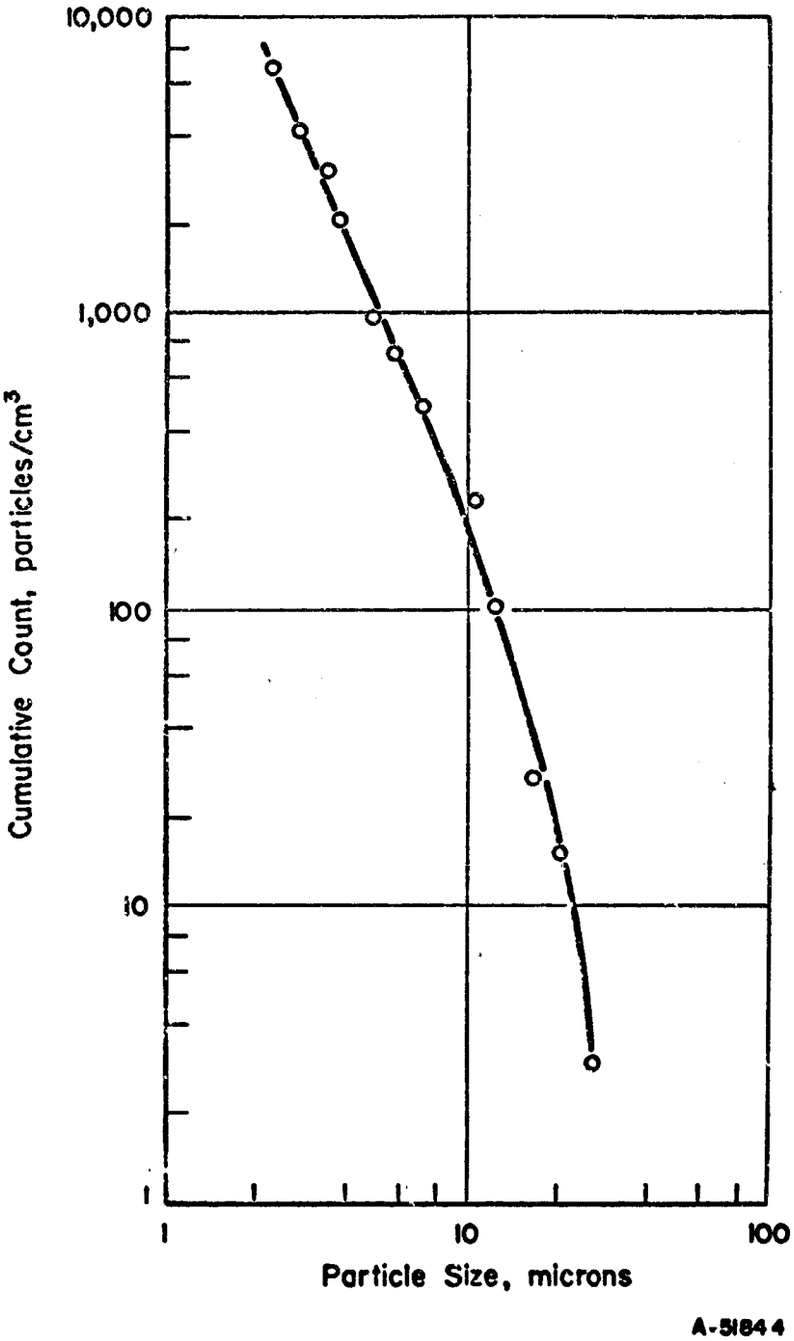

FIGURE 63. FLUID CONTAMINATION COUNT

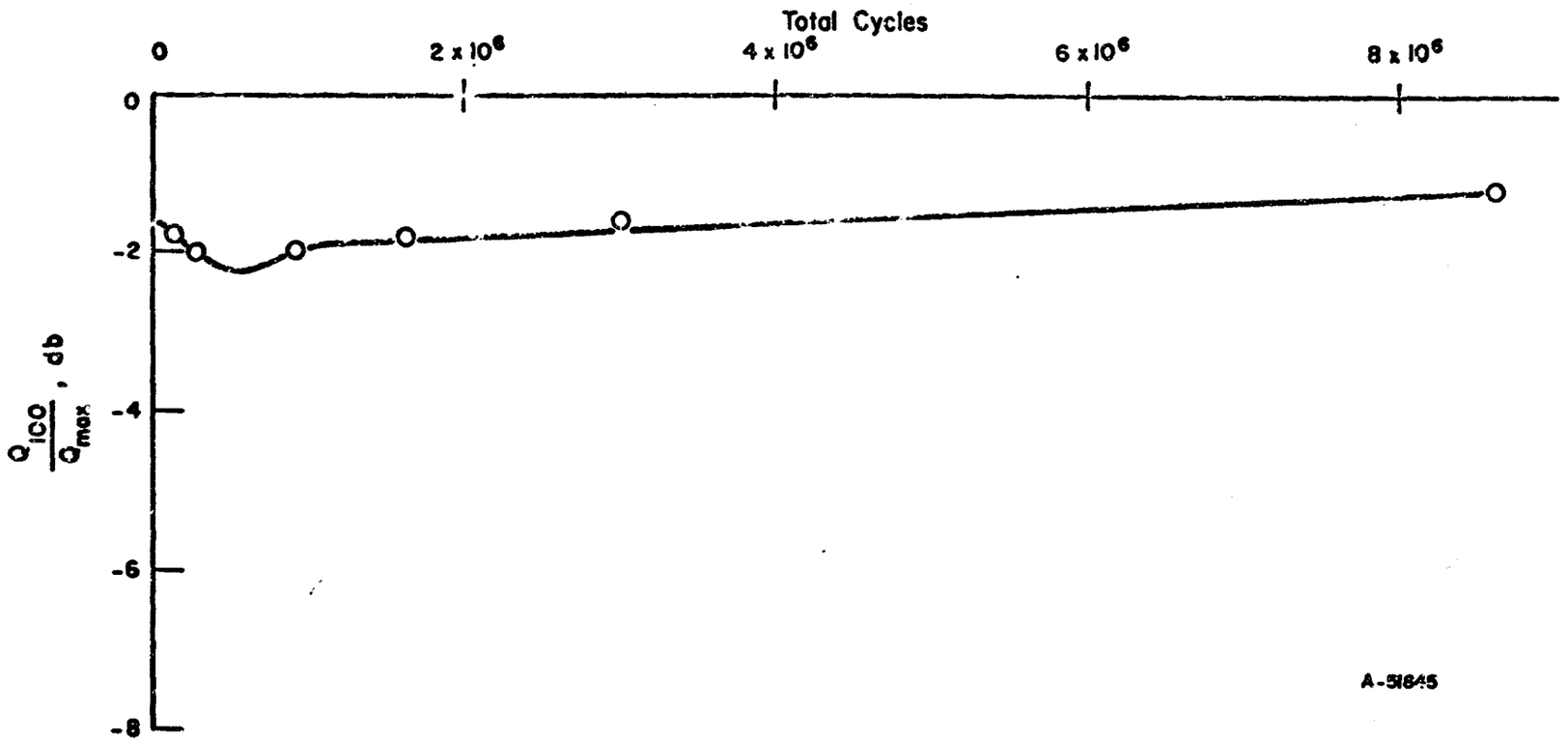

FIGURE 64. FREQUENCY RESPONSE (BLOCKED LOAD) AT 100 CPS VERSUS TOTAL CYCLES

Visual Inspection of Valves

In order to bring to light any specific features that might account for some of the test results, all of the valves were disassembled and inspected after the conclusion of the tests. Table 16 shows a summary of the visual inspection. The two most significant findings were the definite flats worn on the ball ends of the feedback wire of the unmodified valves. The wear on the modified-valve feedback wires was, by contrast, not detectable with a micrometer. Figure 65 is an enlarged photograph of the ball tips of a modified and an unmodified valve at the conclusion of the tests. The magnitude of the feedback-wire wear on the unmodified valves was 0.001 in., or approximately 3 percent of the tip ball diameter. The cause of this difference in wear is difficult to ascertain with certainty. The feedback-wire spring rate of the modified design is lower, but this is balanced by a longer stroke required by the narrower ports. In fact, the spring rate was reduced in order to produce the longer stroke. It is felt that the differences in wear rate are most probably the result of different hardnesses on the ball surfaces. According to the valve manufacturer, this is the most likely explanation. If the feedback-wire wear reduction is an inherent feature of the modified design, it may be significant in improving the performance of the valve near null in the later stages of valve life.

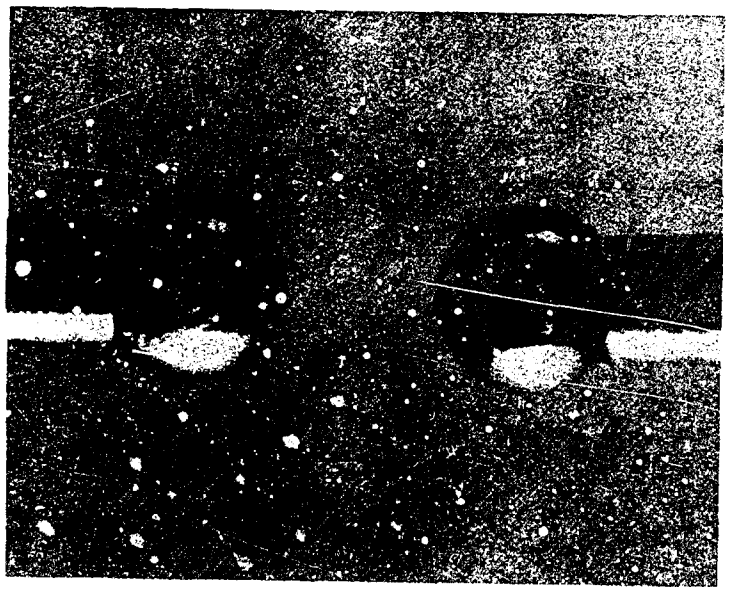

FIGURE 65. BALL ENDS OF FEEDBACK WIRE ON MODIFIED AND UNMODIFIED VALVE DESIGNS AFTER 8,600,000 CYCLES OF OPERATION

TABLE XVI. SERVO-VALVE VISUAL INSPECTION

Valve No.	Spool	Bushing	Feedback Wire	Other
65295 (Unmodified)	Very slight scoring, one outside land	ok	Worn 0.001 in. on ball (Ball diameter 0.031 in.)	Damaged O-ring on one bushing plug
65296 (Unmodified)	Moderate scoring, one outside land	ok	Worn 0.001 in. on ball	Damaged O-ring on one bushing plug
65297 (Modified)	Very slight scoring, center and outside lands	ok	No wear on ball	--
65298 (Modified)	Heavy scoring on middle and at one end. One short, very deep score at end of outside metering edge	ok	No wear on ball	--

One possible effect of the feedback-wire wear experienced in the unmodified valves is a tendency for the valve to be unstable near null with a blocked load. The test best able to reveal such a condition is the differential-pressure versus differential-current test. A check of the original data sheets showed that only one instance of "jumping" instability occurred with the modified valves, as opposed to three for the unmodified valves. The discovery of a possibly important but unanticipated difference between the designs, such as the difference in feedback-wire wear, was one of the goals of the testing program. Such findings help to compensate for the inconclusiveness arising from the low statistical value of the small samples involved.

The other anomalies noted in the visual inspection table — a rather heavy spool scoring in one valve, and damaged O-rings on two valves — did not appear to cause noticeable defects in operation.

Conclusions

The first part of the analytical study employed an analog computer simulation of a two-stage servo valve to obtain partial derivatives of various performance characteristics with respect to valve parameters that are susceptible to degradation. The partial derivatives were calculated and plotted for different values of key design parameters. These plots were evaluated and their interrelationships noted in order to identify design changes

that would reduce the over-all sensitivity of the valve to parameter degradation and to the effects of parameter variations that are introduced in the manufacturing process.

The study showed that the existing design was already close to optimum as far as the critical areas of degradation were concerned, and it was not expected that design changes would bring about significant improvement in the gross reliability of the valve. The critical areas were identified in previous programs as those parts of the spool and bushing that influence the quiescent leakage at null.

The design changes that were ultimately derived did reduce slightly the sensitivity of quiescent leakage to degradation effects, and also reduced the initial value of quiescent leakage and improved the frequency response of the valve. In addition, these modifications reduced significantly the sensitivity of several performance characteristics to degradations in the first-stage orifice and nozzle flow characteristics. Previous experiments, however, have shown that spool and orifice wear are not significant under normal operating conditions.

Even though the improvement in anticipated valve reliability resulting from the derived design modifications was relatively minor, the results of the study are significant because they serve to demonstrate the successful application of the Moment method of reliability analysis to the redesign and improvement of an existing control-system component.

The prediction of the expected reliability improvement in the valve was based on the performance characteristic of quiescent leakage at null.

In the reliability improvement derivation for quiescent leakage, it was shown that in the statistical sense, i.e., for the averaged histories of a large number of valves, a definite improvement in time to failure with regard to allowable leakage would occur. However, the study also showed that, given the normal parameter variations expected among valves, any single modified valve might or might not show improvement over the existing design, depending on its particular combination of initial parameter values. Thus, it was not possible to predict that a small sampling of old and new servo valves would show the relative improvements in average characteristics that were predicted for large samples. Hence, it was concluded that a testing program on a small sample of valves might be more useful in showing up unexpected differences between the designs than in verifying quantitatively the predicted improvements in drift-failure reliability.

When the experimental life-testing program was carried out on a sample of two modified and two unmodified valves, the above conclusions were generally confirmed. The spread in initial characteristics of the valves was relatively quite great, both in the intersample and in the intrasample sense. Although it was not possible to draw firm conclusions regarding relative reliability, an interesting unexpected difference did show up. This difference was a noticeable improvement in the wear of the ball on the end of the feedback wire in the new design. This improvement would lead to significantly better performance of the "aged" valve in the critical area very close to null. It is believed that this wear reduction is the result of increased hardness of the ball tip in the new design.

REFERENCES

(1) Stember, L. H., Jr., Mark, D. G., Mesloh, R. E., Pitman, A. A., "Research and Study of Analytical Techniques for Predicting Reliability of Flight-Control Systems", ASD-TDR-63-287, June, 1963.

(2) Mesloh, R. E., and Mark, D. G., "Variability Analysis of a Precision Mechanical Device", Proceedings of the SAE-ASME-AIAA Aerospace Reliability and Maintainability Conference, June, 1964, pp 576-588 (Printed by the Society of Automative Engineers).

(3) Wertz, J. B., Mesloh, R. E., and Easterday, J. L., "The Moment Method for Predicting the Drift Reliability of Control Systems", Proceedings of the Sixth Joint Automatic Control Conference, June, 1965.

(4) Nichol, K. C., "Research and Investigation on Satellite Attitude Control-Part IV", ASD-TDR-64, September, 1964.

(5) Lyon, Richard, N. (Ed.), "Liquid Metals Handbook", Sponsored by the Atomic Energy Commission and the Department of the Navy, Washington, D. C., First Edition NAVEXOS P-733, June, 1950, Second Edition NAVEXOS P-733 (revised), June, 1955.

(6) Jackson, Carey B (Ed.), "Liquid Metals Handbook — Sodium (NaK) Supplement", Sponsored by the Atomic Energy Commission and the Department of the Navy, Washington, D. C., TID 5277, July, 1955.

(7) Watt, D. A., "A Study of Travelling Field Electromagnetic Pumps for Liquid Metals", A.E.R.E. Report ED/R 1696, June, 1955 (H. M. Stationary Office).

(8) Barnes, A. H., "Pumping of Liquid Metals", Proceedings of the International Conference on the Peaceful Uses of Atomic Energy, Geneva, Paper No. 121, August, 1955.

(9) Blake, L. R., "Conduction and Induction Pumps for Liquid Metals", Proceedings I.E.E., Paper No. 2111 u, July, 1956.

(10) Watt, D. A., "Electromagnetic Pumps for Liquid Metals", Engineering, 1956.

(11) Blake, L. R., "A.C. and D.C. Conduction Pumps for Liquid Metals", Engineer, 1956.

(12) Watt, D. A., "Analysis of Experimental D.C. Pump Performance and Theory of Design", A.E.R.E. Report R/R 2274, May, 1957, (H. M. Stationary Office).

(13) Watt, D. A., "The Design of Electromagnetic Pumps for Liquid Metals", Proceedings I.E.E. Paper No. 2763, December, 1958.

(14) Tompkins, R. E., et al., "Study of Light Weight Liquid Metal Flywheel Systems — Parts I and II", General Electric Report No. 60 GL 193, September, 1960.

(15) McComb, R. D., "Transistors as Rectifiers for Very Low Voltage Loads", General Engineering Laboratory, General Electric Company, GOSAM Conference Paper for January 29, 1962, N.Y.C. Meeting.

(16) Tompkins, R. E., et al., "Study of Materials and Fabrication for Liquid Metal Flywheels", General Electric Report, November 1961.

UNCLASSIFIED
Security Classification

DOCUMENT CONTROL DATA - R&D

(Security classification of title, body of abstract and indexing annotation must be entered when the overall report is classified)

1. ORIGINATING ACTIVITY (Corporate author) Battelle Memorial Institute	2a. REPORT SECURITY CLASSIFICATION Unclassified 2b. GROUP

3. REPORT TITLE

Study of Application of Reliability Prediction Techniques

4. DESCRIPTIVE NOTES (Type of report and inclusive dates)

Technical Report March 15, 1964, to June 30, 1965

5. AUTHOR(S) (Last name, first name, initial)

Wertz, J. B. Hassfurther, M. E. Easterday, J. L.
Goldgraben, J. R. Baum, J. V.

6. REPORT DATE	7a. TOTAL NO. OF PAGES	7b. NO. OF REFS
May 1966	129	16

8a. CONTRACT OR GRANT NO.	9a. ORIGINATOR'S REPORT NUMBER(S)
AF 33 (615)-1527 b. PROJECT NO. 8225 c. d.	AFFDL-TR-65-204 9b. OTHER REPORT NO(S) (Any other numbers that may be assigned this report)

10. AVAILABILITY/LIMITATION NOTICES This document is subject to special export controls & each transmittal to foreign governments or foreign nationals may be made only with prior approval of the Flight Dynamics Laboratory (FDCL), Wright-Patterson Air Force Base, Ohio 45433.

11. SUPPLEMENTARY NOTES	12. SPONSORING MILITARY ACTIVITY
	Flight Dynamics Laboratory, Research and Technology Division, Air Force Systems Command, Wright-Patterson AFB, Ohio

13. ABSTRACT

A previous reliability research effort by Battelle generated an analytical technique called the Moment method for predicting drift-type failures in components and systems. This technique is based on the Propagation of Variance formula, which combines data derived from the system, or system model, and parameter tolerance data, to formulate an estimate of the probability that the system will perform within specifications at the initial or some future time of operation. A discussion is presented on

This report discusses the application of the reliability-prediction technique to a momentum-exchange-type attitude control and stabilization subsystem for a satellite, a liquid-metal servo actuating subsystem, and an electrohydraulic servo valve.

A mathematical model was completed for the momentum-exchange-type attitude control (fluid flywheel), significant system parameters identified, the analysis of the expected system degradation over time was made, and a prediction of efficiency and reliability is presented in the report.

DD FORM 1 JAN 64 1473

UNCLASSIFIED
Security Classification

14. KEY WORDS	LINK A		LINK B		LINK C	
	ROLE	WT	ROLE	WT	ROLE	WT
Reliability Prediction						
Flight Control Equipment						
Servo Control Valves						
Actuation Subsystem						
Liquid Metal Actuation						